CalVal Saral/ Altika

SARAL/Altika validation and cross calibration activities

Annual report 2016

Contract No 14026/00 – 160182 - lot 1.6.3

Reference : CLS-DOS-16-0329

Nomenclature : SALP-RP-MA-EA-23073-CLS

Issue : 1rev 1

Date : March 17, 2017

CLS - 11 Rue Hermès - Parc Technologique du Canal - 31520 Ramonville St-Agne - FRANCE
Telephone 33 5 61 39 47 00 / Fax 33 5 61 75 10 14

Chronology Issues:		
Issue:	Date:	Reason for change:
1.0	Nov 14, 2016	Creation
1.1	Jan 30, 2017	Delivery
1.2	Mar 17, 2017	Revised version

People involved in this issue :				
	AUTHORS	**COMPANY**	**DATE**	**INITIALS**
Written by:	P. Prandi; V. Debout	CLS		
Checked by:	M. Ablain; S. Labroue	CLS		
Approved by:	J.-P. Dumont	CLS		
Application authorised by:				

Index Sheet :	
Context:	
Keywords:	
Hyperlink:	

Distribution:		
Company	Means of distribution	Names
CLS/DOS	electronic copy	mablain@cls.fr slabroue@cls.fr
CNES	electronic copy	thierry.guinle@cnes.fr emilie.bronner@cnes.fr nicolas.picot@cnes.fr amandine.guillot@cnes.fr jean-damien.desjonqueres@cnes.fr aqgp_rs@cnes.fr dominique.chermain@cnes.fr delphine.vergnoux@cnes.fr

List of tables and figures

List of Tables

List of Figures

List of items to be defined or to be confirmed

Applicable documents / reference documents

Contents

1. Introduction

This document presents the synthesis report concerning validation activities of SARAL/AltiKa GDRs in 2016 under SALP contract supported by CNES at the CLS Space Oceanography Division.

The present report covers different topics, which are investigated either as part of routine Cal/Val activities, or following mission events:

- mono-mission validation and monitoring,
- cross-calibration between SARAL/AltiKa and Jason-2,
- particular investigations.

Results presented in this document are mainly based on the current version of GDR data (GDR-T Patch2). Sometimes results using IGDR, OGDR, or updated GDR data are also shown. This is mentioned in the text when needed. The content of the Patch2 reprocessing of SARAL/AltiKa data can be found at chapter 10.2.. A detailed evaluation of the impacts of Patch 2 on mission performance was performed in 2014 when the reprocessing occured by [16, Philipps and Pignot].

1.1. SARAL/AltiKa: a brief history

SARAL/AltiKa is a joint CNES/ISRO mission which was successfully launched on February, 25th, 2013. The spacecraft reached its operationnal orbit on March, 13th, and cycle 1/pass 1 started on March 14th. At this time, the satellite was not exactly on the expected ground track (the historical ERS and Envisat ground track), with a difference up to 2 km at high latitudes. After inclination maneuvers, SARAL/AltiKa reached its nominal ground track on October, 7th 2013 (cycle 6).

During September 2014, several mispointing events occured, attributed to variations of reaction wheel friction. The reaction wheel eventually failed, resulting in SARAL/AltiKa going into safe-hold mode (SHM) from October 6th to 9th. Since then, the satellite has been experiencing occasional mispointing events.

Following the loss of the reaction wheel, station keeping maneuvers have been less accurate, and SARAL/AltiKa's ground track has been drifting (eastward and westward) from its nominal ground track, which has been loosely maintained (from March 2015 onward). On June, 29th, 2016, CNES and ISRO announced that the mission would enter a new phase after a last maneuver: the drifting phase (SARAL-DP). On July 4th, 2016, this last maneuver was performed to raise the spacecraft's altitude by 1 km, and leave him flying free of station keeping maneuvers. This new phase comes with a new numbering of cycles, starting at 100.

1.2. SARAL/AltiKa Cal/Val activities

Since the beginning of the mission, SARAL/AltiKa data have been analyzed and monitored in order to assess the quality of SARAL/AltiKa products. Cycle per cycle reports summarizing mission performance are generated and made available through the AVISO web page (http://www.aviso.altimetry.fr/en/data/calval/systematic-calval/validation-reports.html). Main performance metrics were also summarized in a paper published in the Marine Geodesy special issue on SARAL/AltiKa in 2015 [2]. Each year, the Cal/Val activity is described in a yearly report, which are also available through the AVISO website ([4], [23] and [4]).

The present report documents the activities undertaken in the framework of the SALP contract to assess and monitor Saral/AltiKa data quality. Depending on the sections the period considered may vary slightly. In general, all data from cycle 1 to 103 are considered (corresponding to March 2013 to October 2016). This period might be reduced (to end at cycle 101 or 102) for some plots. We present a detailed description of the main performance metrics of the mission including:

- monitoring of missing and edited parameters,
- analysis of geophysical parameters and corrections,
- accuracy and stability of SLA measurements.

We also present the results of cross-calibration analysis performed between SARAL/AltiKa and Jason-2. Even if both satellites are on different ground tracks comparisons remain possible, and necessary, to ensure the continuity of ocean observations through high precision altimetry.

Routine validation of SARAL/AltiKa mission and cross-calibration with Jason-2 activities generate a large number of graphs, plots and figures. The purpose of the present report is to give the reader a useful and reader-friendly (as much as possible) summary of the most important results of the daily monitoring of the mission performed at CLS.

This report also presents the results of particular investigations undertaken this year on SARAL/AltiKa, either to better characterize mission performance or as a consequence of mission events.

2. Processing status

2.1. Processing history

Four months after launch, SARAL/AltiKa OGDR and IGDR data were available to all users beginning of July 2013. They were first released under the version T label, with some flaws (unit problem for liquid cloud water,...), some corrections voluntarily disabled (atmospheric attenuation set at default value) or with disclaimers of product fields (ice_flag, altimeter wind not to use, ...).

Some of these issues were addressed by Patch 1, whose content is recalled in 10.1.. Beginning of September 2013 the GDR products were released with consistent Patch 1 standards since the beginning of the mission.

A second processing upgrade, labeled Patch 2, containing several improvements for SARAL/AltiKa data, was applied on February 2014. The content of this Patch 2 is recalled in chapter 10.2. This included a full reprocessing of previous GDR cycles.

Further on, orbit standard changed from GDR-D to GDR-E from June 30th, 2015 onwards on IGDR and from cycle 25 (July 3rd) on GDR. To date, previous GDR cycles were not reprocessed. The mean sea surface was also updated from July 4th, 2016 onwards on IGDR data and from cycle 34 (May 12th) on GDR data. Again, previous GDR cycles were not reprocessed to date.

Table 1 summarizes the processing history of SARAL/AltiKa products through the application dates of main product versions.

Data version	Ogdr	Igdr	Gdr
Version T	till cycle 4 segment 0609	till cycle 4 pass 394	-
Version T with Patch1 (chapter 10.1.)	from cycle 4 segment 0611 onwards (2013-07-18 13h44m04)	from cycle 4 pass 0395 onwards (2013-07-10 23h56m18)	from cycle 1 pass 0001 onwards
Version T with Patch2 (chapter 10.2.)	from cycle 10 segment 0407 onwards (2014-02-06 10h46m58)	from cycle 10 pass 0566 onwards (2014-02-11 23h17m37)	from cycle 8 onwards (cycles 1 to 7 have been reprocessed)

Table 1: *Product versions*

2.2. CAL/VAL status

2.2.1. Acquisition/tracking modes

Table 2 shows the acquisition/tracking modes used since the beginning of the SARAL/AltiKa mission.

cycle	pass	start time	stop time	altimeter mode
1	0001-0200	2013-03-14	2013-03-21	DIODE acquisition / median tracking
1	0201-0400	2013-03-21	2013-03-28	DIODE acquisition / EDP tracking
1	0401-0600	2013-03-28	2013-04-04	DIODE acquisition / median tracking
1	0601-0800	2013-04-04	2013-04-11	DIODE / DEM tracking
1	0801-1002	2013-04-11	2013-04-18	DIODE acquisition / EDP tracking
2	0001-1002	2013-04-18	2013-05-23	DIODE acquisition / median tracking
3	0001-0400	2013-05-23	2013-06-06	DIODE acquisition / median tracking
3	0401-0800	2013-06-06	2013-06-20	DIODE acquisition / EDP tracking
3	0801-1002	2013-06-20	2013-06-27	DIODE acquisition / median tracking
4 to 9	0001-1002	2013-06-27	2014-01-23	DIODE acquisition / median tracking
10	0001-0127	2014-01-23	2014-01-27	DIODE acquisition / median tracking
10	0128-0135	2014-01-27	2014-01-27	autonomous DIODE / median tracking
10	0136-1002	2014-01-27	2014-02-27	DIODE acquisition / median tracking
11 to 16	0001-1002	2014-02-27	2014-09-25	DIODE acquisition / median tracking
17	0001-0324	2014-09-25	2014-10-06	DIODE acquisition / median tracking
				.../...

cycle	pass	start time	stop time	altimeter mode
17	0414-0457	2014-10-09	2014-10-11	autonomous DIODE / median tracking
17	0457-1002	2014-10-11	2014-10-30	DIODE acquisition / median tracking
18 to 102	0001-1002	2014-10-30	2016-10-17	DIODE acquisition / median tracking

Table 2: *Acquisition and tracking modes*

2.2.2. List of events

Table 3 summarizes the major events of the SARAL/AltiKa mission.

cycle	pass	start time	stop time	event
1		2013-03-14	2013-03-17	X-band stations acquisition problems (a few missing data)
1	0172-0175	2013-03-20 05:10:03	08:30	calibration I2+Q2 and I&Q for expertise
1	0266	2013-03-23 12:13:52	12:13:55	semi major axis maneuver
1	0372, 0374	2013-03-27		CAL2 long calibrations at 04:51 (28min missing data) and 06:40 (11min missing data)
1	0801	2013-04-11 04:42:00	04:59:45	altimeter gain calibration I2+Q2 (mostly over land)
1	0868	2013-04-13 12:53:52	12:53:54	station keeping maneuver
1	0898	2013-04-14 13:42:00	13:59:45	altimeter gain calibration I&Q (mostly over land)
1	0984	2013-04-17 13:47:00	14:04:45	altimeter gain calibration I2+Q2 (mostly over land)
2	0034, 0035	2013-04-19 9:37	10:25	cross calibration test over S-band station Biak (Indonesia)
2	0057	2013-04-20 04:53	05:12	altimeter gain calibration I&Q (over land)
				.../...

cycle	pass	start time	stop time	event
2	0127	2013-04-22 15:26	15:54	cross calibration maneuver
2	0206	2013-04-25 9:53		pitch maneuver (0.045°) to correct the PF/RF alignment (alignment between the platform and the radiofrequency axis)
2	0355	2013-04-30 14:35	15:03	cross calibration maneuver
2	0782	2013-05-15 12:48:23	12:48:26	station keeping maneuver
3	0438	2013-06-07 12:25:11	12:25:13	station keeping maneuver
3	0887-0890	2013-06-23 05:06:55	06:56:57	no O/I/GDR product due to PLTM lost
3	0926	2013-06-24 13:31:11	13:31:13	station keeping maneuver
4	0498	2013-07-14 14:42:44	14:42:47	station keeping maneuver
4	0556	2013-07-16 15:01:01	15:19:00	altimeter gain calibration I&Q (mostly over land)
4	0586	2013-07-17 16:13:01	16:30:45	altimeter gain calibration I2+Q2 (mostly over land)
4	0911	2013-07-29 00:54:25	00:58:26	inclination maneuver (1 burn on Y and Z axis)
4	0984	2013-07-31 14:08:03	14:08:11	station keeping maneuver
5	0182	2013-08-07 13:48:06	13:48:09	station keeping maneuver
5	0726	2013-08-26 13:51:02	13:51:05	station keeping maneuver
5	0958	2013-09-03 16:02:01	16:20:00	altimeter gain calibration I&Q (mostly over land)
6	0038	2013-09-06 12:44:01	13:01:45	altimeter gain calibration I2+Q2 (over land)
6	0812	2013-10-03 13:55:39	13:57:17	1st inclination maneuver to reach the Envisat ground track (1 burn on Z axis)
				.../...

cycle	pass	start time	stop time	event
6	0926	2013-10-07 13:29:45	13:31:25	2nd inclination maneuver to reach the Envisat ground track
6	0984	2013-10-09 14:07:52	14:07:57	station keeping maneuver
7	0526	2013-10-28 14:11:24	14:11:26	station keeping maneuver
7	0586	2013-10-30 16:11	16:28:45	altimeter gain calibration I2+Q2
7	0812	2013-11-07 13:57:01	13:57:03	station keeping maneuver
8	0326	2013-11-25 14:31:29	14:31:32	station keeping maneuver
8	0812	2013-12-12 13:56:58	13:57:01	station keeping maneuver
9	0240	2013-12-27 14:25:41	14:25:44	station keeping maneuver
10	0128	2014-01-27 16:15	16:32:45	altimeter gain calibration I2+Q2 (mostly over land)
10	0152	2014-01-28 12:38:43	12:38:45	station keeping maneuver
11	0126	2014-03-03 14:50:53	14:50:56	station keeping maneuver
11	0782	2014-03-26 12:47:17	12:47:20	station keeping maneuver
12	0438	2014-04-18 12:24:16	12:24:19	station keeping maneuver
12	0728	2014-04-28 15:12:55	15:30:45	expertise calibration CAL1
13	0326-0327	2014-05-19 14:31:18	14:31:21	station keeping maneuver with two consecutive mis-pointing events between 14:38 and 14:43 and between 15:03 and 15:12
14	0782	2014-07-09 12:47:10	12:47:12	station keeping maneuver
15	0356	2014-07-29 15:22:00	15:39:45	altimeter gain calibration I2+Q2 (mostly over land)

.../...

cycle	pass	start time	stop time	event
15	0782	2014-08-13 12:47:06	12:47:08	station keeping maneuver
16	0539	2014-09-09		No TM from 01:02:30 to 01:06:16 and from 01:09:25 to 01:14:08 due to the update of MNT onboard parameters
16	0640	2014-09-12 13:44:34	13:44:36	station keeping maneuver
16	0406	2014-09-04 09:44:24	09:47:15	several platform mispointing events caused by a rise in reaction wheel friction due to movement of lubricant. Only the 3 largest events are shown.
	0474	2014-09-06 18:38:32	18:41:55	
	0690	2014-09-14 07:36:44	07:38:50	
17	0324	2014-10-06 12:40:00	12:40:02	station keeping maneuver
17	0324-0414	2014-10-06 13:03:22	2014-10-09 16:27:46	safe hold mode
17	0438	2014-10-10 12:14:14	12:14:34	station keeping maneuver
17	0610	2014-10-16 12:26:26	12:26:35	station keeping maneuver
17	0958	2014-10-28 16:02:00	16:19:45	altimeter gain calibration I2&Q2
18	0152	2014-11-04 12:26:39	12:26:41	station keeping maneuver
18	0640	2014-11-21 13:39:10	13:39:12	station keeping maneuver
19	0182	2014-12-10 13:47:02	13:47:04	station keeping maneuver
19	0640	2014-12-26 13:44:42	13:44:45	station keeping maneuver
20		2015-01-12 11:30		software patch applied by ISRO in order to avoid zero-crossings of RW speed
				.../...

cycle	pass	start time	stop time	event
20		2015-01-17	2015-01-18	platform pointing disturbance (fluctuations in RW friction)
20	0412	2015-01-22 14:31:03	14:31:06	station keeping maneuver
20	0586	2015-01-28 16:11		CNG calibration
21	0268	2015-02-21 13:47:56	13:47:58	station keeping maneuver
22	0354	2015-03-31 13:50:16	13:50:18	station keeping maneuver. Delta_Vy twice more than expected.
22	0610	2015-04-09 12:28:10	12:28:14	station keeping maneuver to stop the westward drift.
22	0986	2015-04-22 15:30		CNG calibration
23	0954	2015-05-26 12:51:07	12:51:12	station keeping maneuver. Delta_V applied twice less than expected. thruster firing has taken place between 10:00 to 10:04 UT to control a reaction wheel error guidance has been performed with thrusters (instead of RW)
24	0554	2015-06-16 13:23	13:39	station keeping maneuver (to calibrate satellite rotation with thrusters). The main objective is not to recover the nominal ground track but to calibrate this new way of performing satellite rotation
24		2015-06-30		introduction of a leap second =¿ UTC = TAI-36s The sequence of dates of the UTC second markers is: 2015 June 30, 23h 59m 59s 2015 June 30, 23h 59m 60s 2015 July 1, 0h 0m 0s
24		2015-06-30		First MOE with GDR-E orbit standard
25				Orbit standard = GDR-E
25	0182	2015-07-08 13:40:55	13:40:58	station keeping maneuver (only with thrusters). Thruster activity is expected from 13:31:50 UT to 13:50 UT
25	0758	2015-07-28 16:22		Altika quarterly expertise CNG calibration
				.../...

cycle	pass	start time	stop time	event
26	0152	2015-08-11 12:32:56	12:32:59	station keeping maneuver (to stop western drift and stay in the +/-1km ground track window) only with thrusters
26	0524	2015-08-24 12:24:12	12:24:14	station keeping maneuver, performed only with thrusters.
26		2015-09-05	2015-09-06	mispointing events attributed to sudden changes in friction torque of reaction wheel (RW-4).
27		2015-09-15		Update of CoG historic file: the initial value of Zcog value has been updated by POD team and propagated to IDS teams through CoG historic file ; new value -0.6105 (instead of -0.6583)
28	0182	2015-10-21 13:41:40	13:41:43	station keeping maneuver
28	0195	2015-10-22		mising data due to issues on X-band stations network and the amount of TM_gaps
28	0614	2015-11-05 15:39		CNG Calibration
28	0812	2015-11-12 13:40:32	13:59:33	station keeping maneuver (3 bursts)
29	0210	2015-11-26 13:08:18	13:24:57	station keeping maneuver
30	0412	2016-01-07 14:28:48	14:44:39	station keeping maneuver
30	0986	2016-01-27 15:30:00	15:47:45	CNG calibration
31	0441-0442	2016-03-18 15:08:55	15:25:40	collision avoidance maneuver
33	0010	2016-04-07 13:18:44	13:34:31	station keeping maneuver
33	0528	2016-04-25 15:33:00	15:50:45	CNG Calibration
35	0522	2016-07-04 12:13:35	12:31:15	orbit change maneuver, cycle 35 ends at pass 522
101	0090	2016-08-11 15:54:00	16:11:45	CNG Calibration
				.../...

cycle	pass	start time	stop time	event
103	0290	2016-10-27 15:47:00	16:04:45	CNG Calibration

Table 3: *Main SARAL/AltiKa mission events (red rows indicates safe hold mode event)*

2.3. Models and Standards

Table 4 summarizes the contents regarding altimeter standards and geophysical correction models of the current version (T, Patch 2) of SARAL/AltiKa products.

Model	Product version "T" Patch2
Orbit	Based on Doris onboard navigator solution for OGDR DORIS tracking data for IGDR DORIS+SLR tracking data for GDR. Using POE-D, and POE-E from cycle 25
Altimeter Retracking	"Ocean MLE4" retracking: MLE4 fit from 2nd order Brown analytical model: MLE4 simultaneously retrieves 4 parameters from the altimeter waveforms: • Epoch (tracker range offset) → altimeter range • Composite Sigma → SWH • Amplitude → Sigma0 • Square of mispointing angle "Ice 1" retracking: Geometrical analysis of the altimeter waveforms, which retrieves the following parameters: • Epoch (tracker range offset) → altimeter range • Amplitude → Sigma0 "Ice 2" retracking: The aim of the ice2 retracking algorithm is to make the measured waveform coincide with a return power model, according to Least Square estimators. Retrieval of the following parameters: • Epoch → altimeter range • Width of the leading edge → SWH • Amplitude → Sigma0 • Slope of the logarithm of the waveform at the trailing edge → Mispointing angle/surface slope • the thermal noise level (to be removed from the waveform samples)

.../...

Model	Product version "T" Patch2
	"Sea Ice" retracking: In this algorithm, waveform parameterization based on peak threshold retracking is applied to the Ka-band waveform. From this parameterization, a tracking offset and backscatter estimate are determined. Tests are made on the extent of the tracking offset, and extreme values are flagged as retracking failures. The sea-ice waveform amplitude is determined by finding the maximum value of the waveform samples and the tracking offset is determined by finding the point on the waveform (by interpolation) where the waveform amplitude exceeds a threshold determined from the above sea-ice amplitude. A tracking offset is determined. The Centre Of Gravity offset correction must be included in the range measurement as the correction is not available separately in the L2 product. • Amplitude → Sigma0 • Tracking offset → altimeter range • Centre Of Gravity offset correction → correction to altimeter range measurement N.B.: the Ice2 retracking algorithm has been tuned to Ka-band since Patch2, but not the Ice1 nor the Sea Ice algorithms
Altimeter Instrument Corrections	consistent with MLE4 retracking
Saral/AltiKa Radiometer Parameters	Using on-board calibration
Dry Troposphere Range Correction	From ECMWF atmospheric pressures and model for S1 and S2 atmospheric tides
Wet Troposphere Range Correction from Model	From ECMWF model
Ionosphere correction	Based on Global Ionosphere TEC Maps from JPL
Sea State Bias Model	Hybrid SSB model from [17]
Mean Sea Surface	MSS_CNES-CLS11 , MSS_CNES_CLS15 from cycle 34
Mean Dynamic Topography	MDT_CNES-CLS09
Geoid	EGM96
Bathymetry Model	DTM2000.1
Inverse Barometer Correction	Computed from ECMWF atmospheric pressures after removing S1 and S2 atmospheric tides
	.../...

Model	Product version "T" Patch2
Non-tidal High-frequency De-aliasing Correction	Mog2D high resolution ocean model on (I)GDRs. None for OG-DRs. Ocean model forced by ECMWF atmospheric pressures after removing S1 and S2 atmospheric tides.
Tide Solution 1	GOT4.8
Tide Solution 2	FES2012 + S1 and M4 ocean tides. S1 and M4 load tides ignored
Equilibrium long-period ocean tide model.	From Cartwright and Taylor tidal potential.
Non-equilibrium long-period ocean tide model.	Mm, Mf, Mtm, and Msqm from FES2004
Solid Earth Tide Model	From Cartwright and Taylor tidal potential.
Pole Tide Model	Equilibrium model
Wind Speed from Model	ECMWF model
Altimeter Wind Speed	wind speed model from [14]
Trailing edge variation Flag	Derived from Matching Pursuit algorithm (from J. Tournadre, IFREMER)
Ice flag	Initialized in climatological areas based on wind speed values and updated by comparing the model wet tropospheric correction and the dual-frequency wet tropospheric correction retrieved from radiometer brightness temperatures

Table 4: *Models and standards adopted for the SARAL/AltiKa version T Patch 2 products. Adapted from [9]*

3. Data coverage and edited measurements

This section details the SARAL/AltiKa mission performance regarding data availablity. The ratio of missing and edited measurements is carefully monitored through routine Cal/Val analysis to detect any anomalies, either on the instrument itself or on ground processing.

3.1. Missing measurements

3.1.1. Over land and ocean

Determination of missing measurements relative to the theoretically expected orbit ground pattern is an essential tool to detect missing telemetry or satellite events for instance. The number of missing measurements is routinely monitored by Cal/Val tools. SARAL/AltiKa's performance regarding the number of missing measurements is compared to Jason-2, through the comparison of the percentage of missing measurements estimated in a consistent manner for the two missions.

Missing 1 Hz measurements are estimated by comparing actual measurements to the theoretical ground track, resampled from the ENVISAT one. From cycle 100 onward, the actual ground track is drifting and the theoretical track can't be used any more. Missing measurements are then estimated using a theoretical ground track generated on the fly from predicted orbit files. As long as a record exists for a given date, the measurement is accounted as present, even if there is no useful science data.

SARAL/AltiKa can use several on board tracking modes: median, Earliest Detectable Part (EDP) and Diode/DEM (see chapter 2.2.1.). The median mode is similar to the one used by Envisat and for most cycles of Jason-2. EDP tracker should improve the tracker behavior above continental ice surfaces and hydrological zones. Finally, Diode/DEM mode is a technique using information coming from Diode and a digital elevation model available on board. It was already tested on Jason-2. For more information about the different on board tracker algorithms see [11]. The information about the acquisition / tracking mode used is available in the GDR (fields alt_state_flag_acq_mode_40hz and alt_state_flag_tracking_mode_40hz).

From cycle 4 onwards, SARAL/AltiKa used the **DIODE acquisition / median tracking mode**, except for two short periods of autonomous DIODE acquisition at cycles 10 and 17:

- at cycle 10, the altimeter switched to autonomous DIODE acquisition mode after a CNG I2+Q2 calibration, this mode was used for about 6 hours before switching back to the nominal DIODE acquisition mode,
- at cycle 17, the altimeter switched to the autonomous DIODE acquisition mode after it was turned on again after the SHM, this acquisition mode was used for a day and a half before switching back to the nominal DIODE acquisition mode.

Considering all surface types, SARAL/AltiKa has more data available than Jason-2 (which also uses most of the time the median tracker), independently from the tracker mode used for Saral. Figure 1 shows the percentage of available measurements for SARAL/AltiKa and Jason-2 over all surfaces. Differences appear on land surfaces as shown in figure 2. The missing data are highly correlated with the mountains location. Note that the routine calibrations for SARAL/AltiKa are mainly done over desert regions (Sahara, Australia, south of Africa and Mongolia), the percentage of available data is therefore low in these regions. In periods when the ground track was loosely maintained, and at the beginning of the drifting phase, routine calibrations also drifted and some of them were performed over ocean, resulting in short track sections missing.

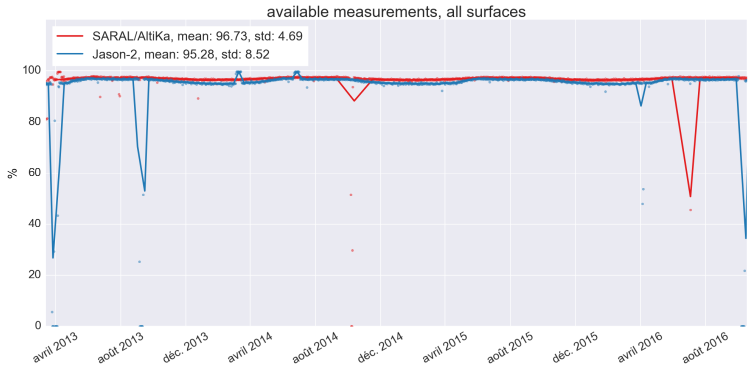

Figure 1: *Percentage of available measurements over all surfaces for SARAL/AltiKa and Jason-2. Dots are daily averages while solid lines correspond to cycle averages.*

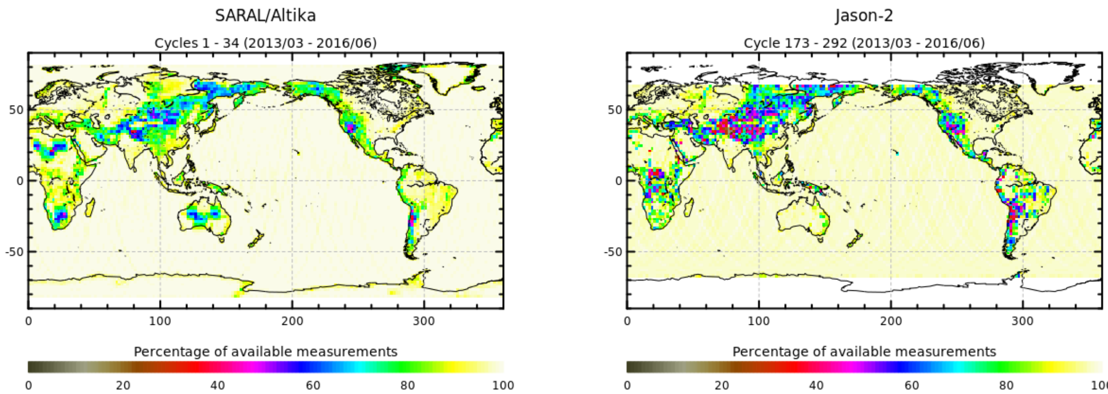

Figure 2: *Map of the percentage of available measurements over land for SARAL/AltiKa (left) and Jason-2 (right) on SARAL/AltiKa's cycles 1 to 34*

3.1.2. Over ocean

When considering only the ocean surface, the same analysis method leads generally to slightly less available data for SARAL/AltiKa compared to Jason-2 data coverage, as shown on figure 3, which represents the percentage of available measurements limited to ocean surfaces. Over the shown period, the mean value is about 97.1% for Jason-2, and 99.2% for SARAL/AltiKa, but please consider that Jason-2 encoutered two safe-hold mode periods and Saral/AltiKa one safe-hold mode period, which explains the globally lower value for Jason-2. SARAL/AltiKa had other periods with reduced data availability. All these events are described in table 3.

By removing days when instrumental events or other big anomalies occurred, the mean value of available measurements increases to 99.98% for Jason-2 and 99.88% for SARAL/AltiKa. These 0.1% of fewer data over ocean for SARAL/AltiKa compared to Jason-2 are likely due to the sensitivity of the Ka-band frequency to rain. This exceeds largely the specifications for SARAL/AltiKa, which were (see [19]) 95% of all possible over-ocean data during a 3-year period with no systematic gaps plus the specific Ka-band limitation (5% of measurements may be not achieved due to rain rates > 1.5 mm/h according to geographic areas).

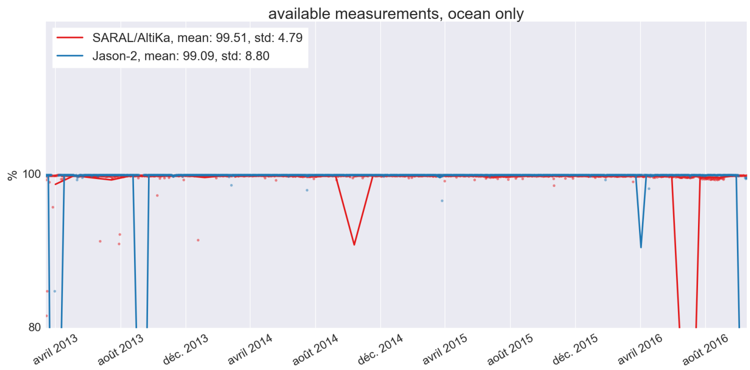

Figure 3: *Percentage of available measurements over ocean for SARAL/AltiKa and Jason-2. Dots are daily averages while solid lines correspond to cycle averages.*

3.2. Edited measurements

The editing step of the Cal/Val process intends to remove from further analysis any measurement that is considered as erroneous. The definition of an erroneous measurement, and on the accepted error level on the final sea level anomaly is of course a trade off between accuracy and data coverage.

3.2.1. Editing criteria definition

Editing criteria are used to select valid measurements over ocean. The editing process is divided into 3 main parts:

- removal of all measurements affected by sea-ice (see section 3.2.2.),
- removal of all measurements which exceed given thresholds on different parameters (see section 3.2.3.),
- further checks on along-track sla consistency (see section 3.2.17.).

For each step of the editing process, the number of edited measurements, per track, per day and per cycle are routinely monitored at Cal/Val level. This allows detection of anomalies in the number of removed data, which could come from instrumental, geophysical or algorithmic changes.

The editing performed here (and more generally SARAL/AltiKa Cal/Val activities) are dedicated to ocean applications. All data over land are removed using a land/water mask prior to the analysis described in this section. There are some variations over time (mainly at the beginning of the missions life) of the number of measurements over land. These variations are directly related to the tracking mode used: when the DEM mode is used, more measurements are acquired over land compared to the median tracking periods.

Furthermore, as a very first step of the editing process, all passes are checked for latitude monotony (either increasing or decreasing). On SARAL/AltiKa this has not led to the removal of a single measurement yet.

Figure 4 gives an overview of the behavior of the edited measurements (all criteria combined) over the mission's lifetime. On average 20.3% of the measurements are edited, the majority of which are removed due to the sea ice flag. Results of the different editing steps applied to the data are presented below.

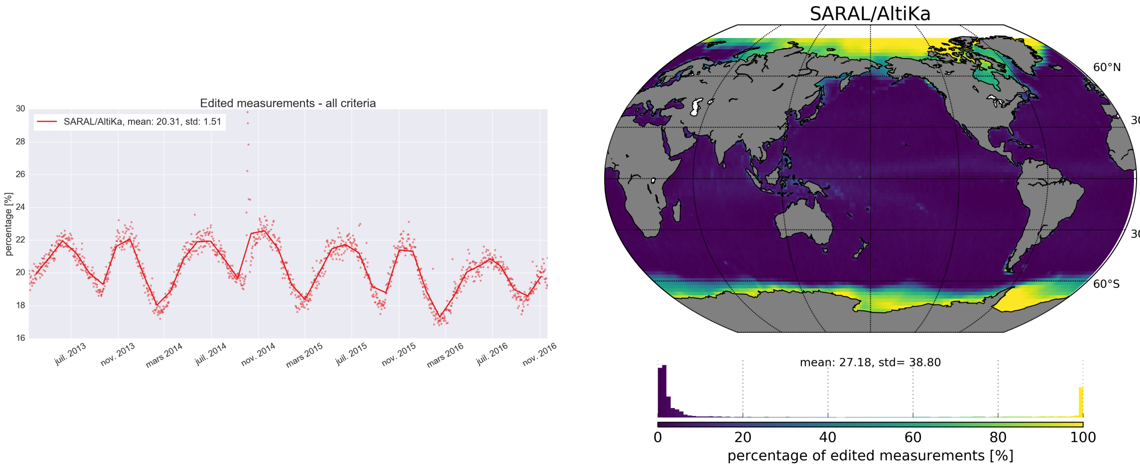

Figure 4: *Total percentage of SARAL/AltiKa edited measurements. [left] monitoring for GDR data and [right] map since the beginning of mission (cycles 1 to 101).*

3.2.2. Flagging quality criteria: Ice flag

The ice flag (ice_flag in the GDR products) is used to remove measurements affected by sea ice in the altimeter footprint. Left panel of figure 5 shows the evolution of the percentage of measurements edited by this criterion. Over the shown period, several characteristics are visible:

- a large seasonal cycle, due to annual growth and retreat of sea ice extent,
- two yearly minimums of the percentage of edited SARAL/AltiKa data (∼16% of edited data) are observed in February and September, corresponding to periods where the Antarctic or Arctic sea ice extension are minimum,
- maximums (∼20% of edited data) are reached around May/June and October/November,
- a general decreasing trend, related to sea ice extent retreat.

The spatial distribution of the percentage of measurements edited by ice flag is plotted in the right panel of figure 5, over the whole mission lifetime.

Please note that an improved ice flag algorithm is available through the PEACHI products. As this is not in the GDR, we do not consider this flag here.

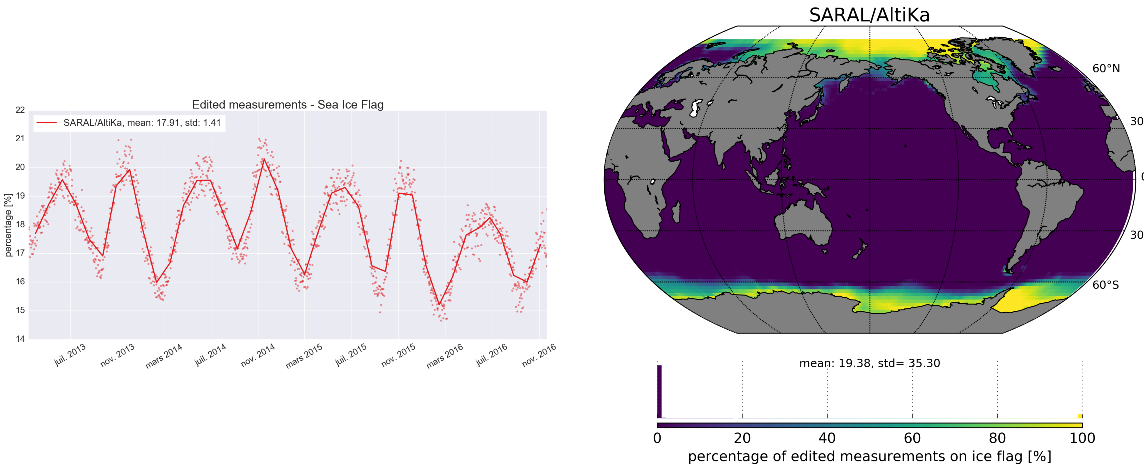

Figure 5: *Percentage of edited measurements by ice flag criterion. [left] monitoring for GDR data (all latitudes and [right] map since the beginning of mission (cycles 1 to 101).*

3.2.3. Threshold criteria: Global

Parameter	Min thresholds	Max thresholds	mean edited
Sea surface height	$-130\,m$	$100\,m$	0.47%
Sea level anomaly	$-2\,m$	$2\,m$	0.82%
Number of range measurements	20	*Not applicable*	1.11%
Standard deviation of range	0	$0.2\,m$	1.49%
Squared off-nadir angle	$-0.2\,deg^2$	$0.0625\,deg^2$	0.37%
Dry troposphere correction	$-2.5\,m$	$-1.9\,m$	0.00%
dynamical atmopsheric correction	$-2\,m$	$2\,m$	0.00%
Radiometer wet troposphere correction	$-0.5m$	$0\,m$	0.07%
Significant wave height	$0\,m$	$11\,m$	0.42%
Sea State Bias	$-0.5\,m$	$0.0025\,m$	0.29%
Number measurements of Ka-band Sigma0	20	*Not applicable*	1.04%
Standard deviation of Ka-band Sigma0	0	$1\,dB$	0.93%
Ka-band Sigma0	$3\,dB$	$30\,dB$	0.34%
Ocean tide	$-5\,m$	$5\,m$	0.18%
Equilibrium tide	$-0.5\,m$	$0.5\,m$	0.17%
Earth tide	$-1\,m$	$1\,m$	0.00%
Pole tide	$-0.15\,m$	$0.15\,m$	0.00%
Altimeter wind speed	$0\,m.s^{-1}$	$30\,m.s^{-1}$	0.29%
All together	-	-	2.60%

Table 5: *Editing thresholds, statistics obtained for cycles 1 to 101*

The quality of instrumental and geophysical parameters is checked with respect to thresholds, after having selected only ocean/lakes measurements and having removed sea ice. Thresholds used are summarized in table 5, along with the average percentage of edited data for each parameter/threshold pair.

Note that no measurements are edited by the following corrections:

- dry troposphere correction,
- dynamical atmospheric correction,
- equilibrium tide,
- earth tide,
- and pole tide.

Indeed these parameters are all derived from models, and are only checked in order to detect default values, which would point to a processing anomaly.

For each parameter and threshold, the percentage of edited data are monitored on a cycle per cycle, day per day and pass per pass basis by Cal/Val routines. Figure 6 presents the monitoring of the percentage of data points edited on all thresholds combined. Considering all parameters and thresholds, the mean percentage of edited measurements is 2.6%. The editing rate is steady over time. The rise of this parameter around October 2014 is a result of the mispointing events before the SHM. Note that one measurement can be edited by several different thresholds, so the sum of individual criterion percentages does not equal the all thresholds combined percentage.

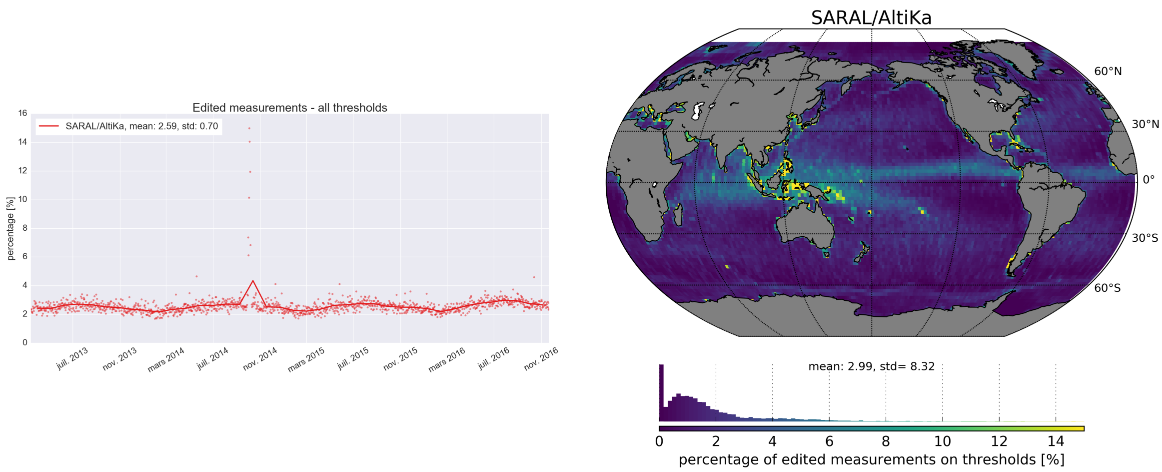

Figure 6: *Percentage of edited measurements on all thresholds combined. [left] monitoring for GDR data and [right] map since the beginning of mission (cycles 1 to 101).*

3.2.4. number of 40-Hz measurements

The percentage of edited measurements because of a too low number of 40-Hz measurements is represented on the left side of figure 7. On SARAL/AltiKa the all 1 Hz measurements resulting from the compression of less than 20 high rate waveforms are discarded from further analysis. No trend nor any anomaly has been detected. The percentage of edited data is similar for SARAL/AltiKa and Jason-2.

The map of measurements edited by 40-Hz measurements number criterion is plotted on the right panel of figure 7 and shows a correlation with heavy rain and wet areas (in general regions with disturbed sea state), as well as regions close to sea ice. Indeed waveforms are distorted by rain cells or sigma bloom events, which makes them often meaningless for SSH calculation. As a consequence, edited measurements due to several altimetric criteria are often correlated with wet areas (rain cells/sigma bloom events).

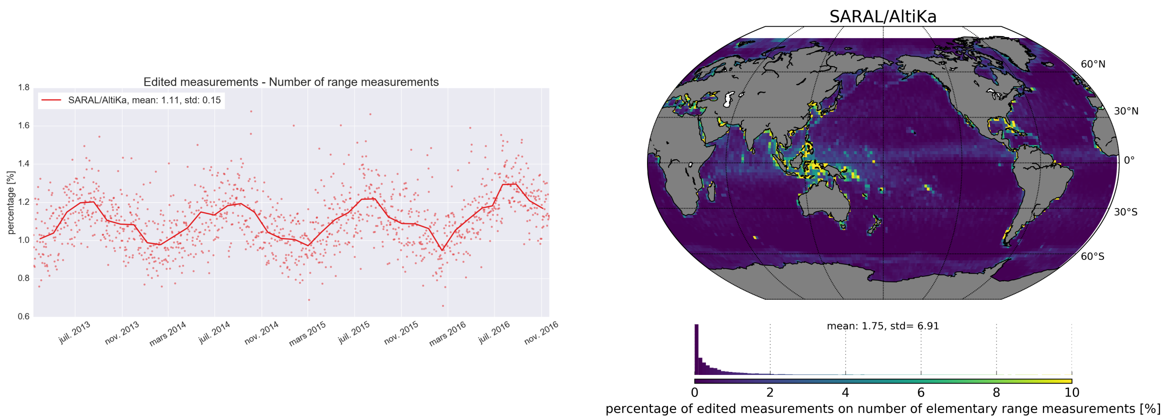

Figure 7: *Percentage of edited measurements on the number of 40-Hz measurements criterion. [left] monitoring for GDR data and [right] map since the beginning of mission (cycles 1 to 101).*

3.2.5. standard deviation of 40-Hz range measurements

The percentage of edited measurements due to a high standard deviation of 40-Hz measurements of the range criterion is shown in figure 8. On average, 1.5% of the measurements are edited on this criterion.

Several days show a slight increase in the percentage of data edited by this criterion. These can mostly be related to mispointing episodes (before the SHM or around maneuver burns). In the latter case, the data a few minutes before and after the maneuver are edited (in general several parameters are out of thresholds) as a consequence of the lower platform pointing accuracy. Since cycle 24, platform pointing during maneuvers is achieved by the thrusters instead of the reaction wheels. The impact of this change on the number of edited GDR data is small.

The right panel of figure 8 shows a map of the percentage of measurements edited by the 40-Hz measurements standard deviation criterion. As in section 3.2.4., edited measurements are correlated with wet areas.

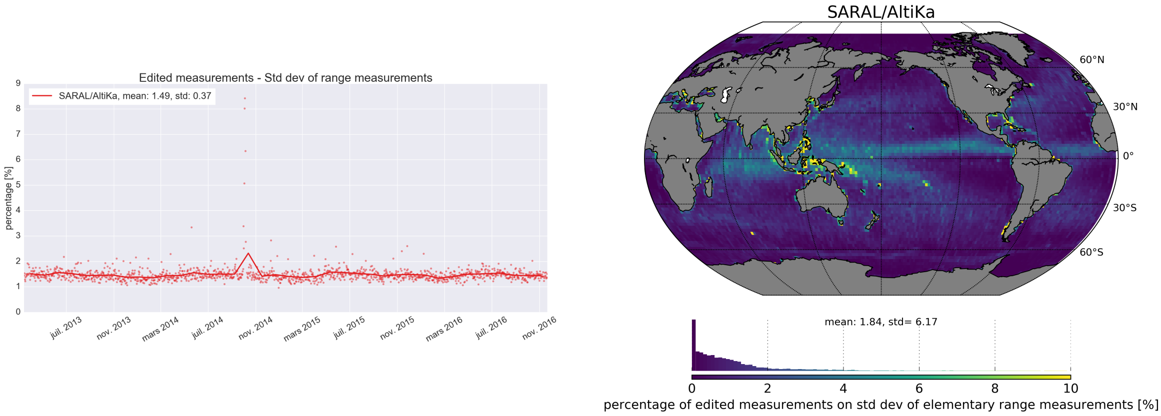

Figure 8: *Percentage of measurements edited due to high standard deviation of 40-Hz range measurements . [left] monitoring for GDR data and [right] map since beginning of mission (cycles 1 to 101).*

3.2.6. Significant wave height

The percentage of edited measurements due to significant wave height out of thresholds is represented on figure 9. On average, 0.42% of the measurements are edited on this criterion.

As for the 40 Hz range standard deviation, several days show an increased number of edited data. Again, this is mostly due to mispointing events and maneuver burns.

Figure 9 (right panel) shows that measurements edited by the SWH criterion are especially found in wet regions where heavy rains and sigma bloom events can occur, as well as in high sea state regions.

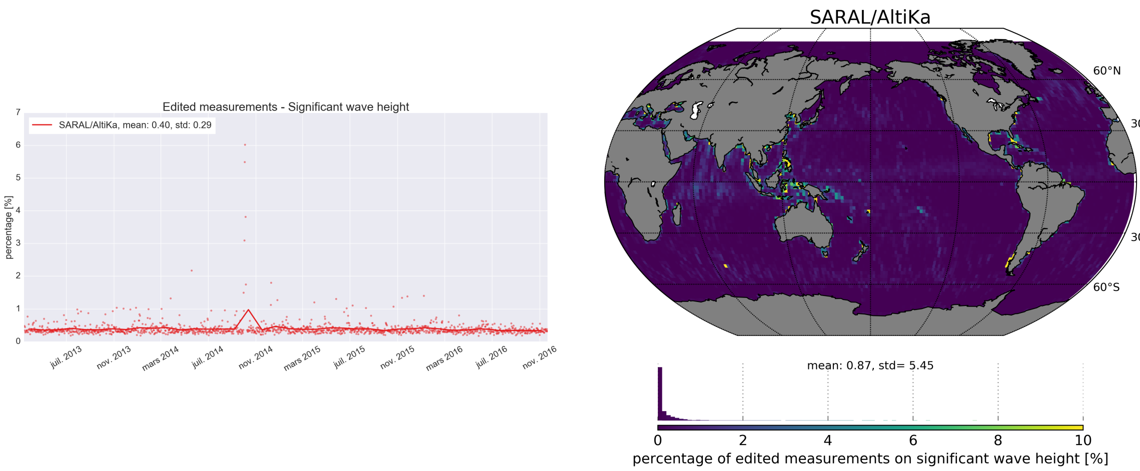

Figure 9: *Percentage of edited measurements by SWH criterion. [left] monitoring for GDR data and [right] map since the beginning of mission (cycles 1 to 101).*

3.2.7. Backscatter coefficient

The percentage of edited measurements due to backscatter coefficient out of thresholds is represented on figure 10. On average, 0.35% of the measurements are edited on this criterion.

High editing rates (see right panel of figure 10) are generally found at the coast, and in rain areas. Again, this quantity is affected by mispointing events, and high editing rates are generally observed close to maneuvers.

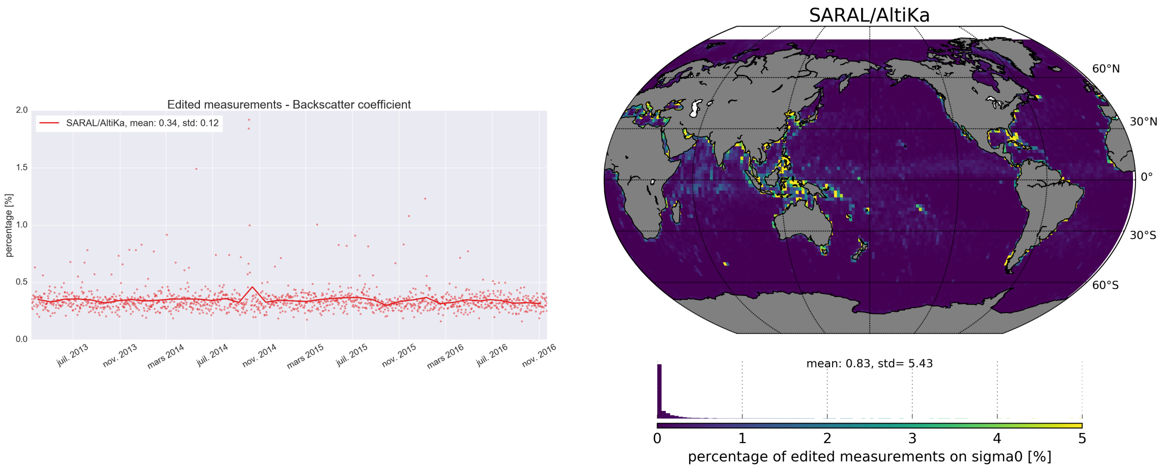

Figure 10: *Percentage of edited measurements by Sigma0 criterion. [left] monitoring for GDR data and [right] map since the beginning of mission (cycles 1 to 101).*

3.2.8. Number of backscatter coefficient measurements

The percentage of edited measurements due to too few high rate backscatter coefficient measurements for each 1 Hz measuremet is represented on figure 11. On average, 1.04% of the measurements are edited on this criterion.

High editing rates (see right panel of figure 11)are generally found at the coast, and in rain areas. This quantity is also affected by mispointing events which lead to high editing rates (close to maneuvers for example). The number of elementary measurements of backscatter is closely related to the number of elementary range measurements, and metrics are very similar.

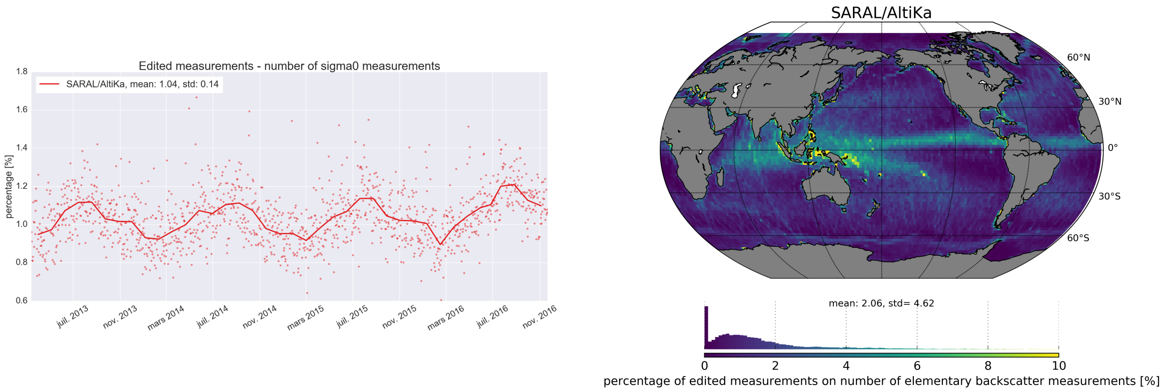

Figure 11: *Percentage of edited measurements by number of high rate backscatter coefficient measurements. [left] monitoring for GDR data and [right] map since the beginning of mission (cycles 1 to 101).*

3.2.9. Standard deviation of backscatter coefficient

The percentage of edited measurements on the 40 Hz backscatter coefficient standard deviation criterion is represented on figure 12. On average, 0.93% of the measurements are edited on this criterion.

The right panel of figure 12 shows that measurements edited on 40 Hz backscatter coefficient standard deviation criterion are found in coastal areas, and in regions affected by rain events, as a result of Ka backscatter attenuation related to atmospheric water content. The spatial distributions of edited measurements due to high standard deviation of backscatter and of range measurements are very similar.

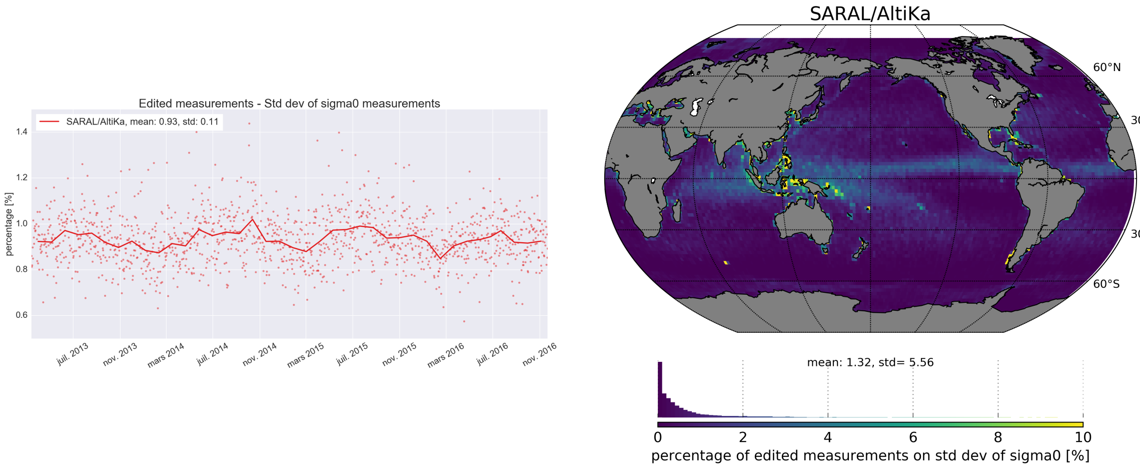

Figure 12: *Percentage of edited measurements by 40 Hz Sigma0 standard deviation criterion. [left] monitoring for GDR data and [right] map since the beginning of mission (cycles 1 to 101).*

3.2.10. Radiometer wet troposphere correction

The percentage of edited measurements due to radiometer wet troposphere correction criterion is represented in figure 13. On average, only 0.07% of the measurements are edited on this criterion. The edited data for Saral/AltiKa are generally due to wet troposphere path delay values larger than the -0.5 m threshold. Large editing percentages are mainly observed in coastal regions suggesting that some land effects on radiometer measurements impacts the quality of the wet troposphere path delay retrievals. Other editing events happen in known wet areas in the inter tropical band where the retrieval algorithm may be less efficient in some cases of high rain rates or unusal sea states (sigma blooms).

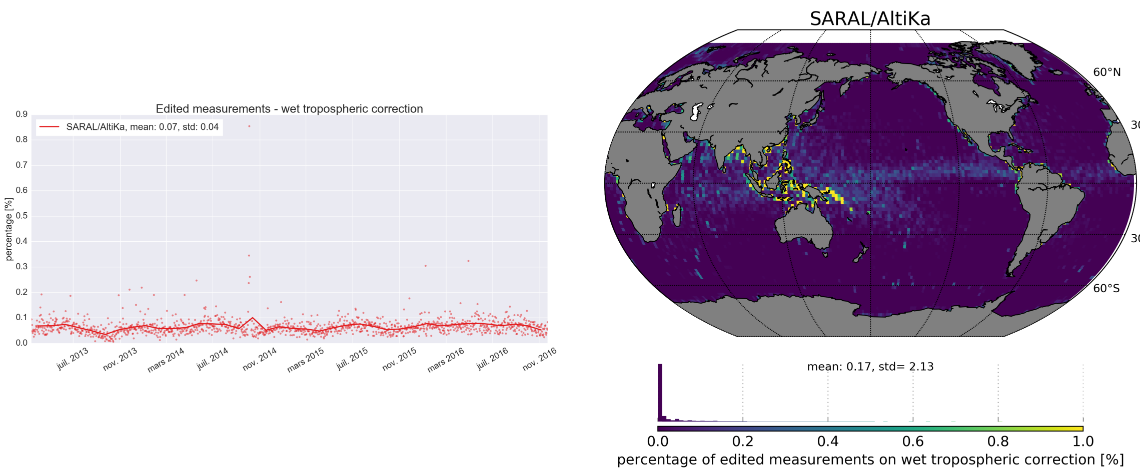

Figure 13: *Percentage of edited measurements due to radiometer wet tropospheric correction out of thresholds. [left] monitoring for GDR data and [right] map since the beginning of mission (cycles 1 to 101).*

3.2.11. Square off-nadir angle

The percentage of edited measurements due to square off-nadir angle criterion is represented in figure 14. On average, 0.37% of all measurements are edited due to high mispointing values. Maneuvers have a strong impact on mispointing values because the platform has to rotate from nadir to geodetic pointing before thrusters activity. As a result, nearly all maneuvers are edited due to high mispointing values. This is visible both on the monitoring (daily points slightly higher around 0.5 to 2 % values) and on the map as all maneuvers where performed in the Indian Ocean, within view on Indian ground stations. After the SHM, systematic mispointing were observed at zero-crossings of reaction wheel (RW) speed, resulting in a slightly higher percentage of edited points. This was corrected and the percentage of measurements edited due to high mispointing values came back to normal values. SARAL/AltiKa is still impacted by random fluctuations in RW friction which explains that several days show a higher percentage of edited measurements.

The spatial distribution of the percentage of edited values (right panel of figure 14) appears very noisy at first. There are several features visible in this map, such as:

- editing due to maneuvers in the Indian Ocean,
- a patch in the North Atlantic Ocean, resulting from zero crossings of RW speed over the regions between Greenland and Svalbard,
- several track-like patterns due to RW friction fluctuations,
- a pattern similar to the one observed for several other parameters: coastal areas and wet areas, as off-nadir angle estimation is based on waveforms trailing edge slope which is impacted by rain cells and surface roughness.

Since the SHM, mispointing is a carefully monitored parameter on SARAL/AltiKa. More information on mispointing events can be found in section 4.3. of this report .

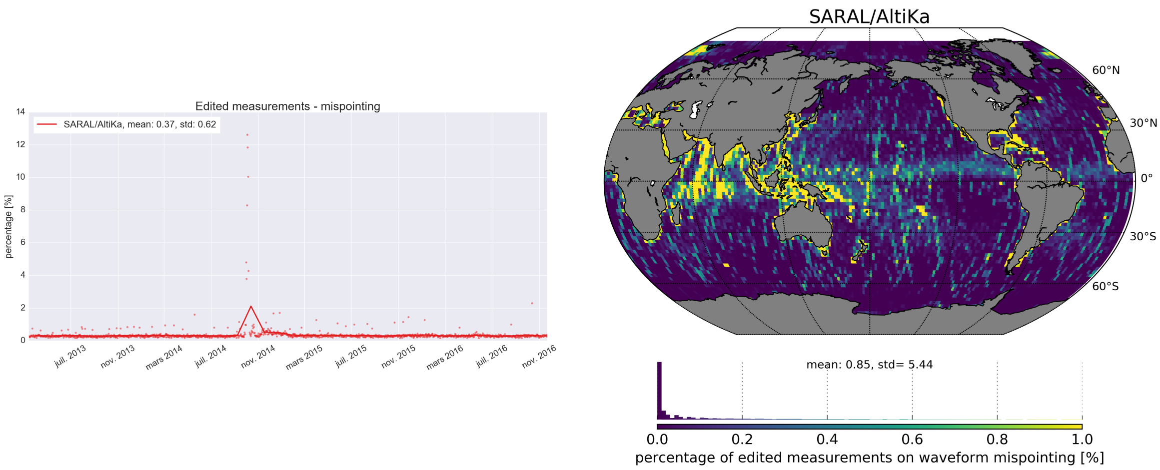

Figure 14: *Percentage of edited measurements by square off-nadir angle criterion. [left] monitoring for GDR data and [right] map since the beginning of the mission (cycles 1 to 101).*

3.2.12. Sea state bias correction

The percentage of edited measurements due to sea state bias correction criterion is represented in figure 15. On average, 0.29% of measurements are edited due to sea state bias values out of thresholds. The percentage of edited measurements is stable over time, although with several days with higher values, mainly due to maneuvers. The spatial distribution is consistent with what is observed regarding editing on SWH values: areas with low sea states may be edited due to erroneous sea state bias estimation. This does not happen for high sea states (high northern and southern latitudes) where no measurements are edited on the sea state bias threshold criterion.

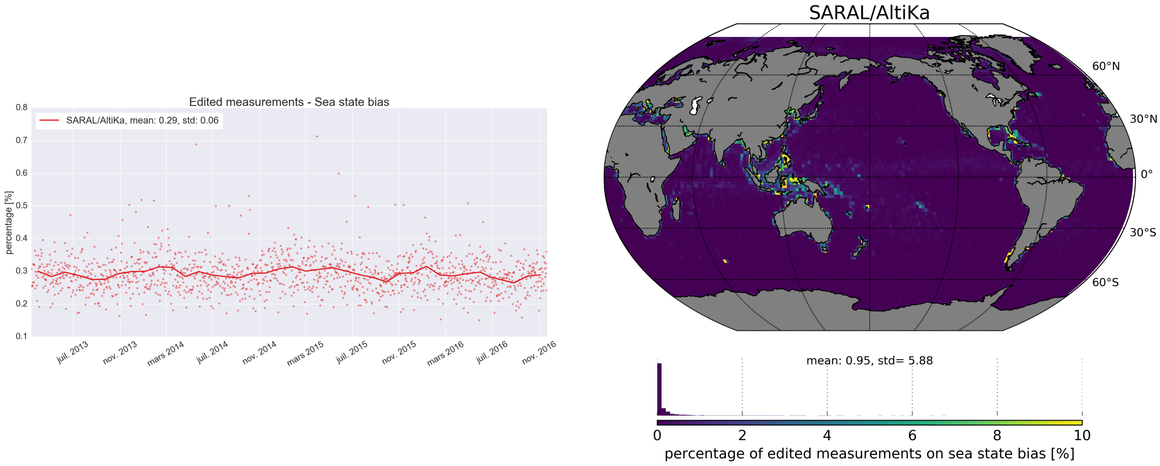

Figure 15: *Percentage of edited measurements by sea state bias criterion. [left] monitoring for GDR data and [right] map since the beginning of the mission (cycles 1 to 101).*

3.2.13. Altimeter wind speed

The percentage of edited measurements due to altimeter wind speed criterion is represented in figure 16. On average 0.29% of measurements are edited. The percentage of edited data on wind speed values is similar to the percentage of data edited on sea state bias values. It indeed concerns mainly the same measurements.

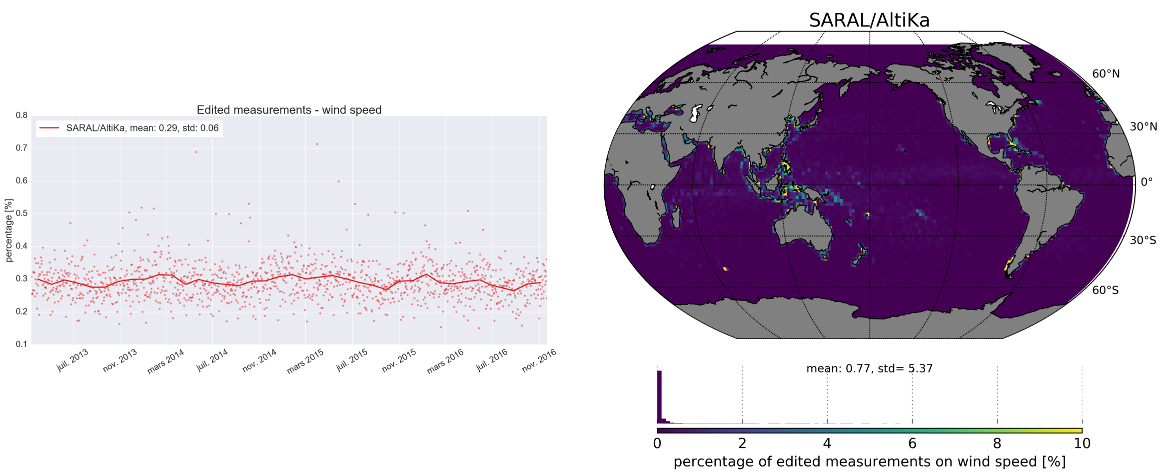

Figure 16: *Percentage of edited measurements by wind speed criterion. [left] monitoring for GDR data and [right] map since the beginning of the mission (cycles 1 to 101).*

3.2.14. Ocean, pole and earth tide corrections

No measurements are edited due to the pole tide or the solid earth tide components whereas some measurements with extreme ocean tide values (GOT 4.8) are edited. The percentage of edited measurements due to the threshold on the latter is represented in figure 17. On average 0.18% of the measurements are edited due to the ocean tide correction. The majority of these measurements correspond to the Caspian Sea. In GDR-T Patch2 version, the geocentric ocean tide has no data over land, including enclosed water bodies such as Caspian Sea, with some impacts on near shore data. This is due to the equilibrium long-period tide height (included in the global ocean tide) which, for Patch2, is computed with FES2012 algorithm, which tests previously if the grid of the FES2012 tide atlas is defined or not. Consequently, the equilibrium tide is set to default values over land (and therefore also the geocentric ocean tide).
This explains the presence of edited data (map 17) near coasts and in Caspian Sea.

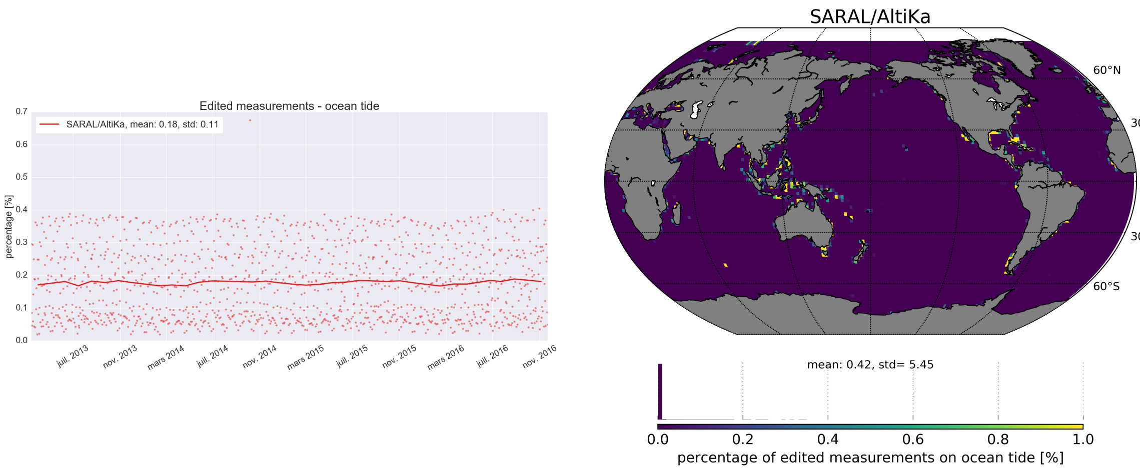

Figure 17: *Percentage of edited measurements by ocean tide criterion. [left] monitoring for GDR data and [right] map since the beginning of the mission (cycles 1 to 101).*

3.2.15. Sea surface height

The percentage of edited measurements due to sea surface height (orbit minus range, no corrections applied) criterion is represented in figure 18. On average, 0.47% of measurements are edited on this criterion. The measurements edited by sea surface height criterion are mostly found near coasts in equatorial and mid-latitude regions, as well as for regions with low significant wave heights (see map 18).

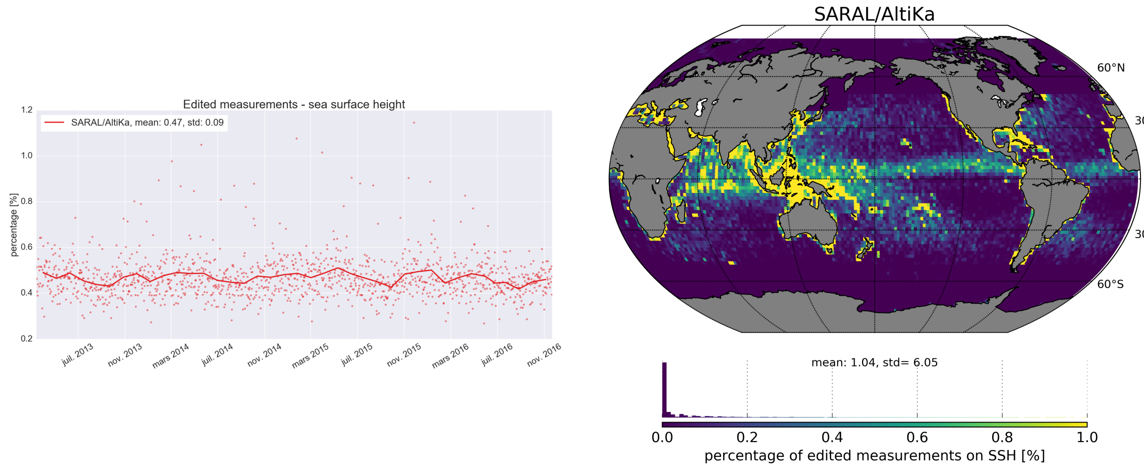

Figure 18: *Percentage of edited measurements by sea surface height criterion. [left] monitoring for GDR data and [right] map since the beginning of the mission (cycles 1 to 101).*

3.2.16. Sea level anomaly

The percentage of edited measurements due to sea level anomaly (all corrections applied) out of thresholds is represented in figure 19. On average, 0.82% of data are edited by this criterion. There is a slight increase of this percentage at the end of the period (since March 2016 approximately) when the ground track was loosely maintained resulting in higher MSS errors.

The map (estimated after applying all other editing steps), shows very few measurements edited, mainly located at the coast. This shows that the editing process is efficent in removing erroneous SLA measurements.

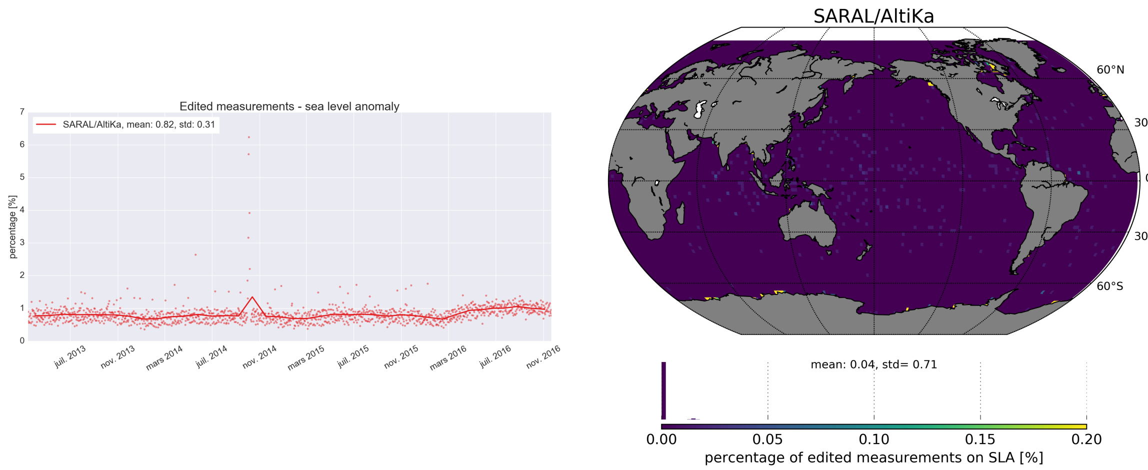

Figure 19: *Percentage of edited measurements by sea level anomaly criterion. [left] monitoring for GDR data and [right] map since the beginning of the mission (cycles 1 to 101).*

3.2.17. SLA consistency checks

The last step of the editing procedure is to check for along-track SLA consistency. Two different checks are performed:

- fitting a spline function to SLA values (after all previously mentionned editing criteria have been applied),
- checking that pass mean and standard deviation do not exceed certain thresholds.

Figure 20 shows the monitoring of the percentage of edited points by these two criteria. Very few points are edited by these two editing steps, 0.04% for splines, and 0.01% for pass statistics. In the latter case, the whole pass is edited, leaving a large gap in the data. This happened 7 times, generally when crossing very large eddies in the Southern Ocean.

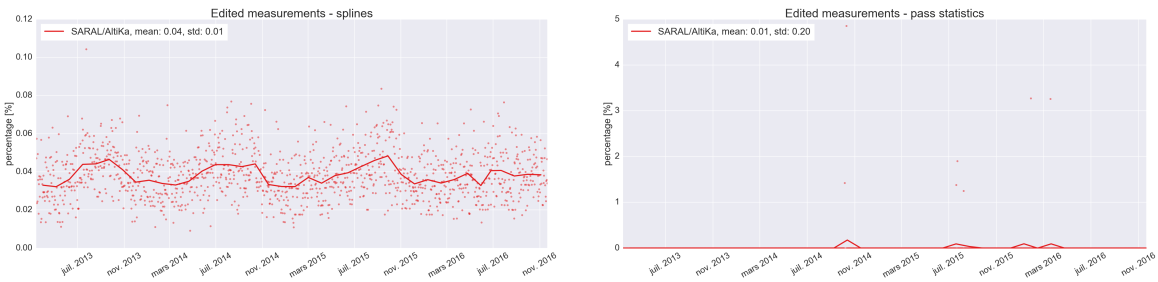

Figure 20: *Monitoring of the percentage of edited measurements by [left] spline criterion and [right] pass statistics.*

4. Monitoring of altimeter and radiometer parameters

4.1. Methodology

Statistics for the main parameters of SARAL/AltiKa have been routinely monitored since the beginning of the mission. Systematic monitoring aims at detecting changes in parameter statistics, that would indicate a problem on the mission. Comparisons with model outputs or other missions (mainly Jason-2) are also performed as part of the systematic Cal/Val activities.

For SARAL/AltiKa, pass by pass, daily and cycle by cycle statistics are computed. In this section, we mainly present results from daily and cycle average estimates.

The measurements distribution is not homogeneous within latitudes, and can skew the statistics to values of the data in high latitudes. This can be important when comparing to another mission, like Jason-2. To overcome this issue when needed, we estimate box averages (generally on a 2 degree cartesian grid) before estimating global averages. For certain parameters, more precise comparisons are performed by estimating short time difference crossovers.

Note that for daily monitoring, due to safe-hold modes on both missions, there are some gaps end of March / early April and in September 2013 for Jason-2 and in October 2014 for SARAL/AltiKa.

Unless otherwise specified, plots in this section are based on GDR data over the full lifetime of SARAL/AltiKa, and averages are estimated over the whole oceanic domain.

4.2. 40 Hz Measurements

Number and standard deviation of 40 Hz elementary range measurements used to derive 1 Hz data are two parameters computed during the altimeter ground processing. For both SARAL/AltiKa and Jason-2 a MQE (mean quadratic error) criterion is used to select valid 40/20 Hz measurements before performing a regression to derive the 1 Hz range from high rate (40 Hz or 20 Hz) data.

The MQE criterion checks that the high rate waveforms can be approximated by a Brown echo model (Brown, 1977 [8], Thibaut et al. 2002 [20]). Then elementary ranges too far from the regression line are discarded, through an iterative regression process, until convergence is reached. Thus, monitoring the number of 40/20 Hz range measurements and the standard deviation computed among them is likely to reveal changes at instrumental level.

4.2.1. 40 Hz measurements number

The mean number of elementary 40 Hz range measurements for SARAL/AltiKa is close to 38.5 (see figure 21, where Jason-2 values were doubled). Before the correction of the PF/RF alignment (alignment between the platform and the radiofrequency axis) on 25th of April 2013 this value was slightly higher (around 38.6). Jason-2 has an average number of elementary 20 Hz range measurements of 19.6, which represents a higher number than SARAL/AltiKa. Jason-2 also shows a smaller day to day variability than SARAL/AltiKa.

Note that before Patch1 version, the MQE threshold was not applied during the 40 Hz to 1 Hz compression (IGDR data till cycle 4, pass 394). As a result, the daily mean of the number of the elementary 40 Hz range measurements was higher at 39.0.

On average 1.5 % of the 40 Hz elementary range measurements are removed during the 40 Hz to 1 Hz compression by the MQE criteria. These removed data might be due to perturbations in the footprint (rain events, sigma blooms). For both missions, the number of elementary range measurements is correlated with the significant wave height (and, for SARAL/AltiKa, with sea ice extent). Figure 22 shows less elementary range measurements around Indonesia, the Mediterranean Sea and close to coasts, which are all regions of low significant wave heights (see also map of SWH 33) and therefore regions where sigma bloom may occur and also rain areas. High latitudes also show a lower number of range elementary measurements, due to the presence of sea-ice.

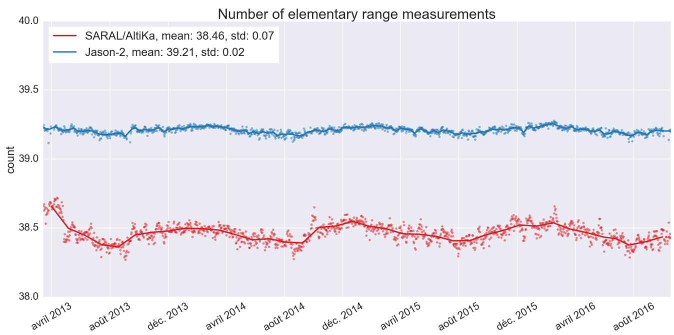

Figure 21: *Daily monitoring of mean of number of elementary measurements for SARAL/AltiKa (ref) and Jason-2 (blue). Dots represent daily averages, the lines corresponds to cycle averages. Jason-2 data are multiplied by two to account for the 40Hz/20Hz difference between the two missions.*

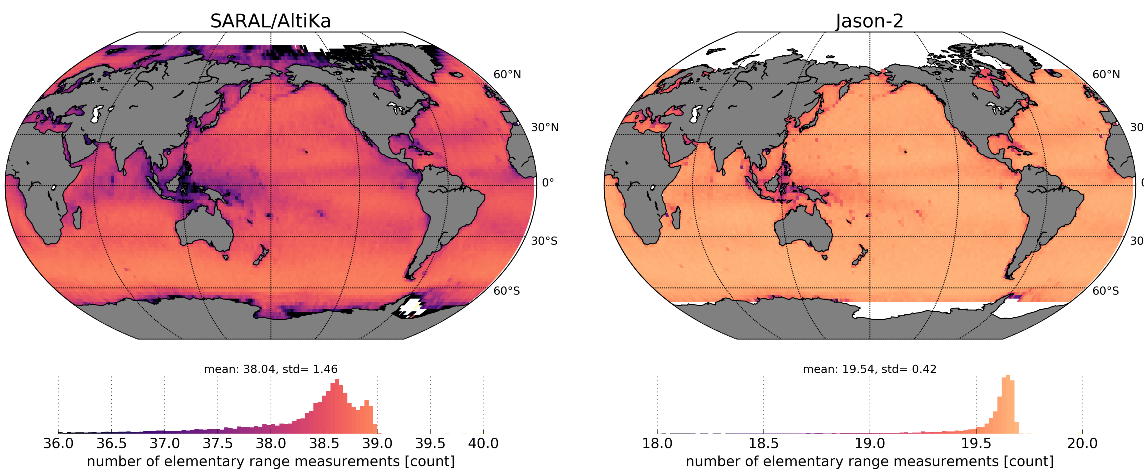

Figure 22: *Average map of number of SARAL/AltiKa elementary 40 Hz range measurements (left) and Jason-2 elementary 20 Hz range measurement (right).*

4.2.2. 40 Hz measurements standard deviation

Considering along-track data, SARAL/AltiKa's standard deviation of 40 Hz measurements is 5.7 *cm*, compared to 8.0 *cm* for Jason-2 (right side of figure 23). When considering latitude weighted box statistics (left side of figure 23), these values decrease to respectively 5.6 and 7.7 *cm*. These values are consistent with power spectrum derived noise level estimates.

A lower value for SARAL/AltiKa compared to Jason-2 is expected due to different band-widths on the two missions: 480 MHz for SARAL/AltiKa instead of 320 MHz for Jason-2 (see [18]). As for the number of elementary range measurements, the standard deviation of the elementary range measurements is correlated to significant wave height (see maps on figures 24 and 33).

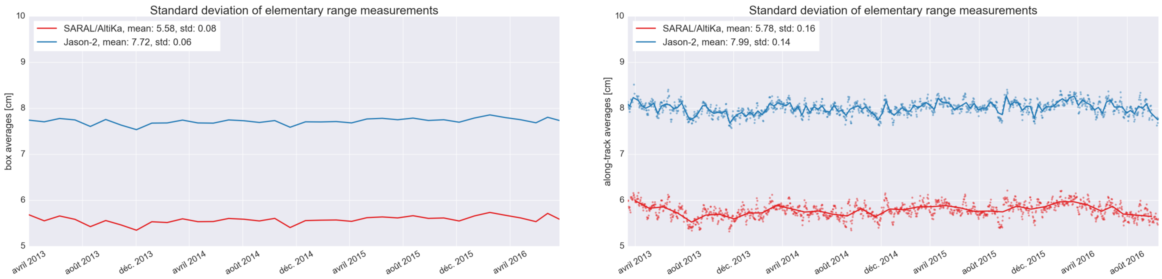

Figure 23: *Monitoring of rms of elementary 40/20 Hz range measurements for SARAL/AltiKa and Jason-2, either computing latitude weighted box statistics (left) or along track averages (right).*

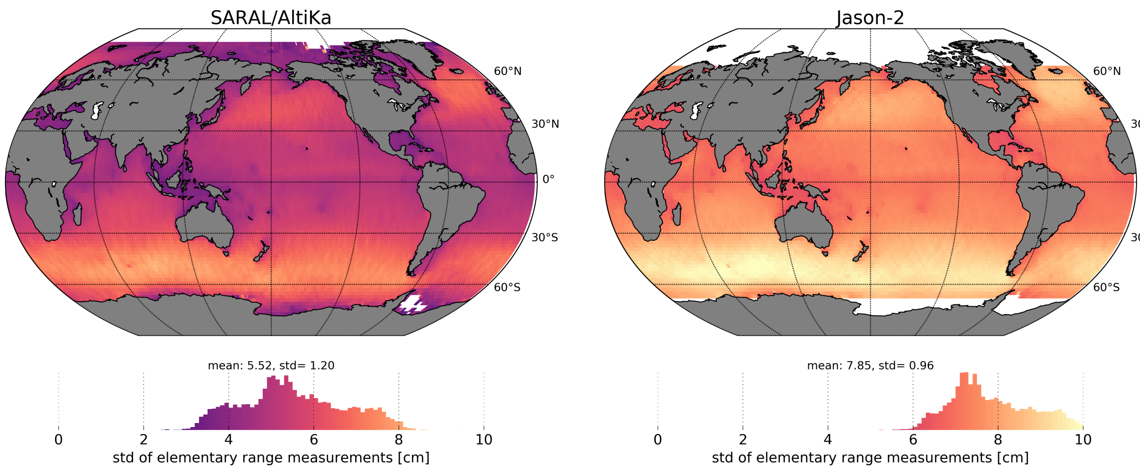

Figure 24: *Average map of rms of SARAL/AltiKa elementary 40 Hz range measurements (left) and Jason-2 elementary 20 Hz range measurement (right) over cycles 1 to 101.*

4.3. Off-Nadir Angle from waveforms

The off-nadir angle is derived from the slope of the trailing edge of the waveform during the altimeter processing. It can either be caused by real platform mispointing or by backscattering properties of the surface. Figure 25 displays the evolution of the mean and standard deviation of this quantity over time for SARAL/AltiKa and Jason-2. Jason-2 shows more variations of the off-nadir angle from waveforms due to its larger antenna aperture, note that these metrics are estimated on valid measurements only. Jason-2 has an antenna beamwidth of 1.29°, whereas SARAL/AltiKa has only 0.6°. In addition Jason-2's orbit is higher, resulting in a larger footprint radius (9.6 km) than SARAL/AltiKa (5.7 km). Therefore the probability of perturbations within the footprint - which modify the backscattering properties of the surface - is higher for Jason-2 than for SARAL/AltiKa.

In the beginning of the SARAL/AltiKa mission the off-nadir angle from waveforms was slightly positive (around $0.003 deg^2$). Following an X-cross calibration maneuver ($+0.3^\circ/-0.3^\circ$ in pitch followed by $+0.3^\circ/-0.3^\circ$ in roll) done on April, 22$^{\text{nd}}$ 2013 (see N. Stenou [18]) a correction of -0.045° in pitch direction was applied from April 25$^{\text{th}}$ onwards. A second X-cross calibration on April 30$^{\text{th}}$, 2013 showed that the correction was successful. Off-nadir angle from waveforms stayed from this day on close to zero and very stable spatially and temporally.

During summer 2014 a rise in reaction wheel friction due to movement of lubricant resulted in an increase of the variability of the off-nadir angle. This event ended with the loss of a wheel and an important increase of the daily mean of the off-nadir angle leading to a safe-hold mode between October 6$^{\text{th}}$ and 9$^{\text{th}}$, 2014. After the safe-hold mode, the spacecraft has been reconfigured to use only three wheels, resulting in a lower pointing accuracy at zero crossings of RW speed. A patch to the command law allowed to avoid these situations. Further mispointing events are now generally associated with random fluctuations of RW torque. A description of mispointing events can also be found in yearly report 2015 ([4]), the main mispointing events are also mentioned in cyclic Cal/Val reports.

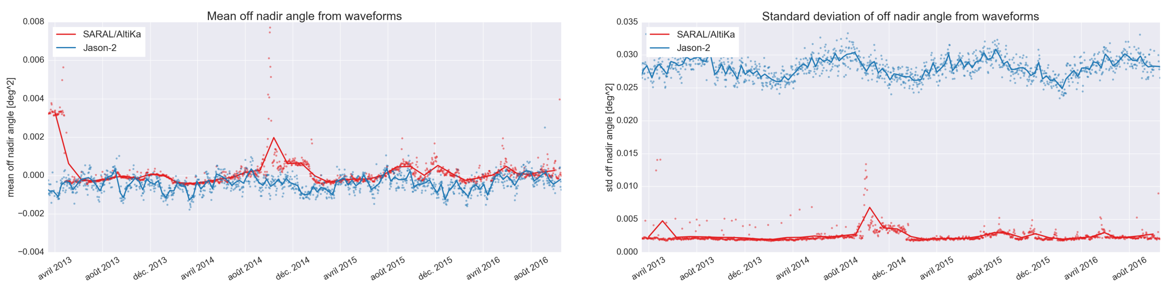

Figure 25: *Monitoring of mean (left) and standard deviation (right) of and Jason-2 off-nadir angle from waveforms. Dots represent daily averages, the lines correponds to cycle averages.*

The map of SARAL/AltiKa off-nadir angle from waveforms (left of figure 26) is not homogeneous. The Indian ocean is impacted by platform mispointing due to maneuvers, and several mispointed tracks are visible due to RW issues. High mispointing values are observed at high latitudes close to sea ice, likley as a result of both platform mispointing and surface heterogeneities. Mispointing is slightly positive around Indonesia and equator and close to coasts. On the other hand, the region around 50°S has slightly negative values. The map of Jason-2 (right of figure 26) is generally slightly negative, except for regions around Indonesia, and close to coasts (especially in the northern hemisphere). Because of platform mispointing events, SARAL/AltiKa map of mispointing is now less correlated to the map of backscattering coefficient (figure 30).

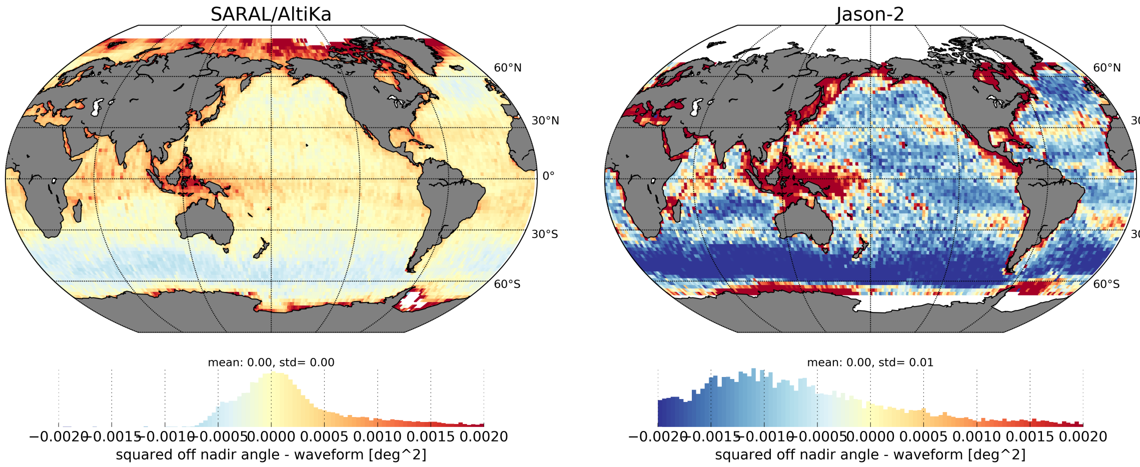

Figure 26: *Average map of off-nadir angle from waveforms for SARAL/AltiKa (left) and Jason-2 (right) over cycles 3 to 101(after the correction of the PF/RF alignment).*

ISRO is now sending platform pointing information derived from onbaord star trackers. These data are routinely ingested in the SARAL/AltiKa Cal/Val database to perform comparisons between platform and waveform mispointing. Figure 27 compares waveform and plaftorm mispointing estimates. Over time, there is a good agreement between waveform and platform estimation. However the map of plaform mispointing is mush more homogeneous than the one derived from waveforms (26), as it is not impacted by pseudo mispointing due to heterogeneous surface properties in the radar footprint.

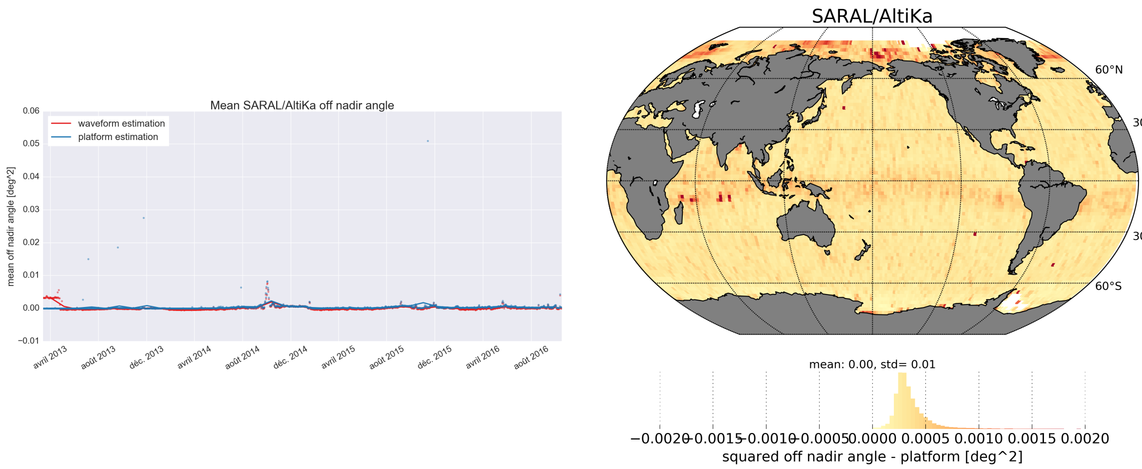

Figure 27: *Monitoring of off-nadir angle from waveform and platform for SARAL/AltiKa (left) and map of platform off-nadir angle (right) over cycles 1 to 101.*

In order to get a better picture of SARAL/AltiKa mispointing events, we detect mispointed track sections. Track sections are defined as 15 consecutive measurements with mispointing values greater than 0.015 deg^2. Results of this detection algorithm are presented in figure 28. There is an excellent agreement between the number of mispointed sections detected from waveforms and platfom data, indicating that, when consecutive measurements are affected by mispoiting, this is likely a real platform pointing issue. Before October 2014, small peaks are associated with maneuvers. From October 2015 to February 2015, mispointed sections are associated with zero crossings of the RW speed. The command low was changed to avoid zero crossings and mispointing events occur randomly since then. No long term evolution of the number of these events is observed.

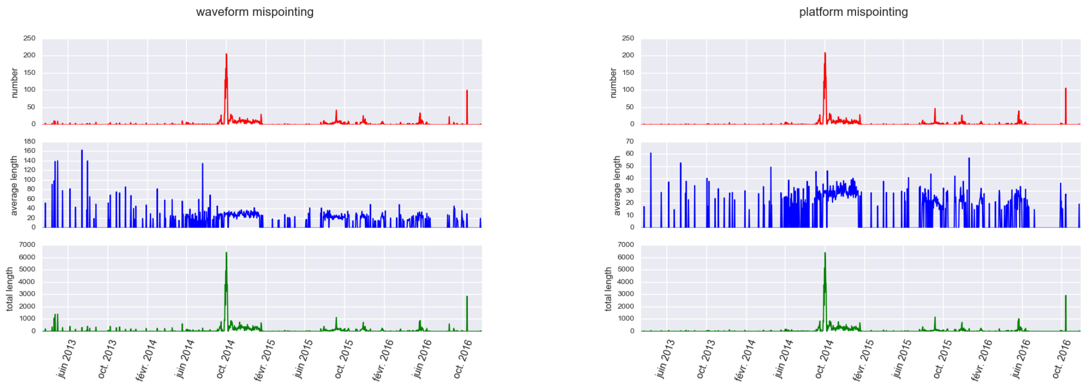

Figure 28: *Monitoring of mispointed track sections from waveform (left) and platform (right) data.*

4.4. Backscatter coefficient

SARAL/AltiKa is the first altimeter mission using the Ka-band frequency and was expected to show a different behavior than altimeters using Ku-band frequency. Several preparatory studies were done before launch, predicting that the Ka-band backscattering coefficient would be about 3.5 dB smaller than the Ku-band backscattering coefficient (see [18]). Note that the backscattering coefficient used here is corrected for atmospheric attenuation.

In flight assessment shows that the difference with respect to Ku-band backscattering coefficient is smaller than expected: 2.5 dB in average (see bottom of figure 29). The daily evolution of SARAL/AltiKa backscattering coefficient shows the same signals as the one of Jason-2 (top left of figure 29), the dispersion diagram of backscattering coefficients at 3h crossover points (31) shows also a good correlation ($r = 0.94$), and maps show consistent patterns (30)

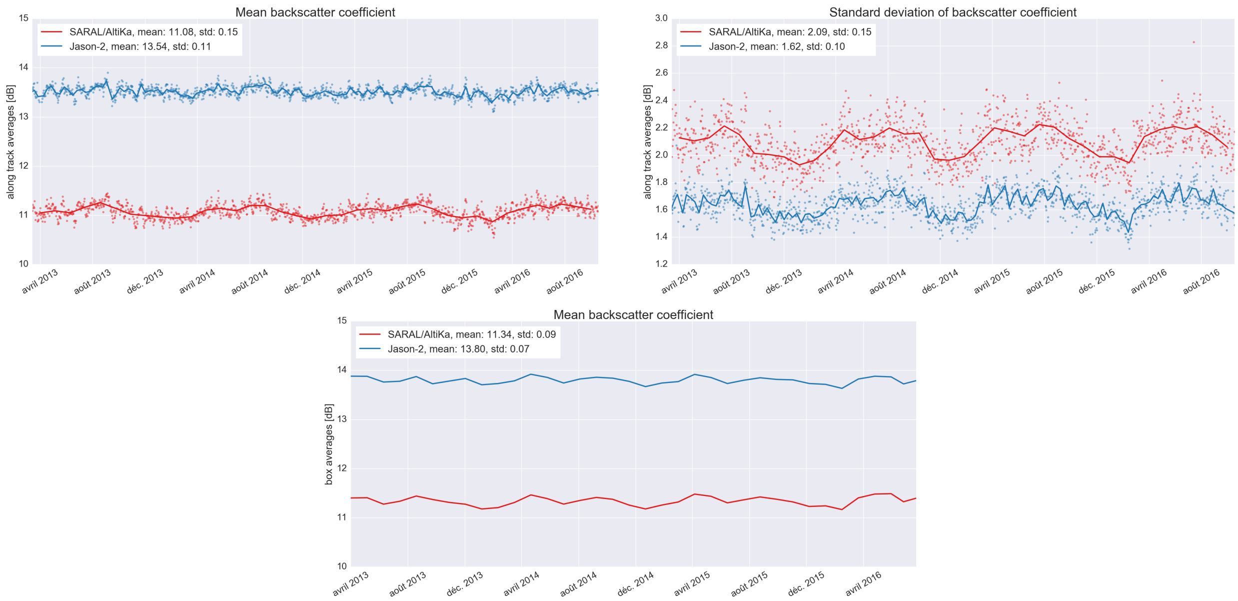

Figure 29: *Daily monitoring of mean and standard deviation of SARAL/AltiKa and Jason-2 backscattering coefficient (top) and cycle per cycle monitoring of latitude weighted box mean for both missions on the bottom.*

However the backscattering standard deviation is higher for SARAL/AltiKa than for Jason-2 (top right of figure 29). While maps (centered around the mean value for better comparison between SARAL/AltiKa and Jason-2) of backscattering coefficient show the same structures for both missions (see top of figure 30), the amplitudes of the observed structures are slightly larger for SARAL/AltiKa than for Jason-2. Also the difference between Ka- and Ku-band backscattering coefficient is not a simple bias, as shown on the difference map (bottom of figure 30), which shows a latitude dependency and/or signals related to waves and rain events. Note that the hotter surface temperature of low latitude also imply a stronger difference between the two bands.

Figure 31 displays the dispersion diagram between SARAL/AltiKa and Jason-2 backscatter, estimated at 3 hours crossovers, as well as the histogram of backscatter. While a good correlation between the two missions is observed, the relation is not strictly linear. The population distribution is different for the Ka- and Ku-band frequencies: the SARAL/AltiKa histogram is tilted with a larger number of measurements at low backscatter values.

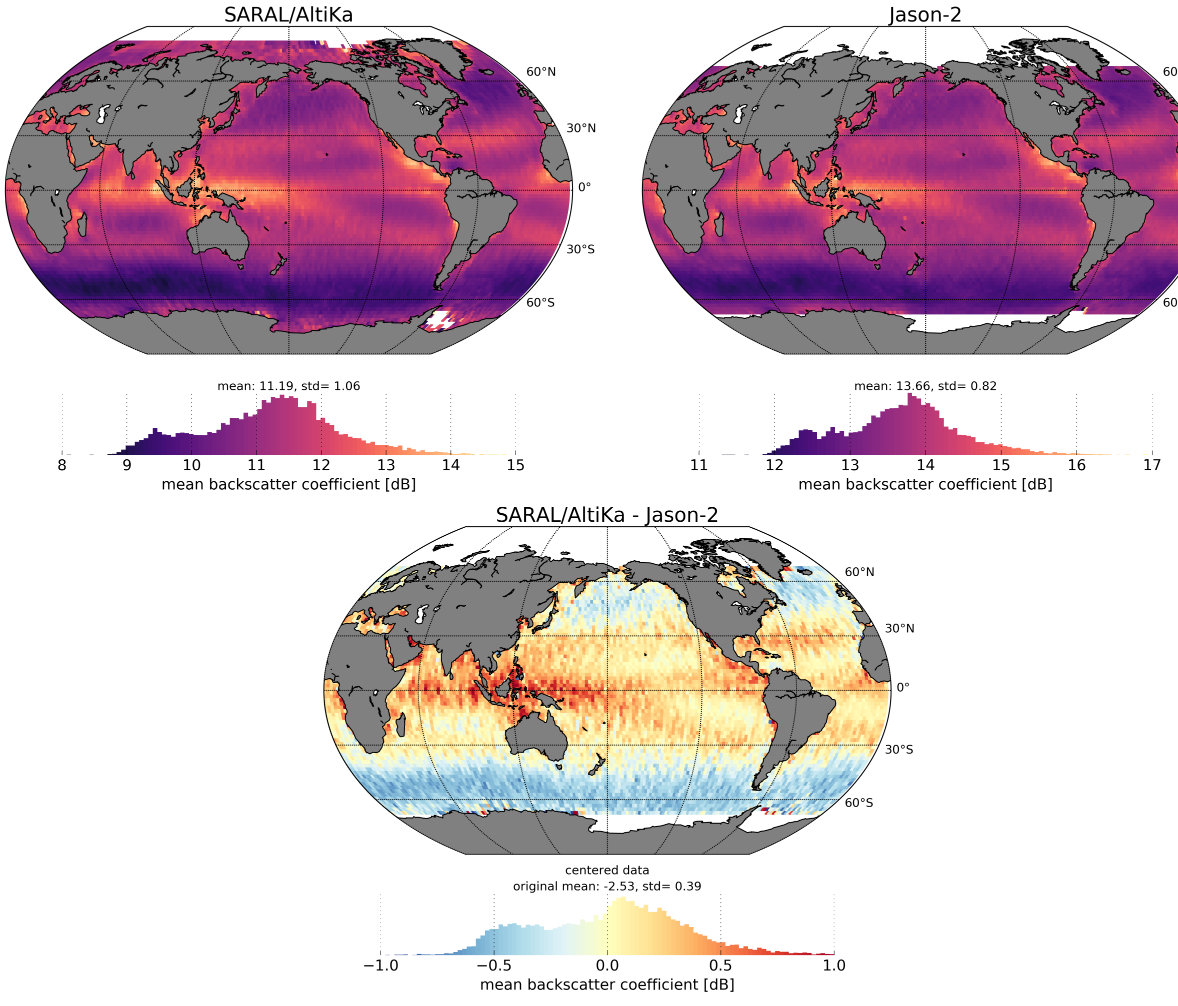

Figure 30: *Average map of backscattering coefficient for SARAL/AltiKa (left) and Jason-2 (right) cycles 1 to 101. Difference map of gridded SARAL/AltiKa and Jason-2 backscattering coefficient for cycles 1 to 101.*

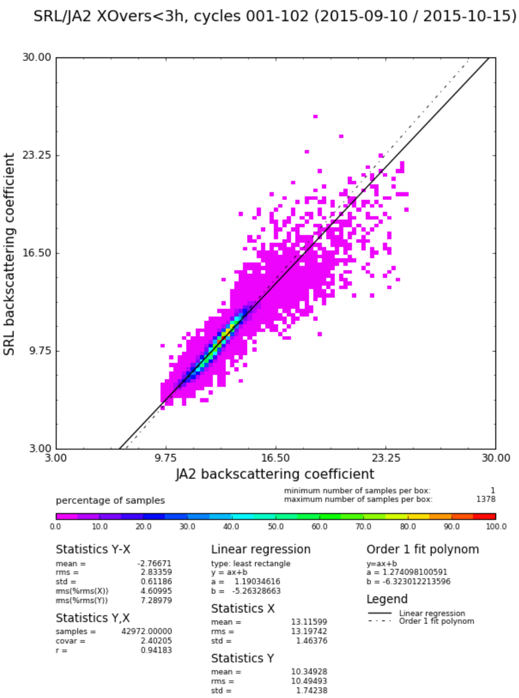

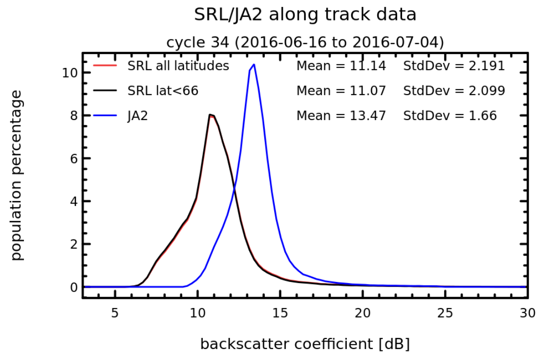

Figure 31: *Dispersion diagram of backscattering coefficient between SARAL/AltiKa and Jason-2 at 3h crossover points (computed for cycles 1 to 101) (left) and histogram of along-track data computed over SARAL/AltiKa cycle 34 (right).*

4.5. Significant wave height

The significant wave height (SWH) is one of the parameters derived from the waveforms. Monitoring of mean and standard deviation of SWH show a very good agreement between SARAL/AltiKa and Jason-2 (see top of figure 32). When accounting for the different data distribution with latitude, the difference between the two mission is only 1 cm. When taking into account all latitudes, SWH is slightly reduced for SARAL/AltiKa as small SWH occur in very high northern latitudes when the sea ice recedes (see also left map of figure 33). The maps of SWH show the same structures: low SWH around Indonesia, in the Mediterranean Sea and the Gulf of Mexico and high SWH around 50°S (as well as in North Atlantic). The difference map between the two satellites (bottom of figure 33) is centered around a difference of 3 cm, with slightly higher values for SARAL/AltiKa. Although this might appear to contradict top left of figure 32, it is only the result of different ways to estimate the mean. Stronger differences occur in high latitudes (in regions, where SWH is higher than 2-3 m). When considering the dispersion diagram between SARAL/AltiKa and Jason-2 SWH at 3h crossovers (left of figure 34), a strong correlation coefficient ($r > 0.98$) is obtained, with an almost perfectly linear relationship between the two missions.

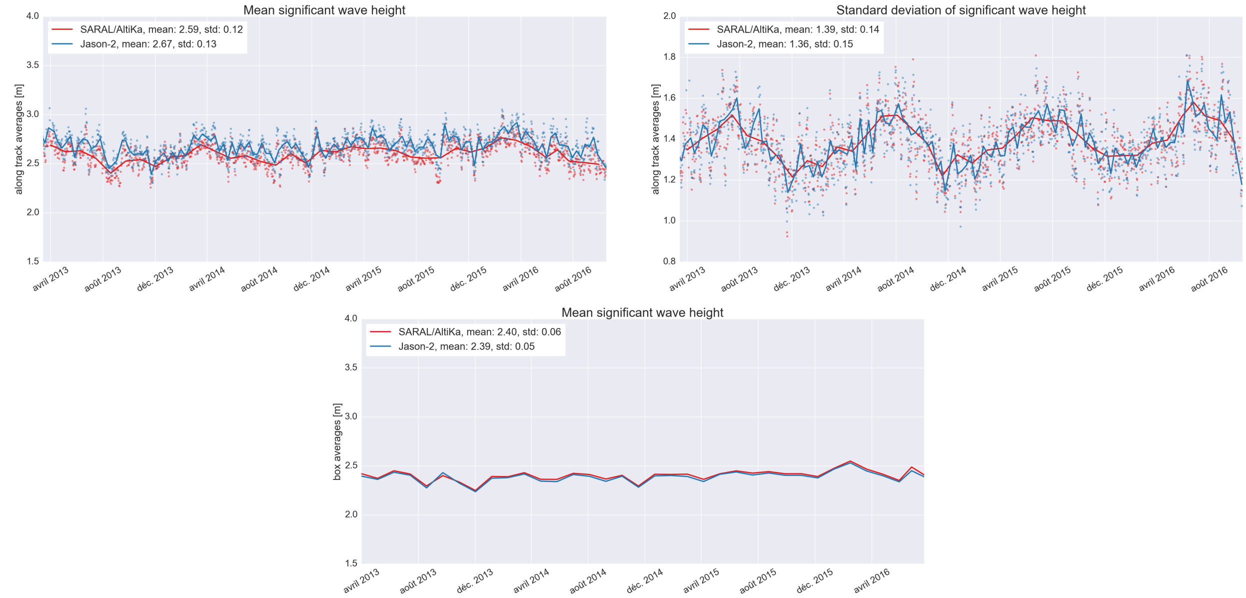

Figure 32: *Daily monitoring of mean and standard deviation significant wave height for SARAL/AltiKa and Jason-2 (top) and cycle per cycle monitoring of latitude weighted box mean for both missions on the bottom.*

When considering 3h crossover points between SARAL/AltiKa and Jason-2 (figure 34, left) mean SWH values are 3.09 m for SARAL/AltiKa and 3.16 m for Jason-2. This is much higher than the mean values of daily along-track SWH (around 2.60 m), and results from the geographical distribution of 3h crossover points: most crossover points are located in high SWH areas (latitudes around 50°), which biases the mean towards high SWH. Nevertheless, this diagnosis shows that for the same positions (SRL/JA2 3h crossovers) with a time difference less than 3h, SARAL/AltiKa SWH is slightly higher than the Jason-2 one. This is also the case when computing latitude weighted box statistics (in order to compensate for uneven data distribution), as shown on bottom of figure 32, where Jason-2 SWH is generally slightly lower than SARAL/AltiKa SWH. When considering along-track statistics (top of figure 32), Jason-2 SWH appears higher than SARAL/AltiKa SWH, this is again an effect of geographical data distribution.

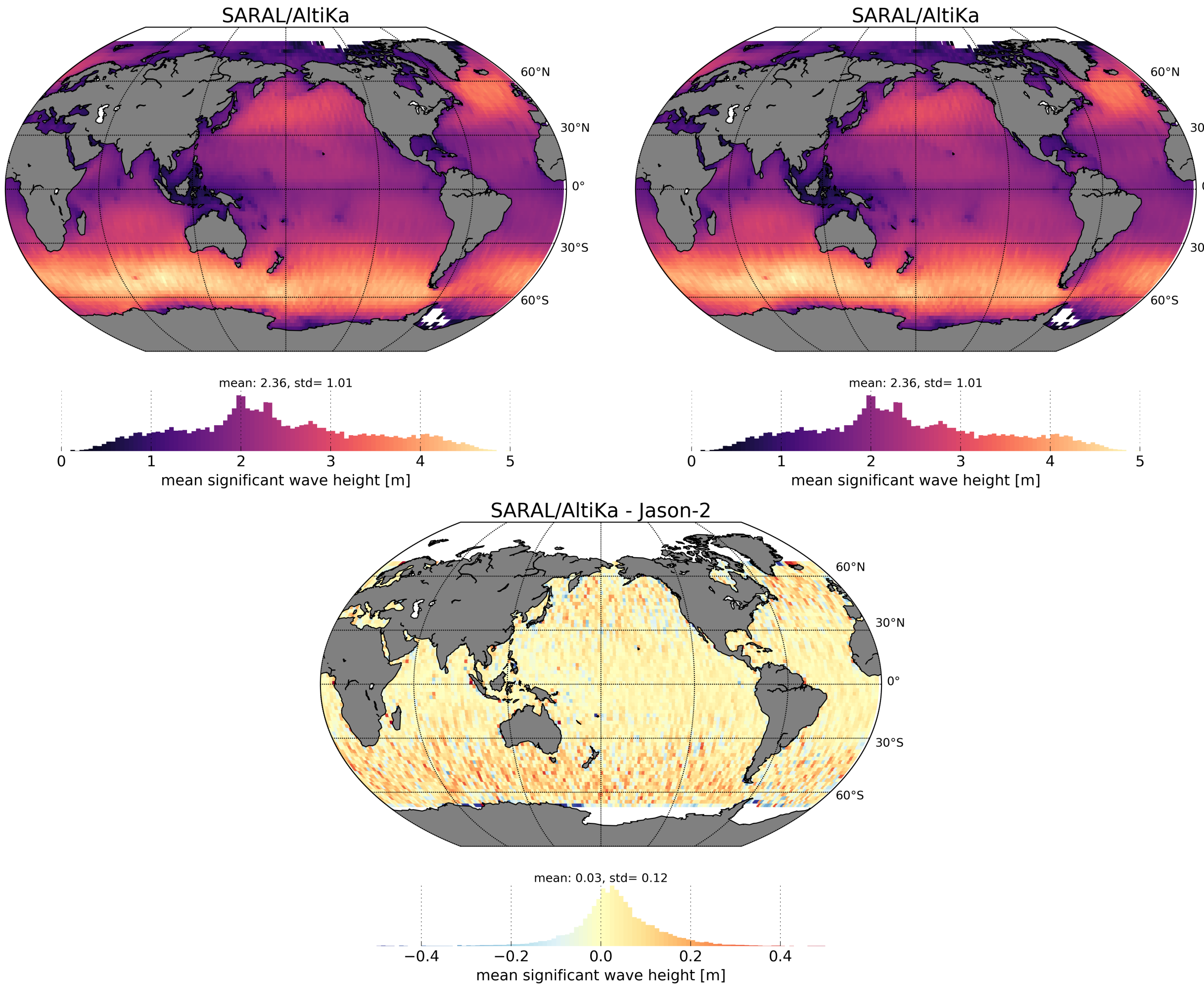

Figure 33: *Average map of significant wave height for SARAL/AltiKa (left) and Jason-2 (right) cycles 1 to 101. Difference map of gridded Saral and Jason-2 significant wave height for cycles 1 to 101.*

The shapes of the histograms are very similar (see right side of figure 34) for Jason-2 and SARAL/AltiKa, except for small SWH. The minimum SWH value of SARAL/AltiKa SWH is 12.6 cm (related to the look-up table), it is 0 for Jason-2. Nevertheless, small SWH of current Jason-2 or Jason-1 data are not precise (errors of about 15 cm), as the look-up table correction for small SWH is not accurate, whereas the SARAL/AltiKa look-up tables were updated for Patch2. Furthermore, the histogram for SARAL/AltiKa shows a small bump for SWH around 50 cm. Note that in the wave forecasting systems of Meteo-France, altimeter significant wave height from Jason-2 and SARAL/AltiKa are only assimilated for values higher than 50 cm. According to L. Aouf, the SARAL/AltiKa SWH data have a positive impact on the wave analysis and forecast of the Meteo-France wave analysis model ([7]).

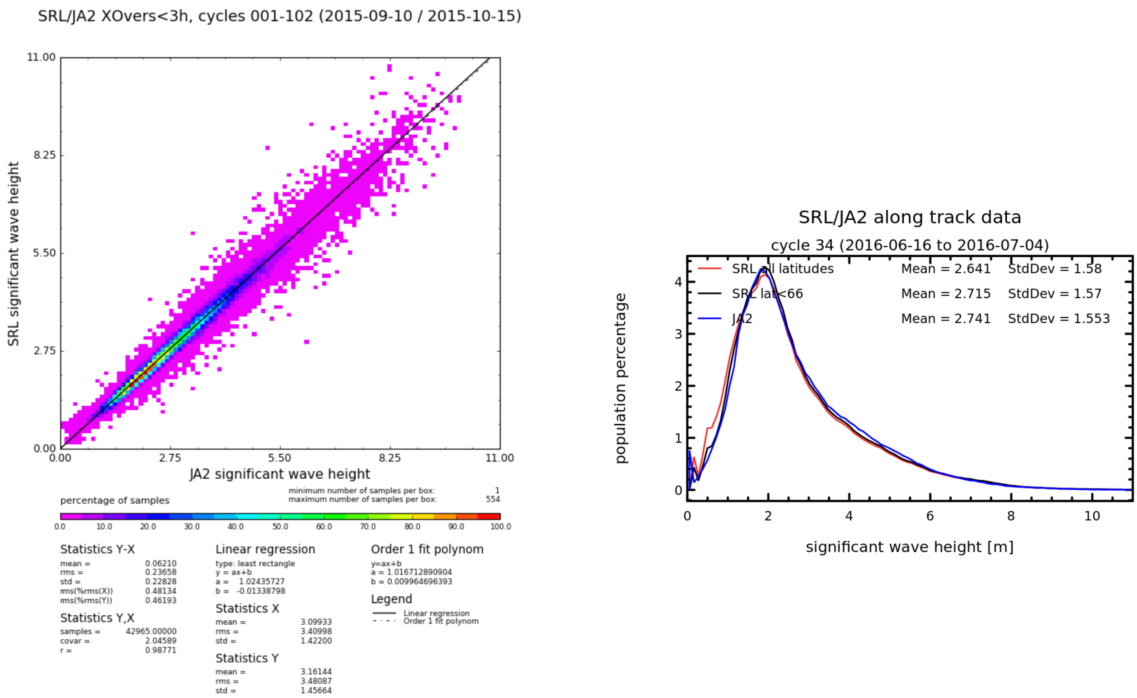

Figure 34: *Dispersion diagram of significant wave height between SARAL/AltiKa and Jason-2 at 3h crossover points (computed for cycles 1 to 101) on the left and histogram of along-track data computed over SARAL/AltiKa cycle 34 on the right.*

4.6. Ionosphere correction

As SARAL/AltiKa uses a single frequence, no dual frequency ionosphere correction is available, GIM model is used instead. This is not an issue as the SARAL/AltiKa altimeter uses a frequency of 35.75 GHz (Ka-band), and ionospheric effects are therefore very small (divided by roughly seven compared to Ku-band frequency). In this section, Jason-2 ionospheric correction values were scaled to be compared to SARAL/AltiKa ones. The scaling factor is based on the radar frequency ratio: $35.75^2/13.575^2 \approx 7$ between instruments. Monitoring the evolution of the ionospheric correction on SARAL/AltiKa and Jason-2 shows very similar evolution (35), with a slightly higher variability for Jason-2, likely related to small scale features the GIM model is unable to reproduce. Effects of varying local times on Jason-2 are alos visible.

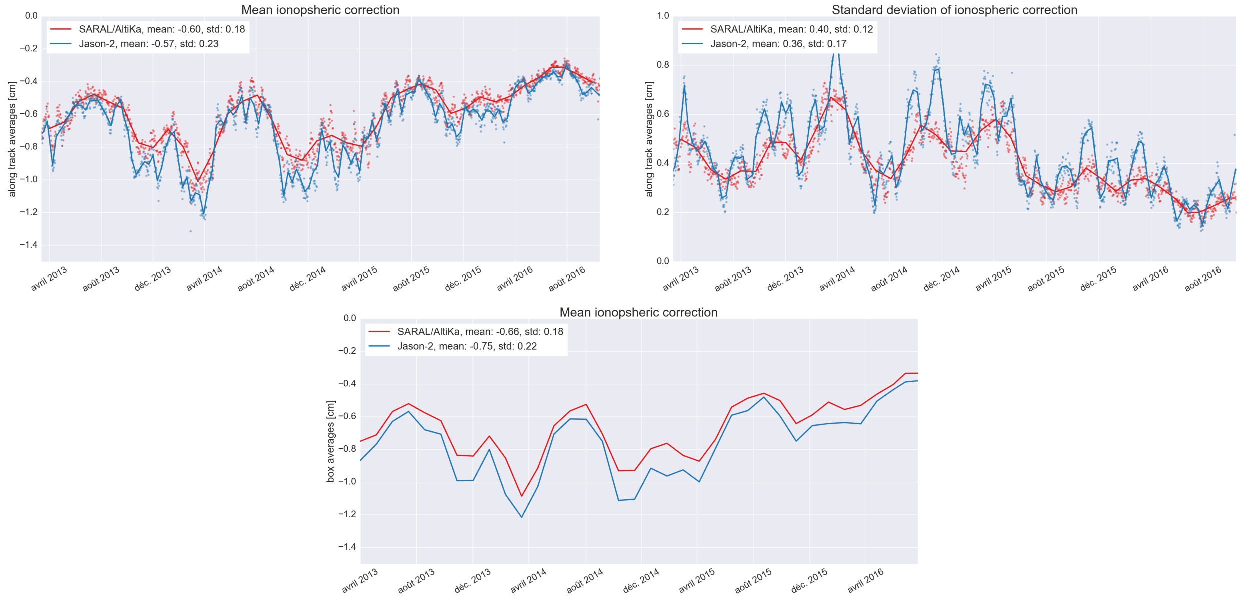

Figure 35: *Daily monitoring of mean and standard deviation ionosphere correction for SARAL/AltiKa (GIM) and Jason-2 (filtered dual-frequency ionosphere correction with scale factor 0.14418 for mean computation) on top and cycle per cycle monitoring of latitude weighted box mean for both missions on the bottom..*

Small differences between the two missions are still observed, may also be due to the fact that SARAL/AltiKa is a sun-synchronous satellite with 6:00 local time for ascending node and 18:00 local time for descending node. As ionosphere correction varies with local time, it is very small for ascending (morning) passes and has absolute values up to 2 cm in the equatorial region for descending (evening) passes. Jason-2 on the other hand is not sun-synchronous and revisits only every 12 cycles the same local hours. Different altitudes between Jason-2 and SARAL/AltiKa might also impact the observed ionospheric content.

Highest ionosphere correction (absolute values) can be found in the same regions (equatorial region) for SARAL/AltiKa and Jason-2 (see maps of figure 36, where Jason-2 data are not scaled), but the amplitude is of course very different (due to the different frequencies).

The dispersion diagram of ionosphere corrections (figure 37, the Jason-2 one is rescaled to Ka-band frequency) at 3h multi-mission crossovers shows a correlation level of 0.84 between the two

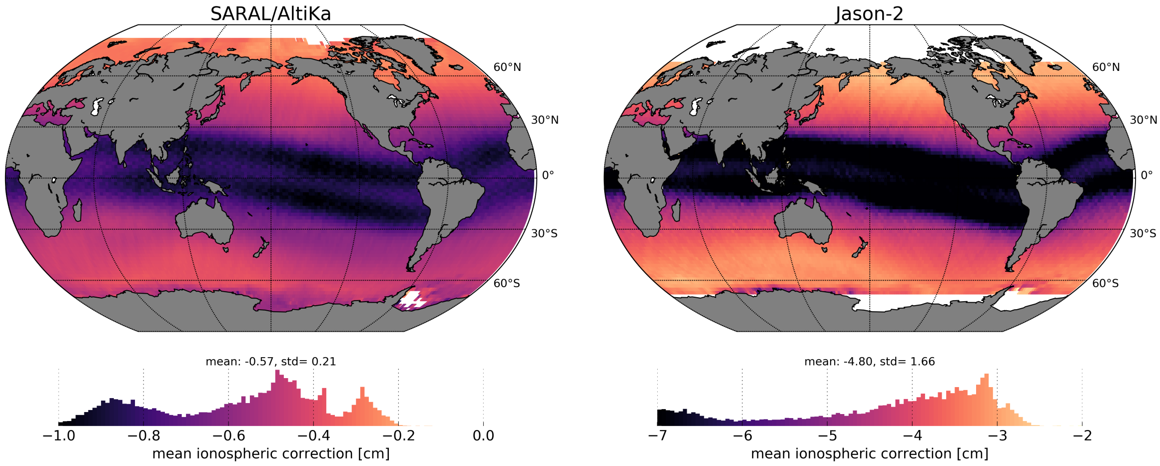

Figure 36: *Average map of ionosphere correction for SARAL/AltiKa (GIM, left) and Jason-2 (filtered dual-frequency ionosphere correction, right) cycles 1 to 101. Note that color scales are different for SARAL/AltiKa and Jason-2.*

missions. Histograms are slightly different, with bi-modal distribution on Jason-2 that is less visible on SARAL/AltiKa.

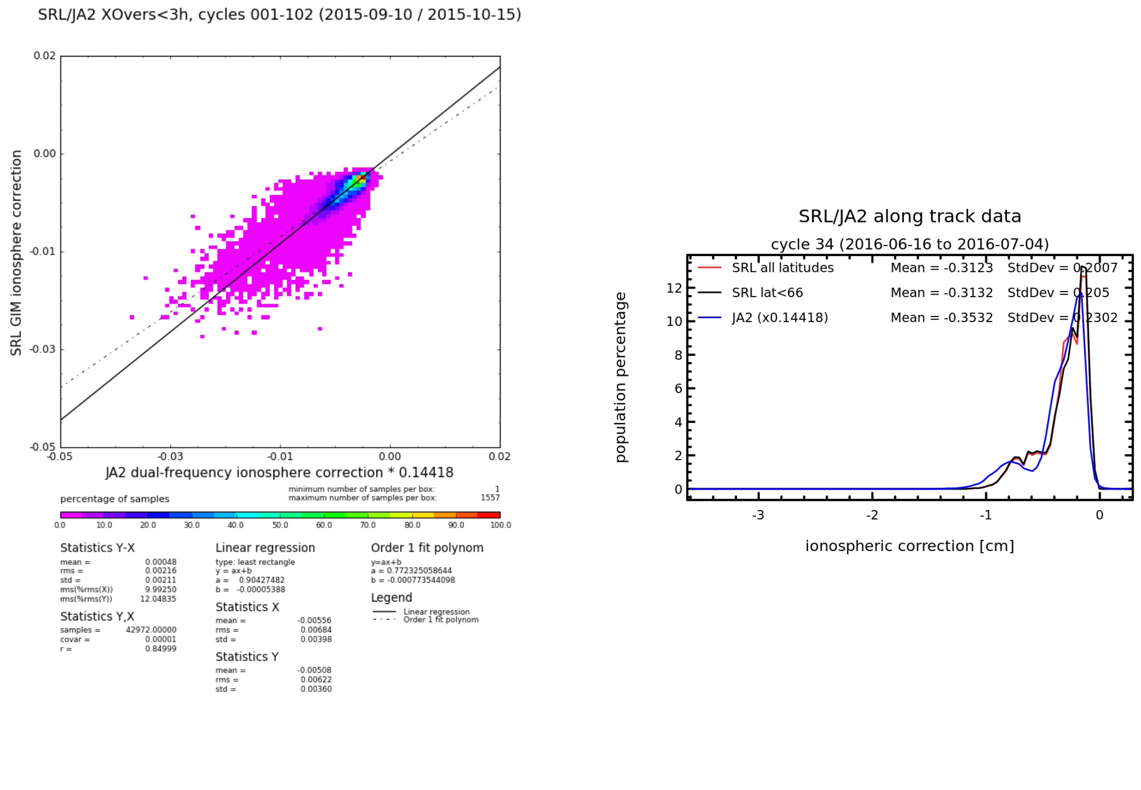

Figure 37: *Dispersion diagram of ionosphere correction between SARAL/AltiKa (GIM) and Jason-2 (filtered dual-frequency with scale factor of 0.14418 for Jason-2) at 3h crossover points (computed for cycles 1 to 101) on the left and histogram of along-track data computed over SARAL/AltiKa cycle 34 on the right.*

4.7. Radiometer wet troposphere correction

4.7.1. Overview

In order to have access to radiometer wet troposphere correction, liquid water content, water vapor content and atmospheric attenuation, SARAL/AltiKa uses a dual-frequency radiometer (23.8 GHz +/- 200 MHz & 37 GHz +/- 500 MHz), whereas Jason-2 has a three-frequency radiometer (18.7, 23.8 and 34.0 GHz). Figure 38 shows the daily mean and standard deviation of radiometer wet troposphere correction for SARAL/AltiKa and Jason-2. Since Patch2, the standard deviation is smaller for SARAL/AltiKa than for Jason-2. Concerning the mean of radiometer wet troposphere correction, Jason-2 has dryer values than SARAL/AltiKa. This is on the one hand related to different radiometer wet troposphere correction retrieval algorithms, but on the other hand, this can also be related to different local times of the satellites (sun-synchronous 6h/18h for SARAL/AltiKa). During several months the radiometer wet troposphere correction of SARAL/AltiKa went dryer, this is related to the saturation of the hot calibration counts, which was corrected on 22 October 2013 (explaining the jump of around 5 mm amplitude visible on the monitoring of figure 39). The safe-hold mode of SARAL/AltiKa did generate a 1 mm bias on the daily mean which is documented in a previous yearly report [4]. Both anomalies will be corrected in the next GDR-E reprocessing, foreseen late 2017.

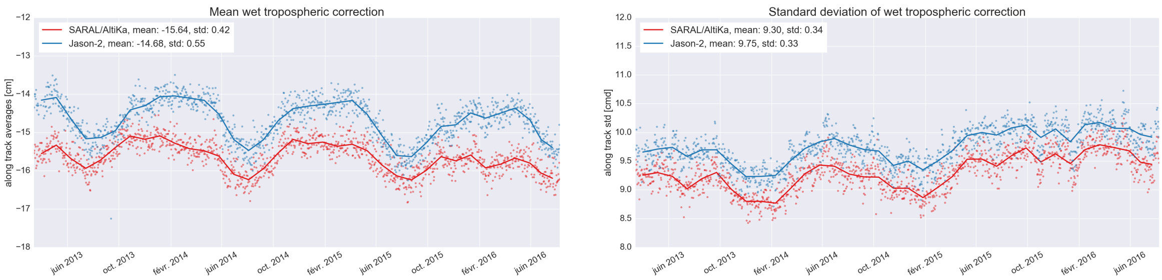

Figure 38: *Monitoring of mean and standard deviation of radiometer wet troposphere correction for Jason-2 (blue) and SARAL/AltiKa (red).*

4.7.2. Comparison with the ECMWF model

The ECWMF wet troposphere correction is used as a reference to investigate small differences between SARAL/AltiKa and Jason-2 radiometer corrections. Daily differences are calculated and plotted in figure 39. The drift in the radiometer wet troposphere correction of SARAL/AltiKa due to the saturation of the hot calibration count is clearly visible on the left part of figure 39. Outside of this drift period the difference between radiometer and ECMWF wet troposphere correction for SARAL/AltiKa and Jason-2 is around 5 mm. The two ECMWF model updates (June and November 2013) occurred during the observed period, which might have an impact on the model wet troposphere correction, did not show any impact on the data.
The standard deviation of radiometer minus model wet troposphere correction is higher for SARAL/AltiKa (around 1.6 cm) compared to Jason-2 (around 1.2 cm), shown on left of figure 39 and also on the histogram on figure 41. Work is ongoing to provide a more accurate wet tropospheric correction for the future GDR-E version of the products, a preview of this correction can be found in section 7.3..

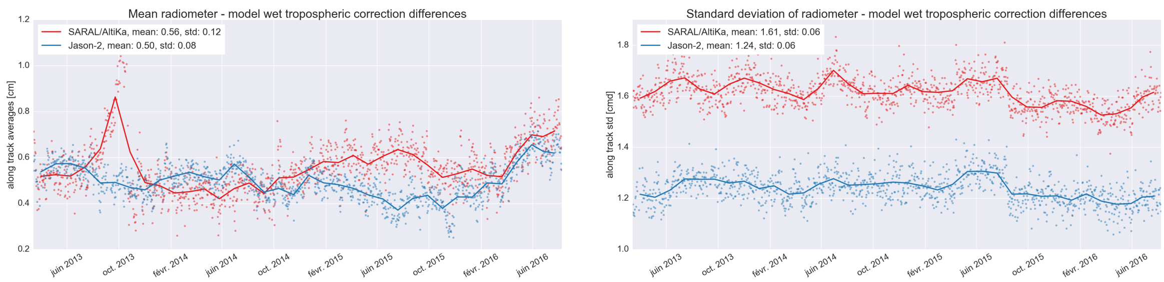

Figure 39: *Monitoring of mean and standard deviation of radiometer minus model wet troposphere correction differences for SARAL/AltiKa and Jason-2.*

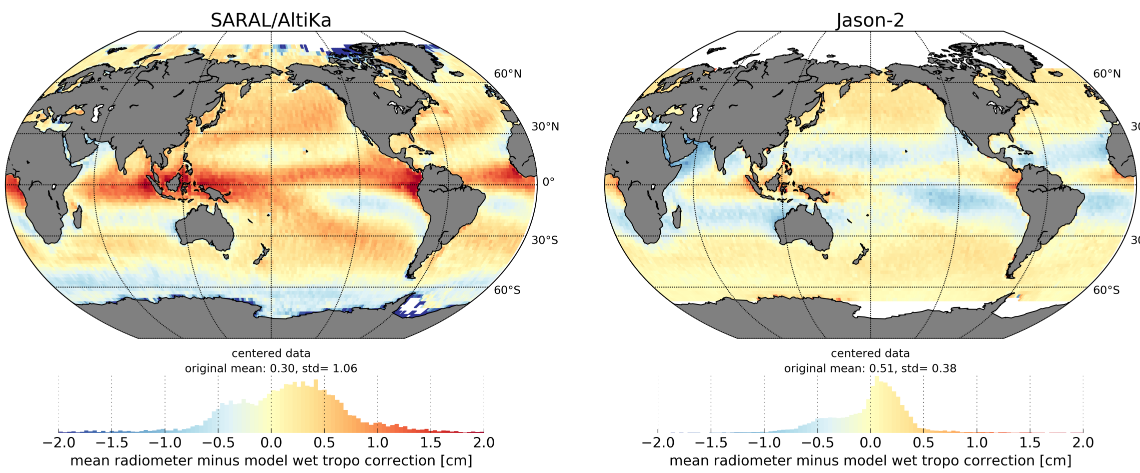

Figure 40: *Average map of radiometer minus ECMWF model wet troposphere correction for SARAL/AltiKa (left) and Jason-2 (right) cycles 1 to 101.*

The maps of radiometer minus ECMWF model wet troposphere correction (figure 40) are centered around the mean value (5 mm for Jason-2, 3 mm for SARAL/AltiKa). The mean of the

SARAL/AltiKa map is impacted on the one side by the saturation of the hot calibration counts (which tends to overestimate the difference) and on the other side by some boxes near the frontier between sea-ice and free water (which tends to underestimate the mean). These boxes with strong negative values are an indication that probably not all sea ice cases are edited. In the frame of Cal/Val activities for the DUACS system, a new ice flagging procedure was tested, and will be implemented in routine Cal/Val analysis. Geographical structures of the radiometer minus model wet troposphere corrections are similar for the two satellites in high latitudes (around $\pm$ 50°), but quite different for low latitudes. This is also observed on the histogram of wet troposphere differences (figure 41) which is slightly wider for SARAL/AltiKa than for Jason-2.

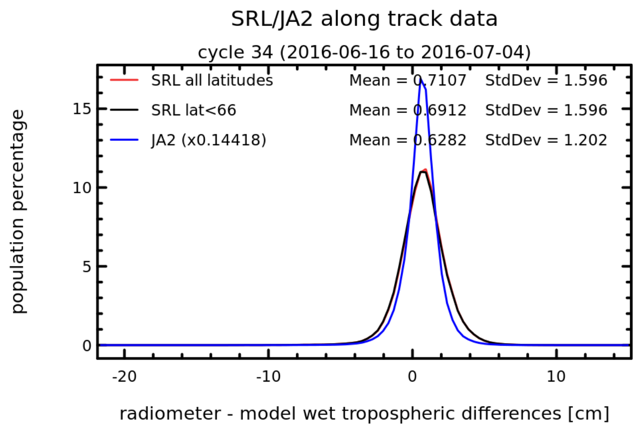

Figure 41: *Histogram (of along-track data) of radiometer minus ECMWF model wet troposphere correction between SARAL/AltiKa and Jason-2 computed for SARAL/AltiKa cycle 34.*

4.8. Altimeter wind speed

The Patch1 version of the products used the wind look-up table from Jason-1 which, with the Ka-band backscattering coefficient produced erroneous wind speeds. In the Patch2 version, the altimeter wind speed algorithm developed by [14] for Ka-band altimetry is used. Figure 42 shows the daily monitoring of the mean and standard deviation of altimeter wind speed for SARAL/AltiKa and Jason-2. The SARAL/AltiKa Patch2 altimeter wind speed has values similar to the Jason-2 altimeter wind speed, despite a sligthly lower mean.
It should be noted that in the current products, the SARAL/AltiKa wind speed is impacted by the saturation of the radiometer hot calibration counts through the estimation of atmospheric attenuation which is then applied on the backscatter coefficient. The maps of altimeter wind speed for both missions are consistent (see 43).
The figure 44 shows a good correlation of wind speed data between the two missions (over 0.95), yet the relationship between Jason-2 and SARAL/AltiKa remains non truly linear. The distribution of SARAL/AltiKa wind speed values shows two modes, this feature is less present on Jason-2 data. SARAL/AltiKa's histogram is also shifted towards lower wind speed values than Jason-2, with a sudden decline above 16 m/s which is not observed on Jason-2 data.

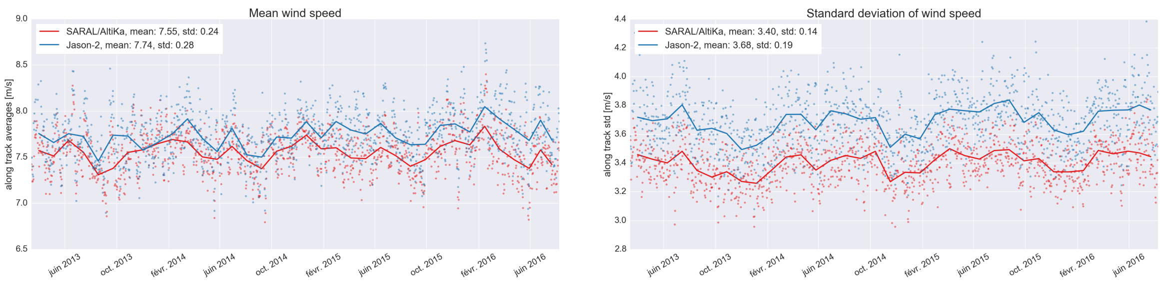

Figure 42: *Monitoring of mean and standard deviation of altimeter wind speed for SARAL/AltiKa and Jason-2. The gold band indicates the safe hold mode on SARAL/AltiKa.*

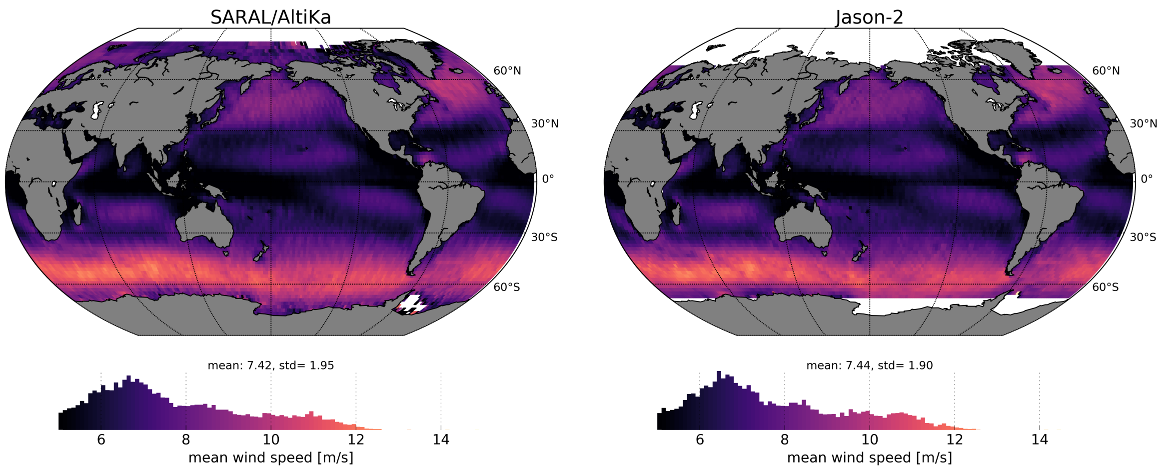

Figure 43: *Average map of altimeter wind speed for SARAL/AltiKa (left) and Jason-2 (right) cycles 1 to 101.*

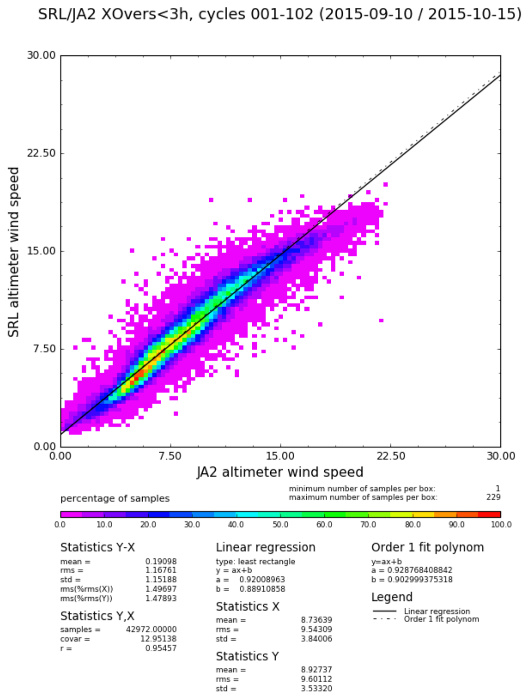

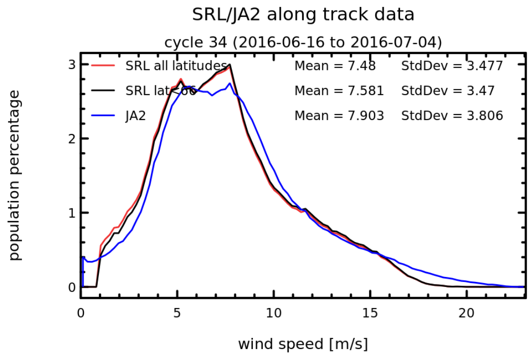

Figure 44: *Dispersion diagram of altimeter wind speed between SARAL/AltiKa and Jason-2 at 3h crossover points (computed for cycles 1 to 101) (left) and histogram of along-track data computed for SARAL/AltiKa cycle 34 (right).*

4.9. Sea state bias

In Patch1 version, the sea state bias was as a first approximation set to -3.5% of SWH.
For Patch2 a hybrid SSB solution developed by R. Scharroo was used (this SSB was computed using the same method as in [17]). The Patch2 SSB solution is in absolute values around 1.8 cm stronger (which increases the Patch2 SLA) than the Patch1 solution. The daily monitoring of the along-track sea state bias for SARAL/AltiKa and Jason-2 shows a similar temporal evolution, but SARAL/AltiKa SSB has higher absolute values (around 2.5 cm higher) than Jason-2 (see left side of figure 45). This is also the case when considering latitude weighted box statistics (bottom of figure 45). The bias between SARAL/AltiKa and Jason-2 SSB is not homogeneous but varies geographically, as shown on bottom of figure 46. Furthermore the daily standard deviation is also slightly larger for SARAL/AltiKa compared to Jason-2 (see right side of figure 45).

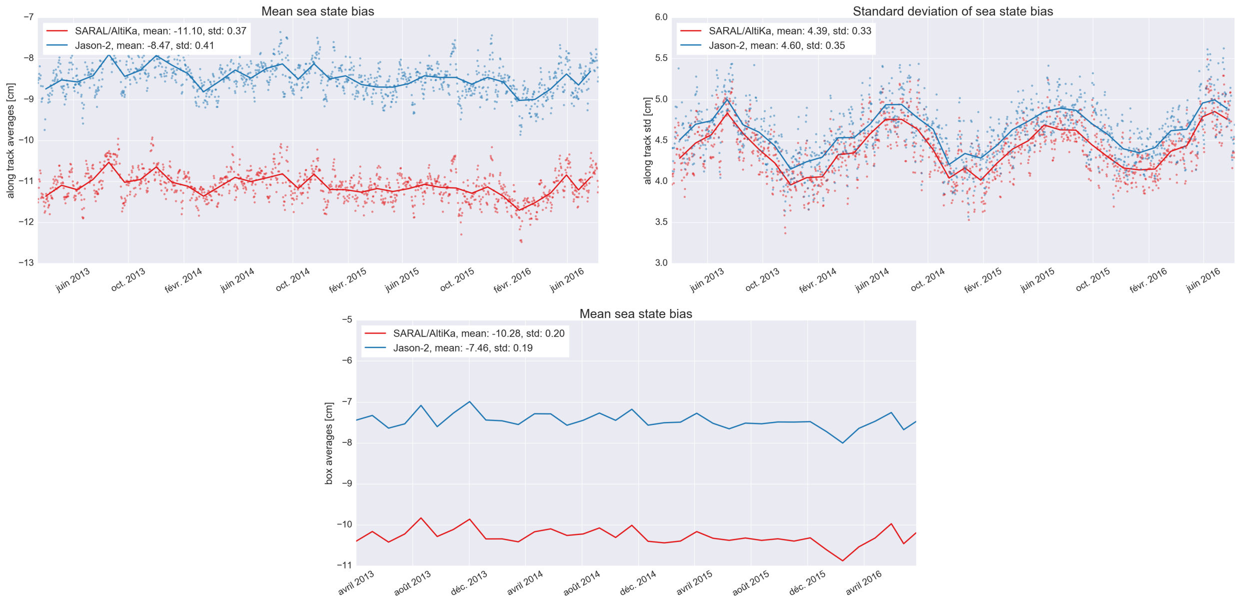

Figure 45: *Monitoring of mean and standard deviation of (along-track) sea state bias of SARAL/AltiKa and Jason-2 on the top. Cycle per cycle monitoring of latitude weighted box mean for both missions on the bottom.*

The map of SARAL/AltiKa sea state bias shows higher values in the region of 50˚S (where SWH is strong) than the map of Jason-2 (top of figure 46). The dispersion diagram of SARAL/AltiKa and Jason-2 sea state bias at 3h multi-mission crossovers confirms that the SARAL/AltiKa SSB is overestimated for high SSB (i.e. for high SWH). The different nature of the SSB models used for SARAL/AltiKa and Jason-2 (dedicated model) is also visible on the right side of figure 47, showing very different shapes of histograms. An updated SSB solution for SARAL/AltiKa is available through the PEACHI project.

This difference in sea state bias between the two missions has also an impact on the geographically correlated biases between the two missions, as shown in chapter 5.3., concerning maps of sea surface height differences at multi-mission crossover points.

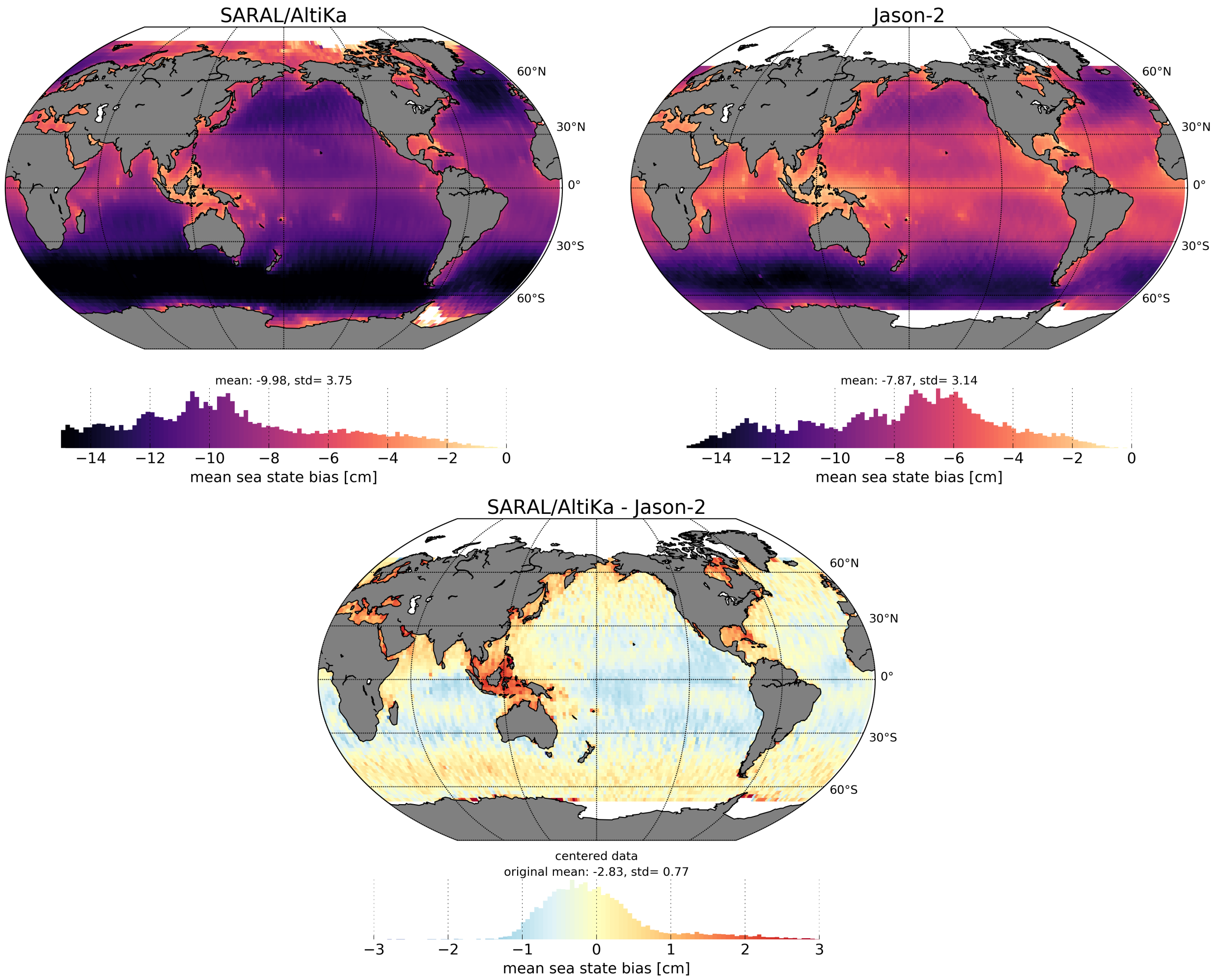

Figure 46: *Average map of sea state bias for SARAL/AltiKa (left) and Jason-2 (right) cycles 1 to 101. Map of differences of gridded SARAL/AltiKa and Jason-2 sea state bias for cycles 1 to 101.*

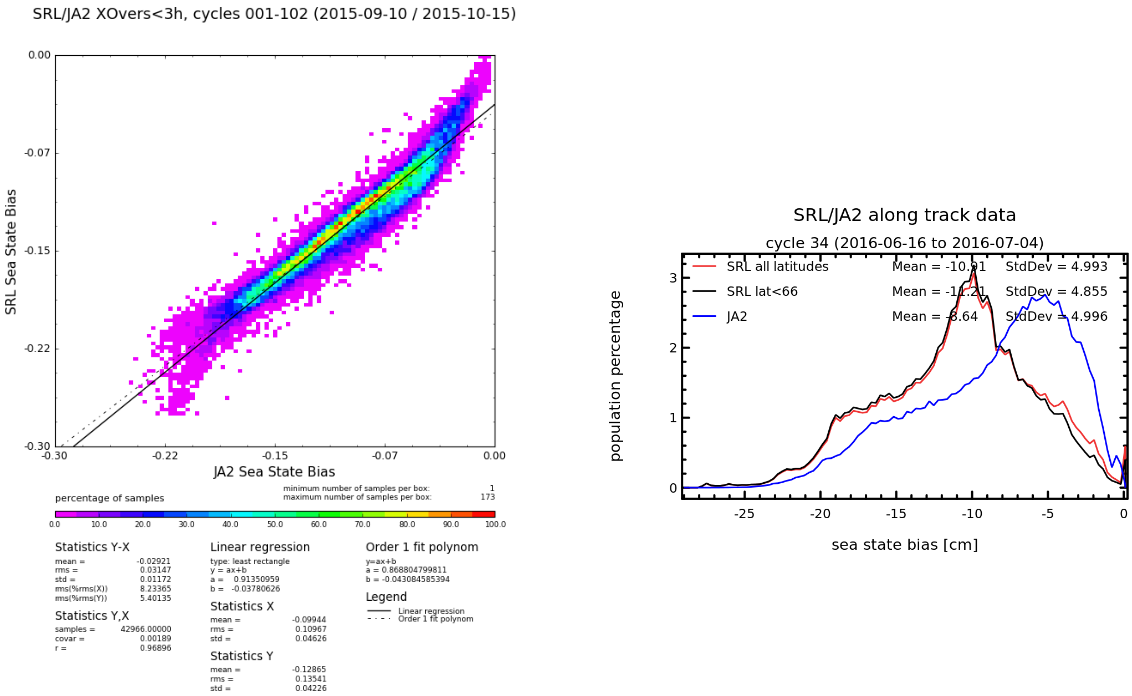

Figure 47: *Dispersion diagram of sea state bias between SARAL/AltiKa and Jason-2 at 3h crossover points (computed for cycles 1 to 101, left) and histogram (of along-track data) computed for SARAL/AltiKa cycle 34 (right).*

5. SSH crossover analysis

5.1. Overview

SSH crossover differences are the main tool to analyze the whole altimetry system performance. Crossovers measure the SSH consistency between ascending and descending passes. At each crossover, the observed difference between SSH measurements between ascending and descending arcs results from the sum of errors in the system and ocean variability. In order to reduce the impact of ocean variability, only crossovers with a maximum time difference of 10 days are selected. This gives a measure of the mission performance on mesoscale time/space scales. Mean and standard deviation of SSH crossover differences are computed from the valid data set to estimate maps and cycle per cycle monitoring over the altimeter period. In order to monitor the performances over stable surfaces, additional editing is applied to remove shallow waters (bathymetry above -1000 m), areas of high ocean variability (variability above 20 cm rms) and high latitudes ($|lat| < 50\,\text{deg}$). Under these conditions, SSH performances are always estimated with equivalent conditions.

The formula used to estimate a fully corrected SSH for SARAL/AltiKa and Jason-2 is defined below:

$$SSH = Orbit - Altimeter\ Range - \sum_{i=1}^{n} Correction_i \tag{1}$$

where the sum of corrections expands as:

$$\begin{aligned}
\sum_{i=1}^{n} Correction_i &= Dry\ troposphere\ correction \\
&+ Dynamical\ atmospheric\ correction \\
&+ Radiometer\ wet\ troposphere\ correction \\
&+ Ionospheric\ correction \\
&+ Sea\ state\ bias\ correction \\
&+ Ocean\ tide\ correction\ (including\ loading\ tide) \\
&+ Earth\ tide\ height \\
&+ Pole\ tide\ height
\end{aligned}$$

The corrections effectively used to generate the metrics presented in this report are summarized in table 6 for SARAL/AltiKa and Jason-2. The standards correspond to the current version of the GDR products: GDR-T Patch2 for SARAL/AltiKa and GDR-D for Jason-2.

Parameter	SARAL/AltiKa	Jason-2
Orbit	CNES POE-D until cycle 24, POE-E afterwards	CNES POE-D (Doris/Laser/GPS)
Dynamic atmospheric correction	Computed from ECMWF atmospheric pressures after removing S1 and S2 atmospheric tides (for inverse barometer) + Mog2D High Resolution ocean model	
Radiometer wet troposphere correction	MWR using P2	AMR
Ionospheric correction	GIM model	dual-frequency altimeter ionosphere correction
Sea State Bias	Hybrid SSB model	MLE4 version derived from 1 year of MLE4 Jason-2 altimeter data with version 'd' geophysical models
Global ocean tide	GOT 4.8 ocean tide	
Earth tide	From Cartwright and Taylor tidal potential	
Pole tide	Wahr [1985]	
Mean Sea Surface	CNES_CLS_2011	

Table 6: Standards used for SSH estimation on SARAL/AltiKa and Jason-2

When not otherwise stated, the standards from table 6 are used.

5.2. Mean of SSH crossover differences

The map of SSH mean ascending/descending differences at crossovers should ideally be close to zero: only time differences shorter than 10 days are selected in order to be as close as possible to the steady ocean hypothesis while maintaining a global sampling by crossovers. Of course this is untrue due to quickly evolving mesoscale ocean features, yet, large geographically correlated patterns on such maps indicate systematic differences between ascending and descending passes, which are generally errors. This can indicate either problems in the orbit computation or in geophysical corrections. Figure 48 shows the map of mean SSH differences at crossovers for SARAL/AltiKa and Jason-2, computed over the same period in a similar way (based on SARAL/AltiKa cycles).

Both missions show geographically correlated patterns of low amplitudes. The mean difference is slightly negative on SARAL/AltiKa and Jason-2, with a larger mean difference observed on

SARAL/AltiKa. Locally differences can reach 2 *cm* on SARAL/AltiKa while they remain below 1 *cm* on Jason-2

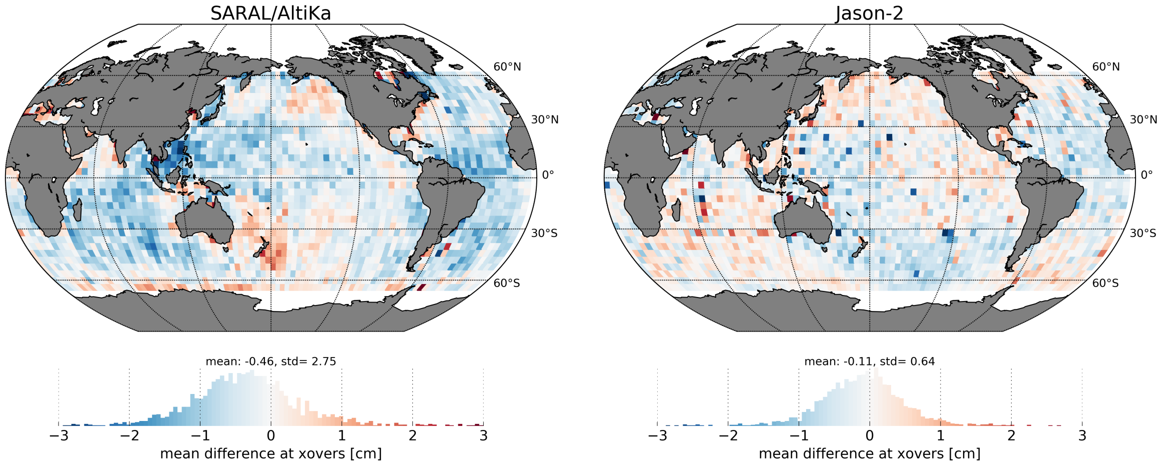

Figure 48: *Map of mean of SSH crossovers differences for [left] SARAL/AltiKa and [right] Jason-2. Mean differences are expressed in cm, estimates are based on SARAL/AltiKa cycles 1 to 100.*

In addition to mapping the differences accumulate over the whole mission's lifetime, the global mean of SSH differences at crossovers is estimated for each cycle. This quantity is monitored over time to detect any issue on the mission.

Over SARAL/AltiKa cycles 1 to 103 the evolution of the cycle-average mean SSH difference at crossovers is plotted on figure 49 for SARAL/AltiKa and Jason-2. The left and right panels correspond to two different selections of crossovers used to estimate the mean (no selection at all and selection on bathymetry, latitude and oceaninc variability), while plain and dotted lines correspond to two ways of averaging the SSH differences at crossovers (a simple ensemble mean and a latitude weighted based on the crossovers theoretical density). The weighted averaging method was described in the SARAL/AltiKa yearly report 2014 [23]. For SARAL/AltiKa, the mean difference is slightly negative $\approx -2/-4$ *mm* depending on the averaging method and the crossovers selection, Jason-2 being closer to zero at ≈ -1 *mm*. The mean value is very stable over time for both missions, with a slightly larger cycle to cycle variability on Jason-2 than on SARAL/AltiKa, but note that the samples used for Jason-2 are smaller than for SARAL/AltiKa due to different cycle lengths. One can also note a periodic signal around one year on SARAL/AltiKa, which is related to the β angle (see [3] for an in-depth analysis of such signals).

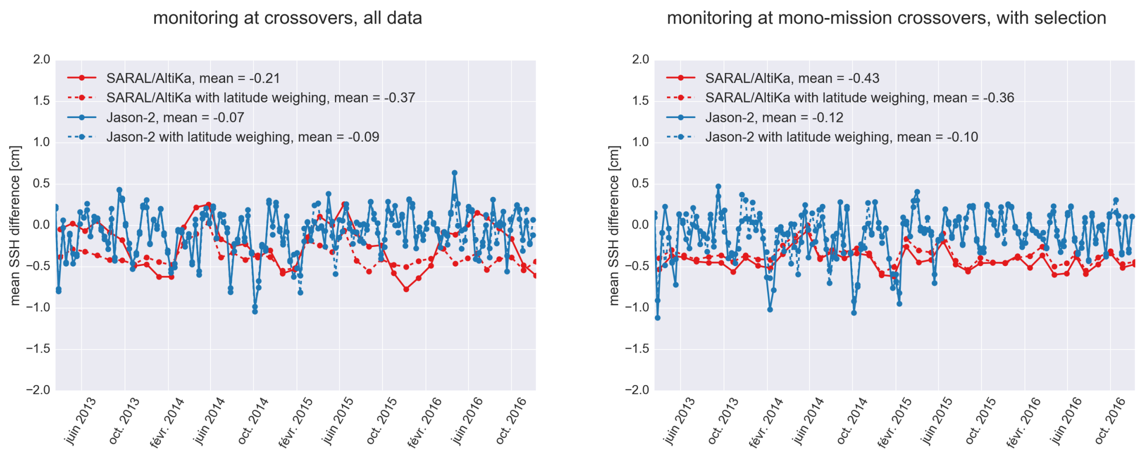

Figure 49: *Cycle per cycle monitoring of ascending/descending SSH differences at mono-mission crossovers for SARAL/AltiKa and Jason-2 for Saral cycles 1 to 101.*

5.3. Mean of SSH crossover differences between SARAL/AltiKa and Jason-2

On top of monomission crossovers that allow to detect systematic biases on one mission, crossovers are also estimated between missions. In this case they are used to check for geographically correlated biases or drifts that could happen between two missions. Here SARAL/AltiKa is compared to Jason-2 through their SSH differences at crossovers.

The temporal evolution of the mean of SARAL/AltiKa minus Jason-2 SSH differences at crossovers is shown on figure 50. On both panels a selection for latitudes lower than 50°, deep ocean and low oceanic variability areas is used. The left panel uses an ensemble mean estimation while the right panel is based on a latitude weighed average. The green line uses the radiometer wet tropospheric correction while the orange line is based on the model correction. In all cases the temporal evolution of SSH differences at crossovers between SARAL/AltiKa and Jason-2 is very similar:

- the mean bias between the two missions is around 45 *mm*,
- there is no significant drift between SARAL/AltiKa and Jason-2 on the period.

However at some periods, differences up to 2 *mm* can be found when comparing the radiometer and model wet tropospheric corrections. There are two explanations for these differences:

- saturation of hot calibration counts, resulting in a drift of the SARAL/AltiKa radiometer wet tropospheric correction around October 2013,
- a 1 *mm* shift in wet tropospheric path delay after the SHM on SARAL/AltiKa (October 2014, [4]).

Rather than looking at the temporal evolution, mapping the SSH differences between SARAL/AltiKa and Jason-2 over the first 38 cycles of SARAL/AltiKa provides information about geographically correlated biases between the two missions. Such maps are shown on figure 51, where both maps are centered before plotting. Large scale biases are visible between the two missions with amplitudes up to ±3 cm. Using the radiometer on both missions (left of figure 51) shows a negative patch in the western tropical Pacific Ocean centered on Indonesia and a large positive patch in

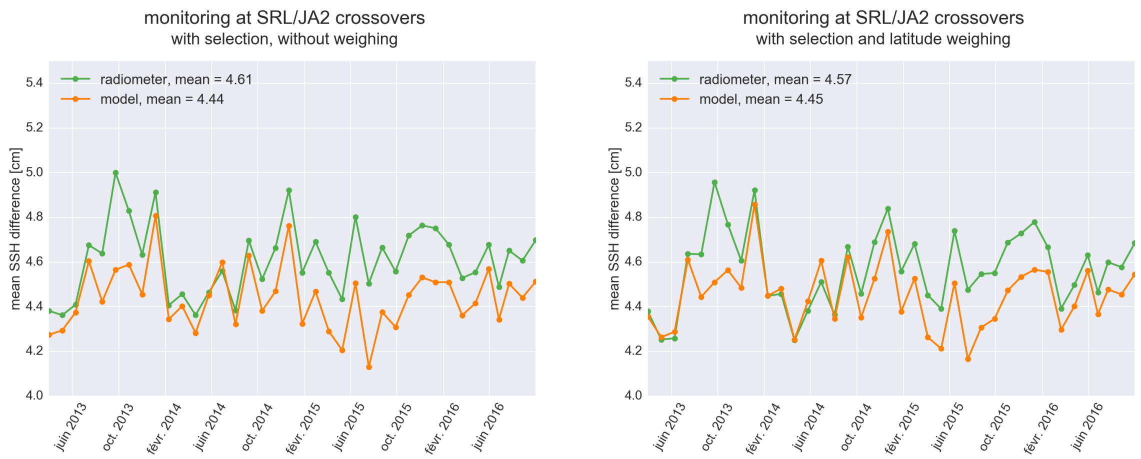

Figure 50: *Monitoring of mean of SARAL/AltiKa minus Jason-2 differences at crossovers using radiometer wet troposphere correction (green line) or ECMWF model wet troposphere correction (orange line) for GDR data, [left] ensemble mean and [right] latitude weighed mean.*

the Southern Ocean, which extends towards the north in Atlantic Ocean. As for mono-mission crossover differences, part of the observed pattern might come from orbit related issues and/or from geophysical corrections. Using the model wet tropospheric correction on both missions (right of figure 51) reduces the Southern Ocean patch and to a lesser extent the negative Indonesian patch, as well as a positive patch at the southern tip of Greenland. However the positive patch in the southern Atlantic Ocean remains. Improvements are expected from an improved radiometer retrieval algorithm, as well as a new SSB model for SARAL/AltiKa as part of GDR-E.

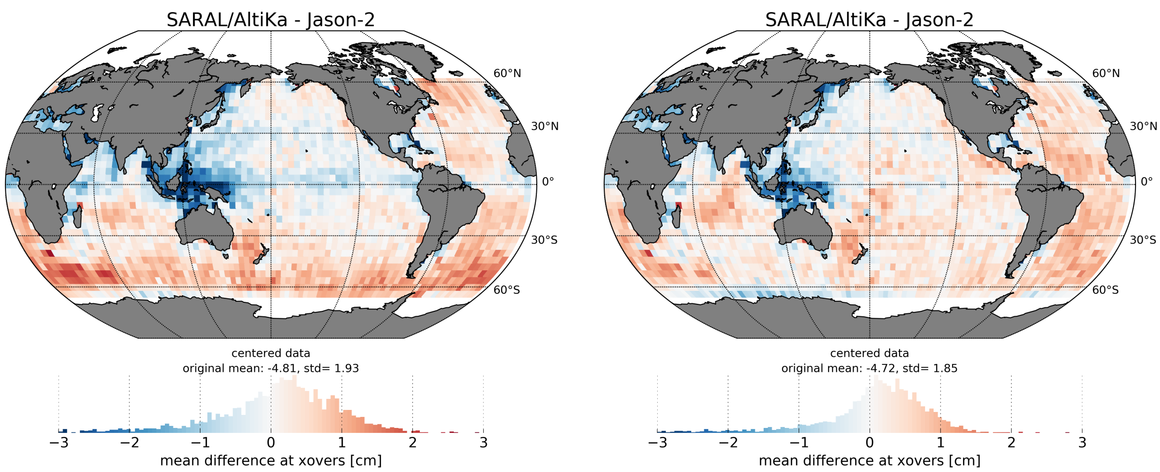

Figure 51: *Map of mean of SSH crossovers differences between SARAL/AltiKa and Jason-2 using [left] the radiometer wet tropospheric correction or [right] ECMWF model wet troposphere correction for both missions. The maps are centered around the mean.*

5.4. Standard deviation of SSH crossover differences

The standard deviation of SSH differences at crossovers is a key performance metric for satellite altimetry missions. In this section the standard deviation of SSH differences at crossovers is investigated for SARAL/AltiKa and compared to Jason-2.

The cycle per cycle standard deviation of SSH differences at crossovers is plotted on the left of figure 52 for different selections and averaging methods:

- solid black: no selection is applied, and the ensemble standard deviation is estimated without any weighting. In this case the standard deviation amounts to 6.8 cm and its temporal evolution is impacted by an annual signal due to varying sea ice extent.
- dotted black: selection is applied on the crossovers, but the standard deviation is estimated after weighting the crossovers following the method described in [23]. This process slighlty reduces the standard deviation (6.3 cm) due to downweighting of crossovers at high latitudes and reduces the amplitude of the annual signal.
- solid red: shallow waters (bathymetry $< -1000\ m$), high latitudes and high variability areas have been removed. This is as close as possible to the steady ocean hypothesis and the standard deviation of SSH differences drops to 5.3 cm, no more annual cycle is observed.
- dotted red: uses the same selection as above, combined to a latitude weighting of the crossovers before estimating the standard deviation. Using this method leads to a small increase of the standard deviation of SSH differences at crossovers (at 5.5 cm)

The right part of figure 52 displays the geographical distribution of the standard deviation of SSH differences at crossovers. This map shows the expected patterns with high standard deviation observed in high ocean variability areas and in the Arctic Ocean (where some geophysical corrections such as tides, are less accurate).

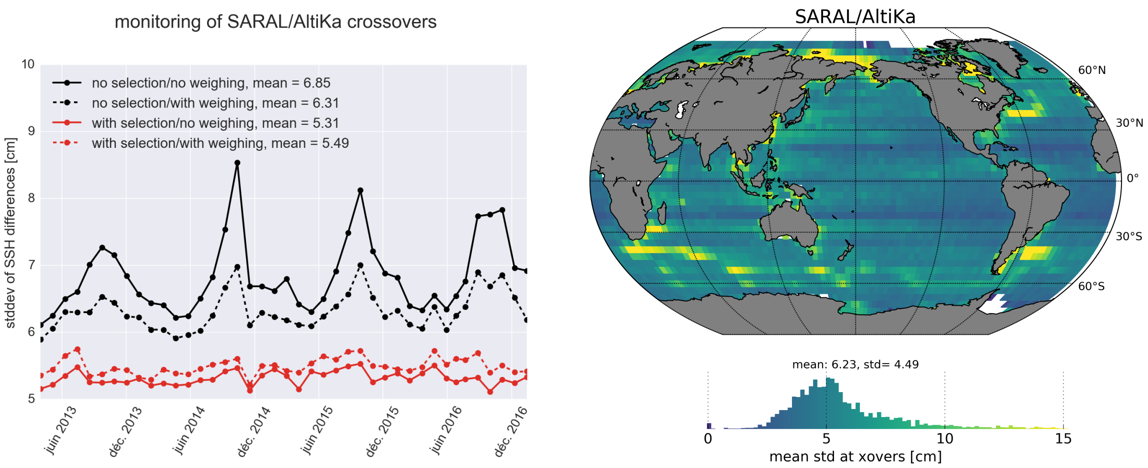

Figure 52: *[left] Cycle by cycle standard deviation of SSH crossover differences for SARAL/AltiKa using different selections and averaging methods and [right] map of standard deviation at crossover points from cycle 1 to 103. In both cases the radiometer wet tropospheric correction is used.*

As part of the routine Cal/Val activities, the performance of SARAL/AltiKa is compared to Jason-2 through the use of the standard deviation of SSH differences at crossovers. Figures 53 and 54 display comparisons between SARAL/AltiKa and Jason-2 performance at crossovers for different selections and weighting methods. In each case the performance using the radiometer and the model are displayed.

Figure 53 displays the ensemble standard deviation with no weighting applied. However, as we compare SARAL/AltiKa to Jason-2, only latitudes below 66° are selected, thus the differences with respect to figure 52(left) which has no such limitation.

When using the model, SARAL/AltiKa consistently shows a better performance than Jason-2. However when using the radiometer wet tropospheric correction, both missions show similar performances. This suggests that there is still room for improvement of the wet tropospheric path delay retrieval algorithm on SARAL/AltiKa.

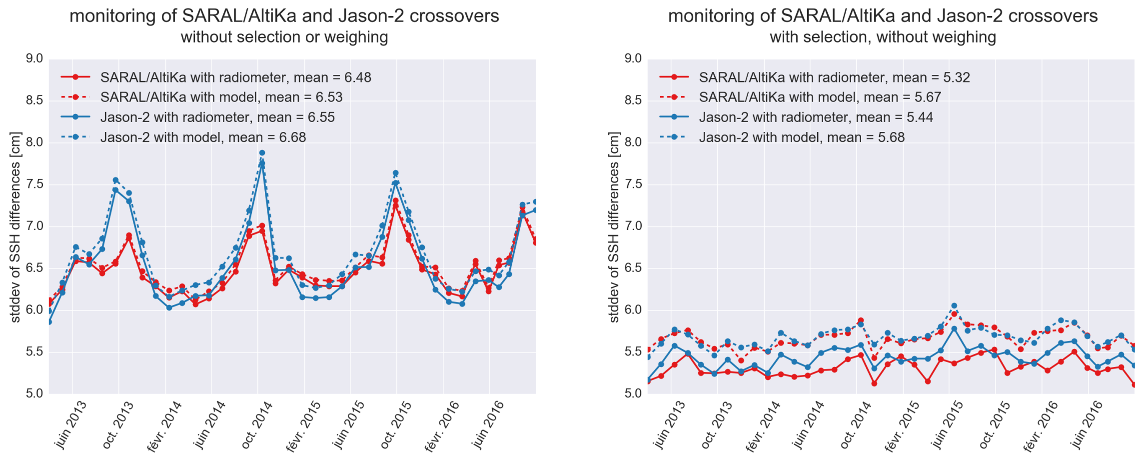

Figure 53: *monitoring of the standard deviation of SSH differences at mono-mission crossovers for SARAL/AltiKa and Jason-2 for Saral cycles 1 to 100 using radiometer (dotted lines) or model (plain lines) wet troposphere correction. [left] is without selection while [right] is after removing high latitudes, shallow waters and high variability areas.*

To account for the uneven distribution of crossover points, we also estimate weighted statistics (figure 54) where the weights applied are a function of latitude based on the crossovers density. This allows to better compare two missions that do not share the same ground track. Similar results are obtained with these weighted statistics: depending on the wet troposphere correction choosen, SARAL/AltiKa's performance is equivalent or slightly better than the Jason-2 one.

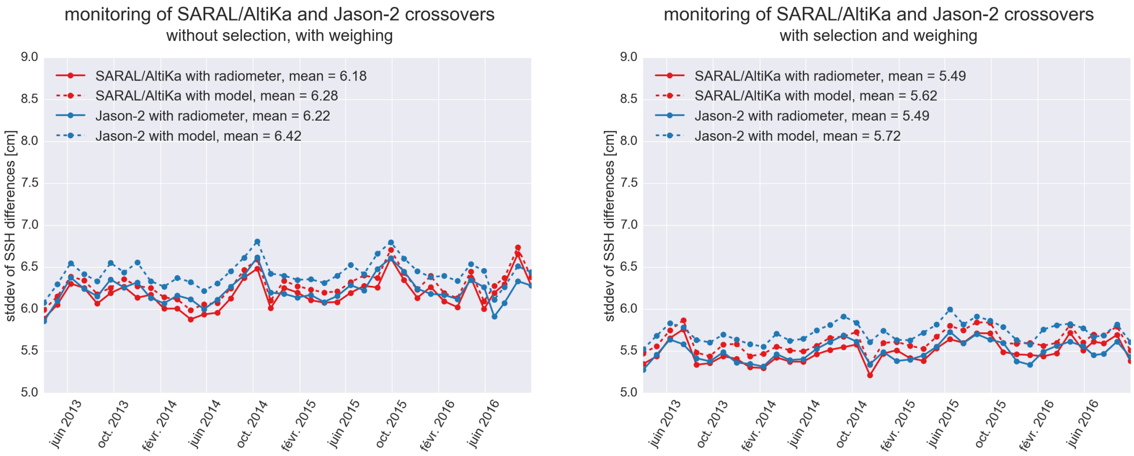

Figure 54: *monitoring of the standard deviaiton of SSH differences at crossovers for SARAL/AltiKa and Jason-2 for Saral cycles 1 to 101. [left] is without selection while [right] is after removing high latitudes, shallow waters and high variability areas. A weighting based on crossovers theoretical density is applied*

5.5. Performances of the different product types

Saral/AltiKa data are also available as OGDR and IGDR products, which are more rapidly available than GDR products. The main differences between the different data products are listed in table 7.

Auxiliary Data	Impacted Parameter	OGDR	IGDR	GDR
Orbit	Satellite altitude, Doppler correction, ...	DORIS Navigator	Preliminary (Doris MOE)	Precise (Doris + Laser POE)
Meteo Fields	Dry/wet tropospheric corrections, U/V wind vector, Surface pressure, Inverted barometer correction,...	Predicted	Restituted	Restituted
Pole Location	Pole tide height	Predicted	Predicted	Restituted
Mog2D	HF ocean dealiasing correction	Not available	Preliminary	Precise
GIM	Ionosphere correction	Predicted	Restituted	Restituted

Table 7: *D*ifferences between the auxiliary data for the O/I/Gdr products (from [9])

Figure 55 displays the monitoring of the cycle per cycle mean and standard deviation of SSH differences at crossovers for the OGDR, IGDR and GDR products. Regarding the mean, all three products show a good stability, of course the temporal variablity is greater for OGDR and IGDR than for GDR data. As expected GDR products provide the best performance with a standard deviation of the differences at crossovers of 5.3 cm. But IGDR data also exhibit a very good performance, with an average standard deviation of the differences of 5.5 *cm*, very close to the GDR value despite degraded standards (GDR-T and GDR-T Patch1) at the beginning of the period and a less accurate orbit solution (MOE vs. POE). OGDR data show a higher standard deviation at $\approx$ 7 cm.

5.6. Estimation of pseudo time-tag bias

The pseudo time tag bias is found by computing at crossovers the regression between SSH differences and orbital altitude rate ($\dot{H}$), also called satellite radial speed :

$$\Delta SSH = \alpha \dot{H}$$

This method allows to estimate the time tag bias but also absorbs other errors correlated with $\dot{H}$ as for instance orbit errors. Therefore it is called "pseudo" time tag bias.

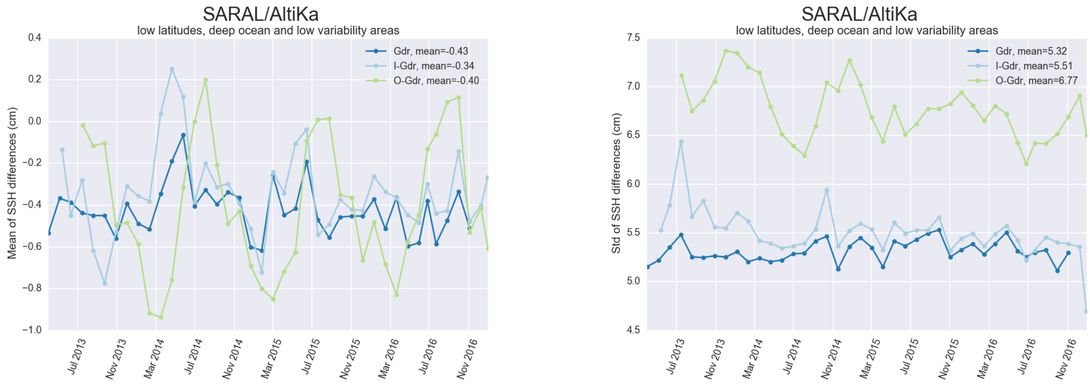

Figure 55: *Cycle per cycle monitoring of mean and standard deviation of SSH crossover differences for SARAL/AltiKa using radiometer wet troposphere correction and geographical selection (|latitude| < 50°, bathymetry < -1000 m and ocean variability < 20 cm rms).*

Figure 56 shows the monitoring of the pseudo datation bias for SARAL/AltiKa and Jason-2 on a cycle basis. On average SARAL/AltiKa has a slightly larger pseudo time-tag bias than Jason-2, around -0.03 ms, but which appears to be more stable over time.

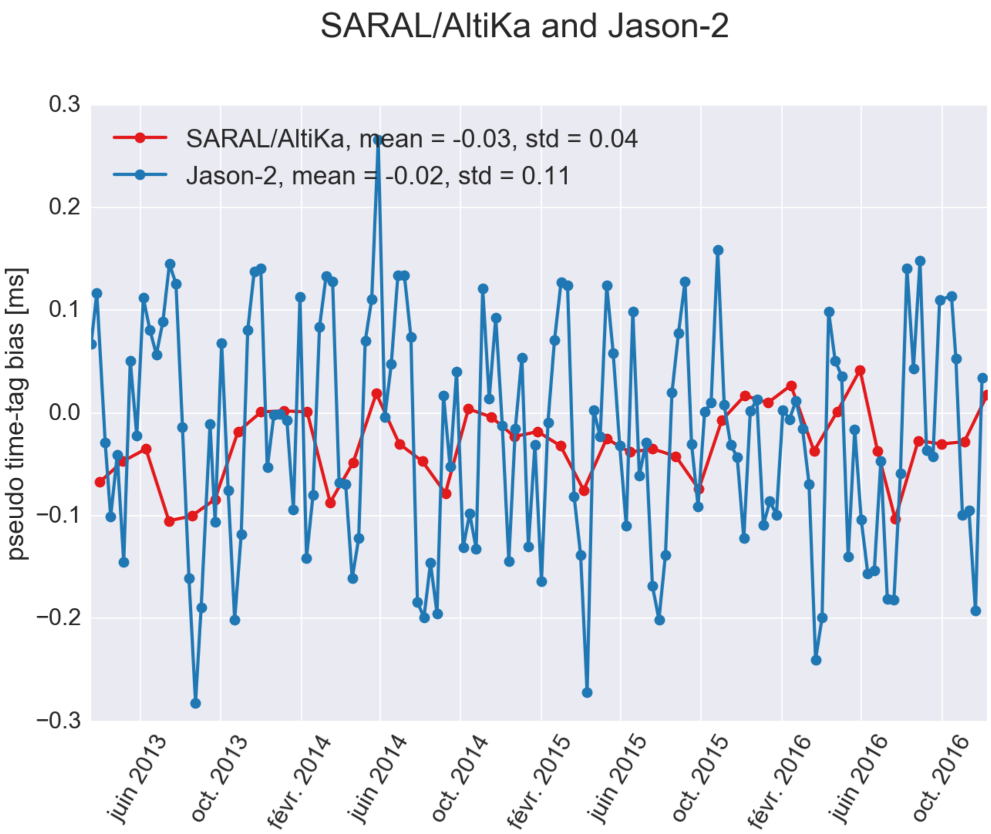

Figure 56: *Cycle per cycle monitoring of the pseudo time tag bias for SARAL/AltiKa and Jason-2*

6. Sea Level Anomalies along-track analysis

6.1. Overview

The Sea Level Anomalies (SLA) are computed along track from the SSH minus the mean sea surface where the SSH is estimated as defined in the previous section (5.1.):

$$SLA = SSH - MSS$$

where the mean sea surface is the CNES/CLS 15 model.

Figure 57 shows two maps of SLA from SARAL/AltiKa and Jason-2 over one cycle of SARAL/AltiKa (here cycle 100). The two maps show very similar patterns.

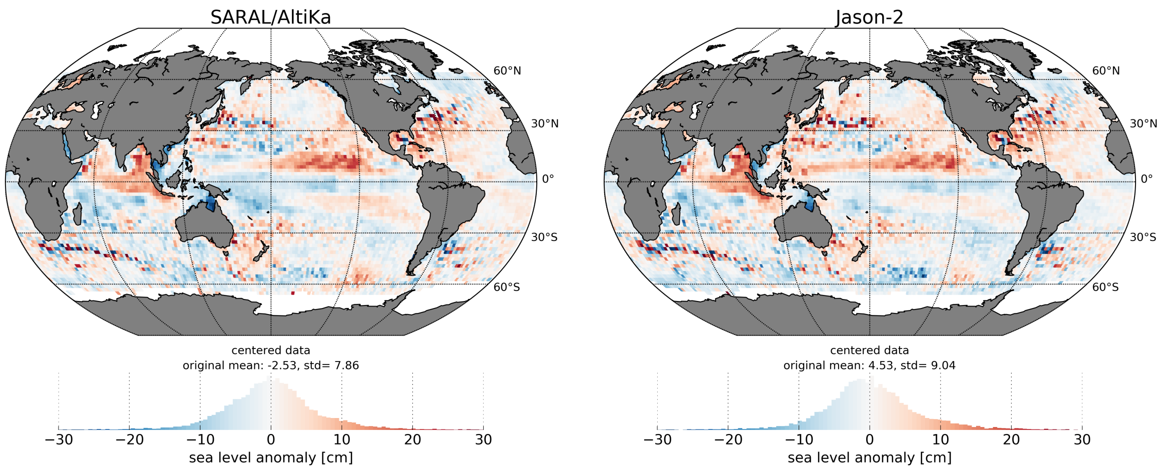

Figure 57: *SLA map for SARAL/AltiKa cycle 100 using the radiometer wet tropospheric correction [left] from SARAL/AltiKa data, and [right] from Jason-2 data over the same period.*

Computing differences between SARAL/AltiKa and Jason-2 allows for better appreciation of potential discrepancies between the two missions than individual maps. Figure 58 displays the average SLA differences between SARAL/AltiKa and Jason-2 over the first 36 cycles on SARAL/AltiKa, for the radiometer and the modeled wet tropospheric correction. Both maps show geographically correlated differences with amplitudes up to ≈ 2 cm. The patterns are very similar to the ones observed at SARAL/AltiKa/Jason-2 crossovers with a positive patch in the Atlantic Ocean and a negative one around Indonesia. The amplitude of the differences is slightly reduced when using the model wet tropospheric correction on both missions.

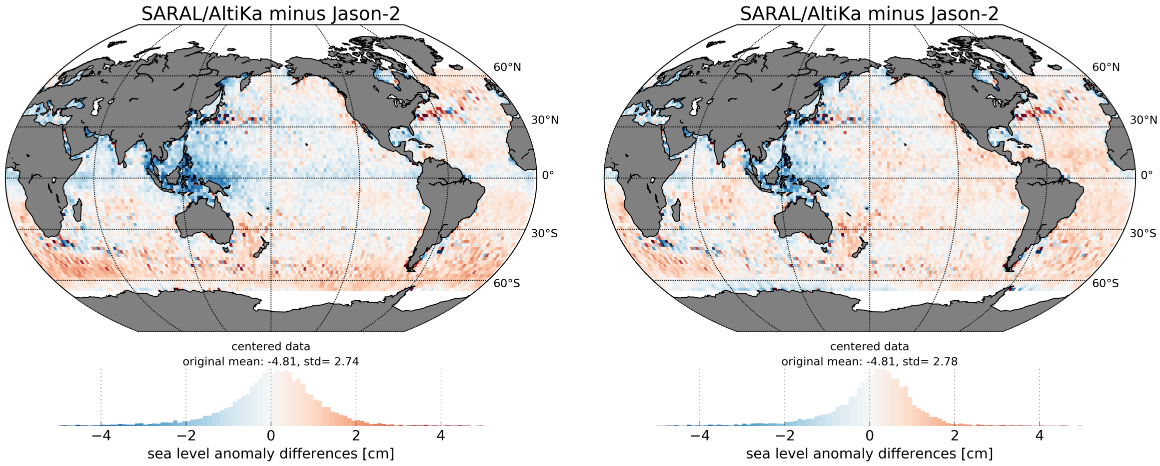

Figure 58: *Map of mean SLA differences between SARAL/AltiKa and Jason-2 using [left] the radiometer and [right] model wet tropospheric correction for the 36 first cycles of SARAL/AltiKa.*

6.2. Along-track SLA performances of Saral/AltiKa and Jason-2

Looking at along-track SLA provides additionnal metrics to estimate the altimetry system performances. The evolution of the mean SLA allows for the detection of shifts, drifts or geographically correlated biases, while looking at the SLA variance may also highlight changes in the long-term stability of the altimeter system performance. Figure 59 displays the temporal evolution of the mean and standard deviation of SARAL/AltiKa and Jason-2 SLA, while figure 60 shows the SLA difference between the two missions.

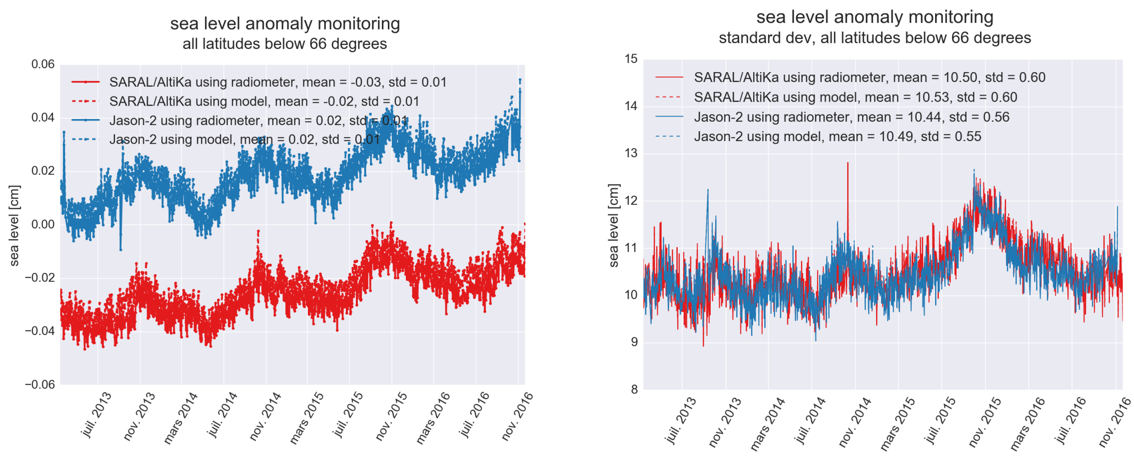

Figure 59: *Monitoring of daily mean [left] and daily standard deviation [right] of SLA of GDR data using the radiometer (plain lines) and the model (dotted lines) wet tropospheric corrections. Global statistics are estimated for all latitudes between* -66 *and* $66\,\mathrm{deg}$

SARAL/AltiKa and Jason-2 daily mean of SLA show similar signals and evolution. There is an offset between SARAL/AltiKa and Jason-2 SLA of around $-4.4\ cm$, which is consistent with multi-mission crossovers analysis. The standard deviation of daily mean global SLA averages is below $5\ mm$. No statistically significant drift is observed between the two missions. Switching from

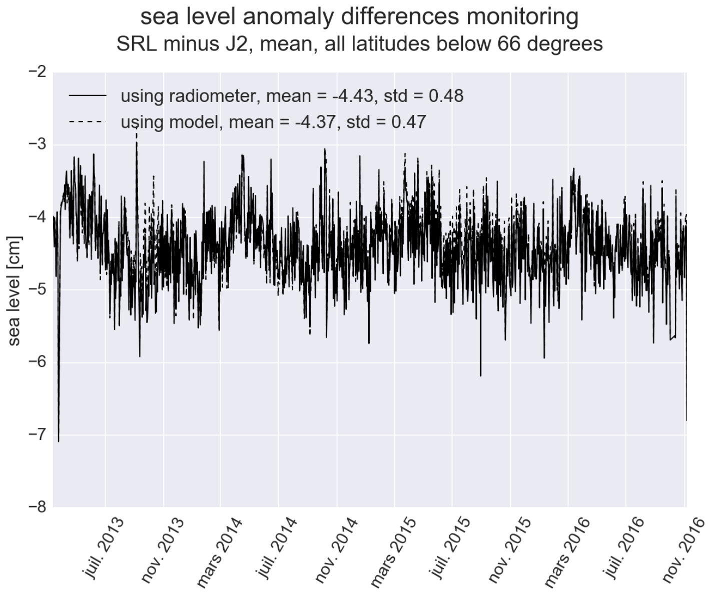

Figure 60: *Monitoring of the daily mean SLA difference between SARAL/AltiKa and Jason-2, using the radiometer and model wet tropospheric corrections.*

the radiometer to the model wet tropospheric correction has little impact on daily averages SLA differences between SARAL/AltiKa and Jason-2, as daily SLA variations are much larger than the difference between wet tropospheric corrections.

6.3. Along-track performances of the different product types (OGDR/IGDR/GDR)

SARAL/AltiKa products are available for three data types (with different latency and precision): OGDR, IGDR and GDR. These products show somes differences in the product content which are summarized in table 7). Figure 61 displays the evolution of the mean and standard deviation of global SLA, as it is in the different products currently available. There are several shifts on the mean OGDR and IGDR values:

- in Feb 2014, when OGDR and IGDR, changed from Patch 1 to Patch 2,
- in July 2014, due to mean sea surface and editing changes.

There is one shift on the mean GDR timeseries corresponding to a mean sea surface standard change from the 2011 to 2015 CNES/CLS MSS in June 2016. Regarding standard deviation, GDR products show the lower standard deviation with 10.9 *cm*, while IGDR and OGDR data show a higher SLA variability, which is expected from less accurate orbit solutions and some geophysical corrections.

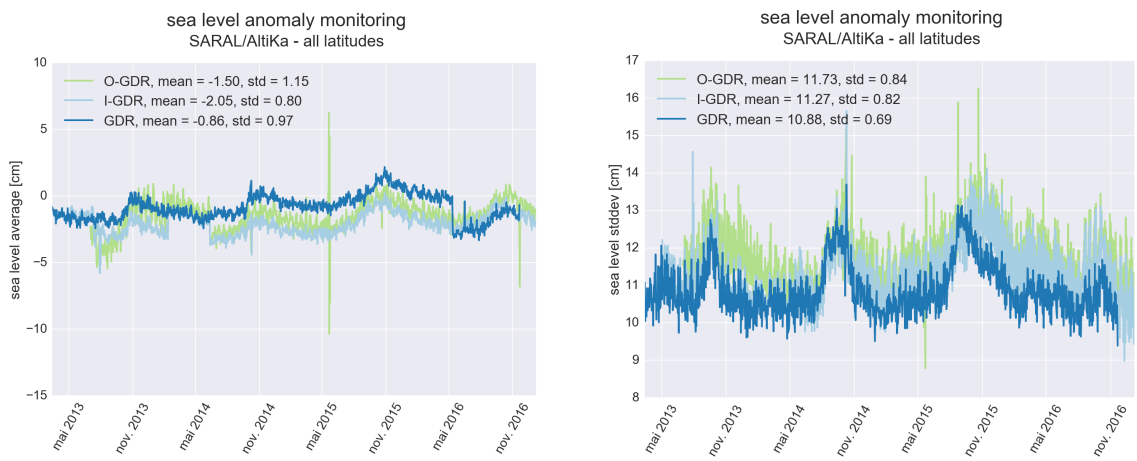

Figure 61: *Daily monitoring of the mean [left] and standard deviation [right] of global average SARAL/AltiKa SLA, using the radiometer wet tropospheric correction, for OGDR, IGDR and GDR products.*

6.4. SARAL/AltiKa as part of the GMSL record

SARAL/AltiKa data can easily be merged to the global Global Mean Sea Level (GMSL) record. Figure 62 presents two ways to do this. Left displays how SARAL/AltiKa blends in with the reference GMSL record while right is a zoom on the SARAL/AltiKa period where actual biases between missions are kept. With now more than three years of data, and Jason-2 available over the same period, we can give some credit to global sea level trends estimates. Over the same period, and the same area, SARAL/AltiKa and Jason-2 show very similar global mean sea level rise rates at 6, 1 and 6, 6 mm/yr respectively.

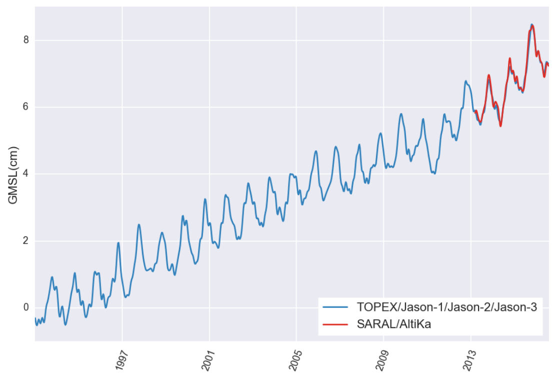

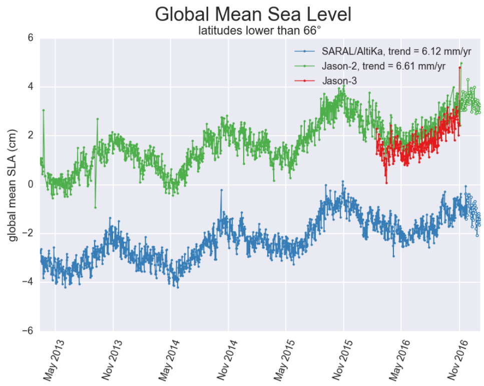

Figure 62: *[left] SARAL/AltiKa global mean record compared to the reference global mean sea level from TOPEX/Poseidon, Jason-1 and Jason-2 and Jason-3, and [right] a zoom on the SARAL/AltiKa period with biases between missions retained*

7. Particular investigations

The present section of the report presents the output of several particular investigations performed in 2016. These investigations include:

- a preview of the future SARAL/AltiKa performance,
- an assessment of the impact of using thrusters rather than reaction wheels during maneuvers,
- an assessment of the impact of the change to a drifting orbit on data availability and quality,
- an investigation on the dependency of SARAL/AltiKa noise level on waves.
- an experimental method to reduce submesoscale errors.

7.1. Maneuver impacts on data quality

From May 2015 onwards, following the issues on reaction wheels, the pre and post maneuver platform rotations have been performed using thrusters instead of RW. We performed a quick investigation to look for impacts on data from this new way of performing station keeping maneuvers. For each pass with maneuver, we estimated the data loss rate, the data editing rate and the variance of remaining SLA measurements.

Figure 63 displays the percentage of missing and edited data on all passes with maneuvers since the beginning of the mission (and up to April 2016). On average, only 4.8% of data were missing when maneuvers where performed using the reaction wheels. When thrusters are used the percentage of missing data rises to 13%, and clearly indicates a different behavior. A majority of thrusters maneuvers show between 10 and 20% of missing data while reaction wheel maneuvers generally show very few missing data, except for three maneuvers. The data editing rate also rises after the maneuver strategy change, rising from 25 to 41%, however there is a large variance from pass to pass and this result is not statistically significant. No change was observed on the variance of remaining SLA measurements, suggesting that the editing process efficiently removes erroneous data points.

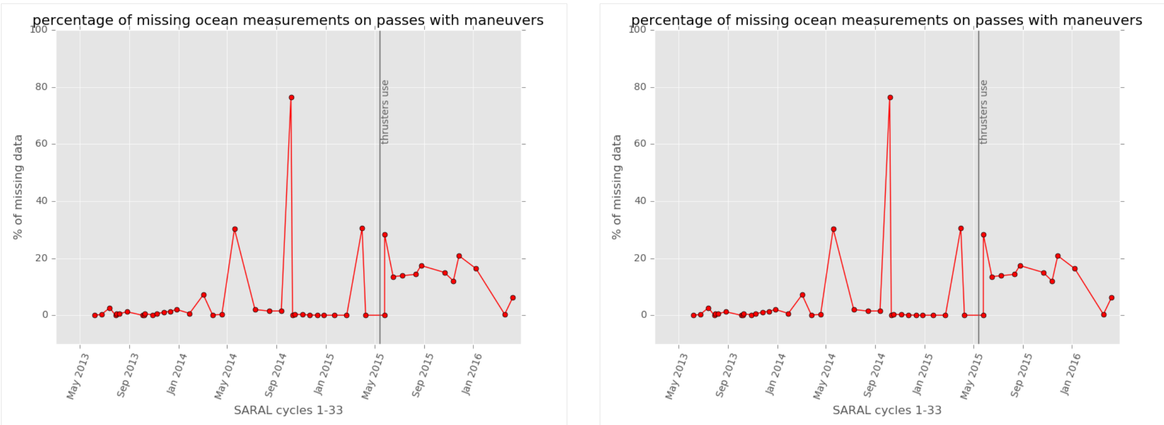

Figure 63: *percentage of [left] missing and [right] edited data on passes with maneuvers, the vertical line indicates the date after which thrusters were used*

7.2. Performance assessment of SARAL/AltiKa drifting phase

On July 4th 2016, SARAL/AltiKa performed its last maneuver: altitude was raised by one kilometer and the spacecraft is now freely drifting, with no station keeping. This started SARAL/AltiKa's drifting phase: there is no 35-day repetitive cycle anymore. However products are still generated consistently with the repetitive phase with cycles of 35 days and 1002 passes. To separate the drifting from the repetitive phase, cycles were renumbered beginning at cycle 100. Cycle 35 is the last repetitive cycle, it has only 522 passes and ends on 04-07-2016 at 11:12:20. Cycle 100 which starts on 04-07-2016 at 12:52:57 is the first cycle of the drifting phase. For this orbit change, product dissemination was stopped in order for Cal/Val team to check the data quality. This took a few days, and as no large impacts on data quality were found, product dissemination quickly resumed. In this section, we present the results of the investigations performed on Cal/Val side to check the quality of the first O/IGDR data of SARAL/AltiKa cycle 100: data availability, parameter monitoring and analysis of the resulting SLA content. The analysis were performed on a relatively short time span, but other results presented in this report based on a longer period and on GDR data (sections 3 and 4) confirm that the system performance remains nominal during the drifting phase.

7.2.1. Data availability

Data availability is key mission performance metric. The final data availability rate results from both missing and edited measurements. Continuity of missing data and edited data rates were checked at the orbit change. Figure 64 displays the monitoring of the percentage of available and edited measurements (thresholds only) per pass for IGDR data around the maneuver. As now theoretical ground track is not available for the drifting phase, the determination of missing measurements is performed with respect to a ground track resampled at 1Hz from predicted orbit files. Both missing and edited data rates are consistent before and after the maneuver. On this sample, the editing rate appears slightly lower during the drifting phase than during the repetitive phase, this behavior was not confirmed with GDR data (see section 3.2.3.).

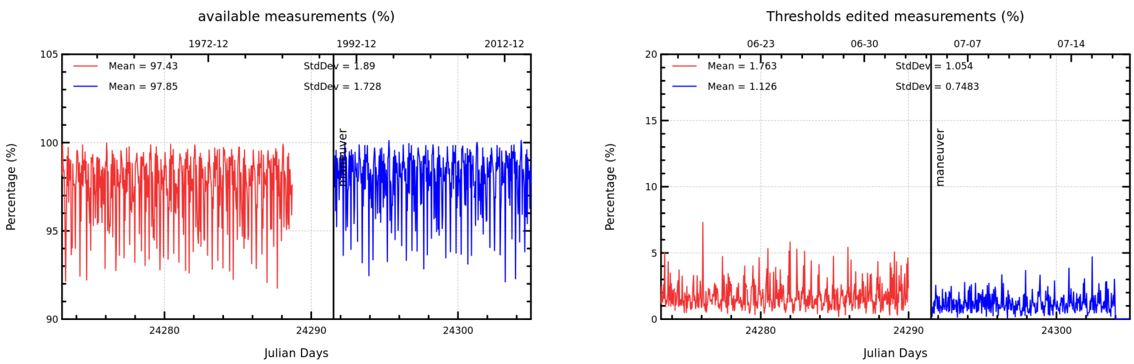

Figure 64: *percentage of available [left] and edited data [right] per pass around the start of SARAL/AltiKa drifting phase*

The geographical distribution of edited points is also consistent with what is observed during the repetitive phase, as shown on figure 65 which compares edited data from SARAL/AltiKa cycle

100 to Jason-2 over the same period. There is no sign of a systematic regional editing bias at the beginning of the drifting phase. This was confirmed by GDR data later on.

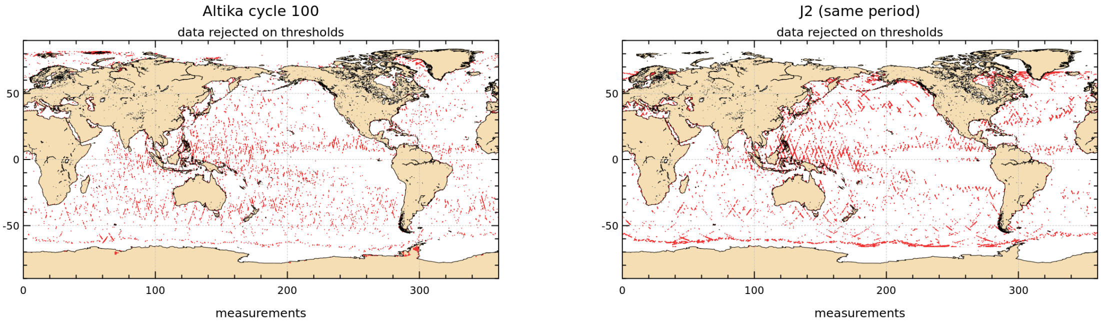

Figure 65: *map of edited data on thresholds for SARAL/AltiKa [left] and Jason-2 [right] estimated over the same period at the beginning of SARAL/AltiKa cycle 100*

7.2.2. Altimeter parameters

The main altimeter parameters where checked to detect and before/after maneuver inconsistencies. Figures 66 and 67 displays the temporal evolution of the number and standard deviation of the high resolution measurements used in the 1Hz compression algorithm for the range, backscatter and significant wave height. No change is observed on these parameters: the mean number of elementary measurements and their standard deviations remain the same before and after the orbit change for all three parameters considered here. In addition the parameters themselves, at least for backscattering and waves remain largely unchanged, as shown on figure 68. Per pass variances are not shown here but also remain unchanged. The results presented here were confirmed by analysis of GDR data later on.

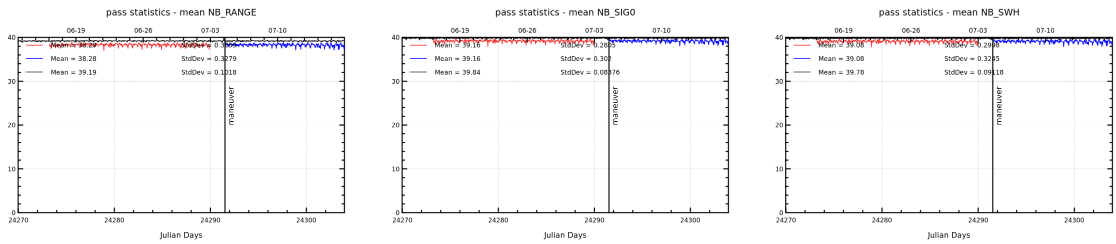

Figure 66: *Evolution of the mean per pass of the number of elementary measurements of the range [left], backscatter [middle] and SWH [right], before (red) and after (blue) the orbit change. Jason-2 data (with a factor two) is indicated in black*

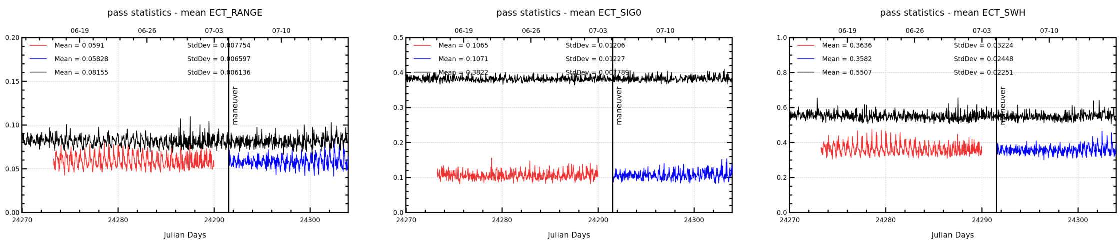

Figure 67: *Evolution of the mean per pass of the standard deviation of elementary measurements of the range [left], backscatter [middle] and SWH [right], before (red) and after (blue) the orbit change. Jason-2 data is indicated in black*

Another closely monitored parameter on SARAL/AltiKa is the mispointing (section 4.3.), and of course we checked that the maneuver had no impact on mispointing statistics. Figure 69 displays the evolution of the mean and standard deviation of the squared mispointing angle. No change of the statistics is observed, however analysis on a longer period on GDR data does show that mispointing events can still occur randomly in the drifting phase of SARAL/AltiKa.

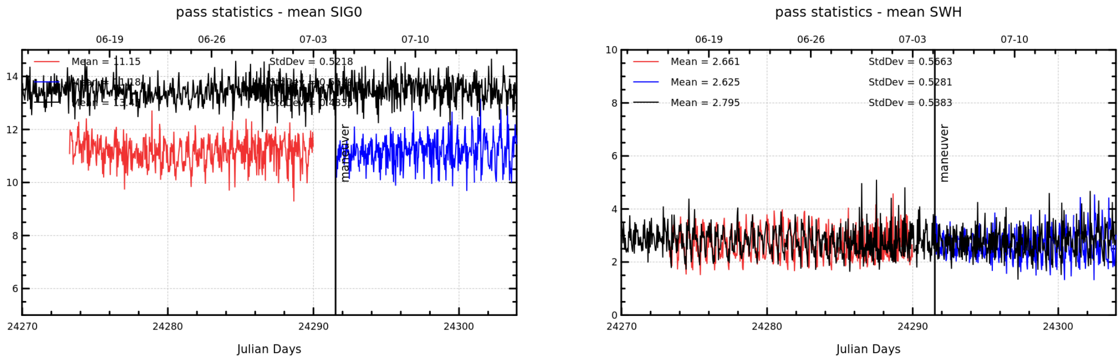

Figure 68: *Evolution of the mean per pass of backscatter [left] and SWH [right], before (red) and after (blue) the orbit change. Jason-2 data is indicated in black as a reference.*

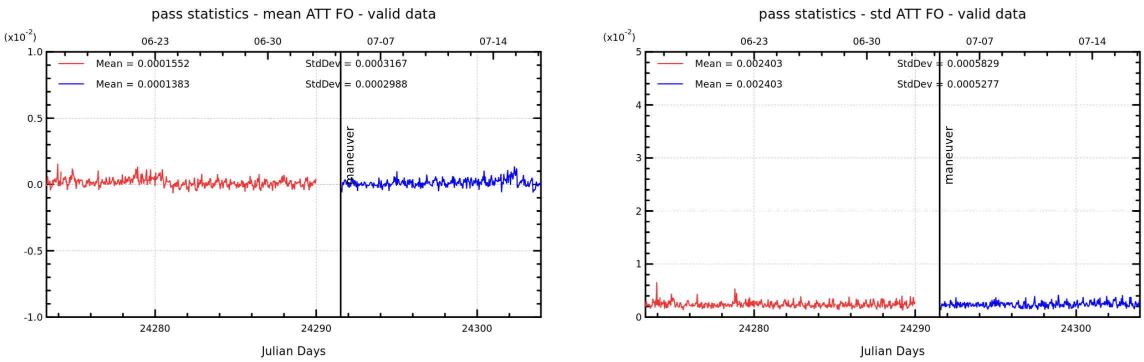

Figure 69: *Evolution of the mean [left] and standard deviation [right] per pass of the squared off-nadir angle from waveforms, before (red) and after (blue) the orbit change.*

7.2.3. Radiometer parameters

Radiometer parameters were also monitored carefully before and after the orbit change, in order to highlight any impact on the brightness temperatures, that would result in a change on the wet tropospheric correction. Regarding brightness temperatures, mean values go from 174.2 to 174.9 K for the 23.8 GHz channel and from 171.4 to 171.7 K for the 35 GHz channel, with a standard deviation of at least 3 K which makes the changes non significant over the available time span. As a result, the differences between the radiometer and the model wet tropospheric corrections do not change neither regarding the mean nor the standard deviation with the orbit change, as shown on figure 70. The mean radiometer minus model wet tropospheric difference remain around 6 mm, with a standard deviation around 1.6 cm.

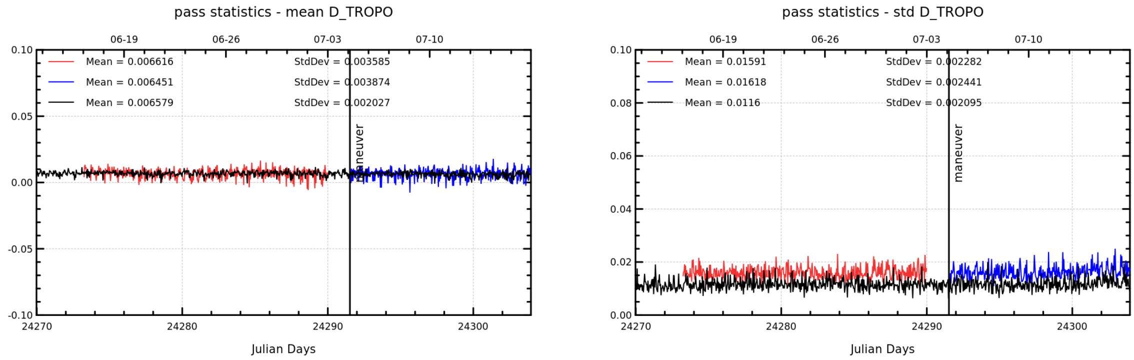

Figure 70: *Evolution of the mean [left] and standard deviation [right] per pass of the differences between the radiometer and the model wet tropospheric corrections, before (red) and after (blue) the orbit change. Jason-2 data is plotted in black as a reference.*

7.2.4. Sea level anomaly

With no measurable impacts on altimeter or radiometer parameters, one expects a seamless transition when considering sea level anomalies. This is verified when comparing SLA statistics right before and after the maneuver, as shown on figure 71. No shift or sudden variance change is observable on SARAL/AltiKa SLA statistics at the beginning of the drifting phase.

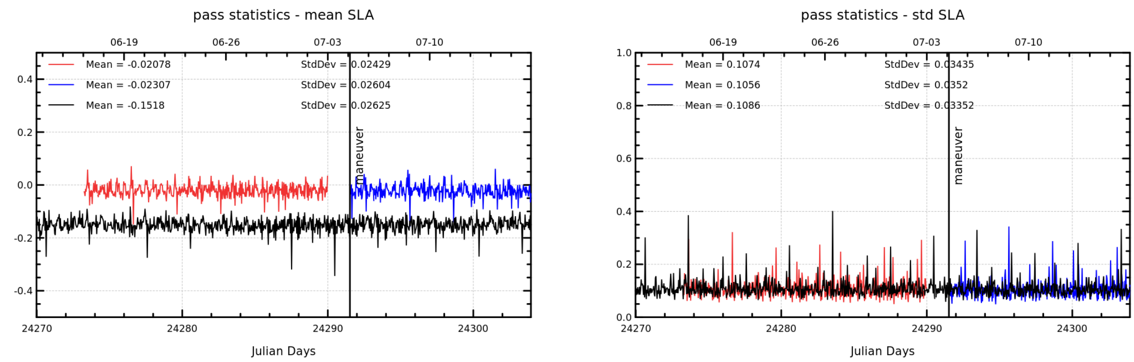

Figure 71: *Evolution of the mean [left] and standard deviation [right] per pass of sea level anomaly, before (red) and after (blue) the orbit change. Jason-2 data is plotted in black as a reference.*

However this does not mean that there is no impact at all of a drifting orbit on SLA estimation. Figure 72 compares the results of three spectral analysis performed with a similar methodology on SARAL/AltiKa data. During cycle 5, SARAL/AltiKa was precisely maintained over the historical ERS/Envisat ground track where the MSS is well known. With a now drifting orbit, SARAL/AltiKa overflies regions where the MSS has more error, due to a lower number of historical observations, which results in an energy increase at small scales (roughly below 100 km, blue curve on figure 72). Switching to a more recent and more accurate MSS model, the CNES/CLS 15 reduces this error, with a much lower energy increase at small scales (green curve).

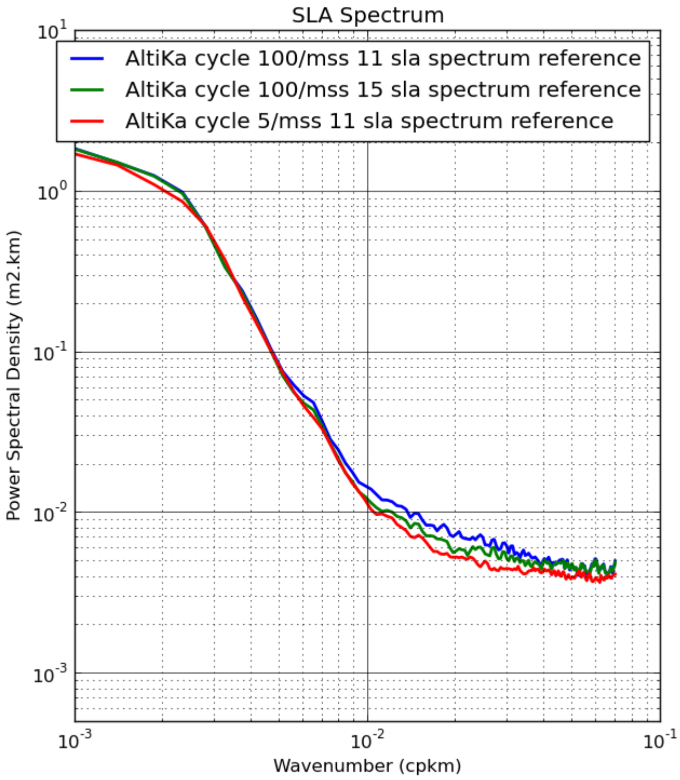

Figure 72: *Sea level anomaly power spectra for SARAL/AltiKa cycle 5 and cycle 100, using the CNES/CLS 11 and 15 MSS models for the latter.*

7.2.5. Other considerations

The July 4th maneuver raised the spacecraft's altitude by 1 km. This orbit should provide good mesoscale observation capabilities, without the need for any station keeping maneuvers. This choice is supported by Dibarboure [1, Dibarboure et al., 2017], where they predicted an orbital decay rate and the corresponding sub-cycle periodicity and associated sampling. How is the actual orbit performing with respect to these predictions ?

Figure 73 is adapted from Dibarboure [1] with the observed POE overlaid in red. The actual orbital decay is in the lower range of the predictions with about $-30\ cm/day$. This indicates that SARAL/AltiKa will achieve a good mesoscale sampling for a longer period than expected (provided that no other issue impacts the mission).

Regarding the time/space sampling provided by this new orbit, figure 74 displays equator crossings in the longitude/time plane. The left panel corresponds to the 35 days repeat cycle while the right panel is estimated from cycles 100 & 101 of the SARAL/AltiKa drifting phase. This illustrates how the ocean sampling changes from the repeat to the drifting phases:

- there is no more exact repeat after 35 days,

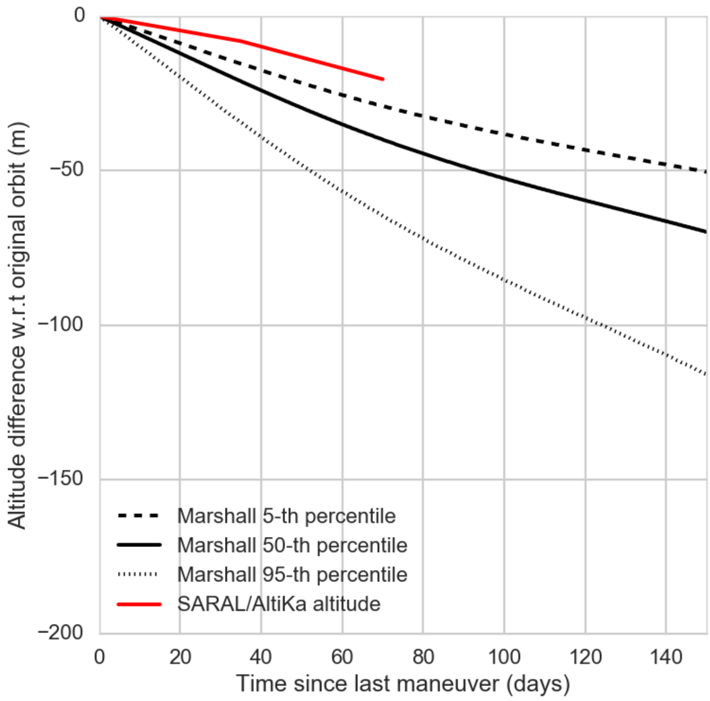

Figure 73: *Predicted and observed orbital decay for SARAL/AltiKa drifting phase*

- periods of subcycles are changed (from 16 to 13 days).

For an easier view of the current SARAL/AltiKa spatial sampling, figure 75 displays all measurements from descending SARAL/AltiKa tracks in a small area around Corsica for cycles 100 to 104. The spatial sampling is relatively well distributed and data gathered during the SARAL/AltiKa drifting phase will therefore be valuable for future mean sea surface models estimation.

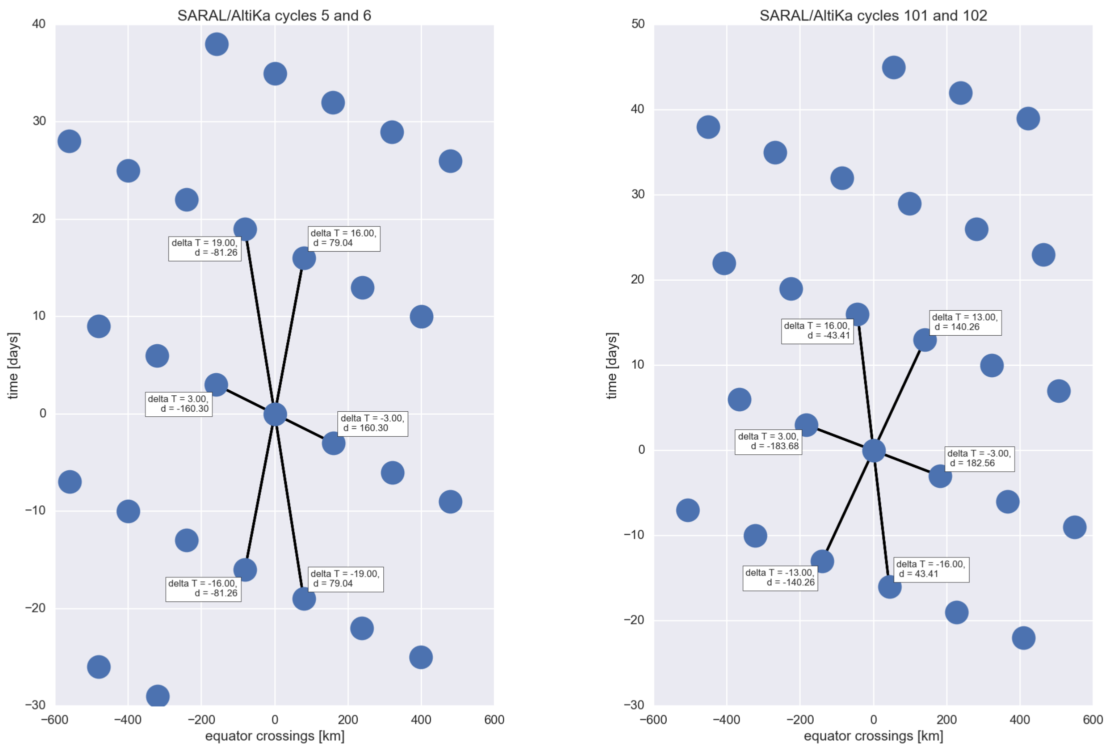

Figure 74: *Evolution of the mean [left] and standard deviation [right] per pass of sea level anomaly, before (red) and after (blue) the orbit change. Jason-2 data is plotted in black as a reference.*

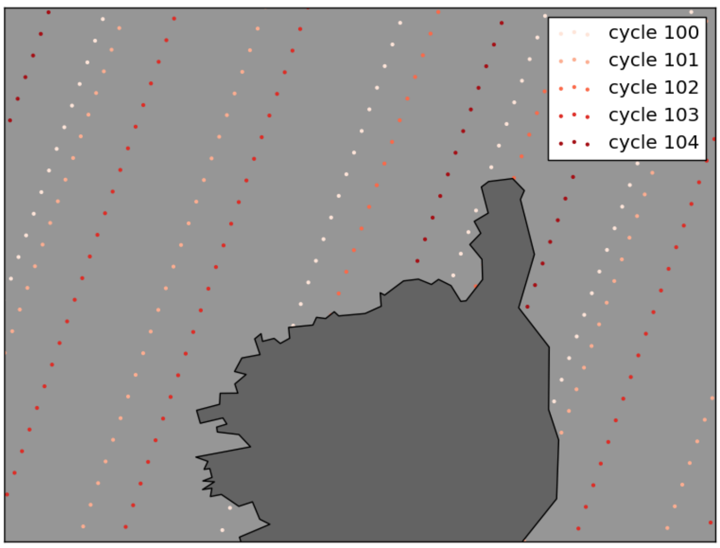

Figure 75: *SARAL/AltiKa drifting phase sampling around Corsica*

7.3. A preview of SARAL/AltiKa's future performance

SARAL/AltiKa GDR-E products will include a new algorithm for the wet tropospheric path delay retrieval, based on a five parameters inversion. At the moment only three parameters are used, the two radiometer brightness temperatures and the backscatter coefficient. Here we briefly evaluate the performance increase of two wet tropospheric path delay retrieval algorithms that could be included in future product evolutions. The first one is based on a observation/model training sample where actual observations are compared to modeled outputs (called P3) while the second one is based on a fully modeled training sample (called P4). Please note that the naming used here does not presume of any inclusion of these algorithms in future reprocessings of SARAL/AltiKa data.

Figure 76 presents the mean and standard deviation at crossovers for the current product, and the two wet tropospheric correction solutions presented above. Clearly these updated algorithms improve the performance at crossovers, with a reduction of the standard deviation of SSH differences. The overall variance reduction observed is unequally distributed over the global ocean. Figure 77 displays the map of SSH differences variance reduction when moving from one algorithm to another. While the P3 algorithm reduces both the bias and the variance with respect to the ECMWF model, this is not the case for the P4 algorithm, despite a better performance at crossovers. P3 and P4 provide a variance reduction at mid-latitudes. The overall impact is almost always a variance reduction, unless for a few pixels in the Southern Ocean and at the coast.

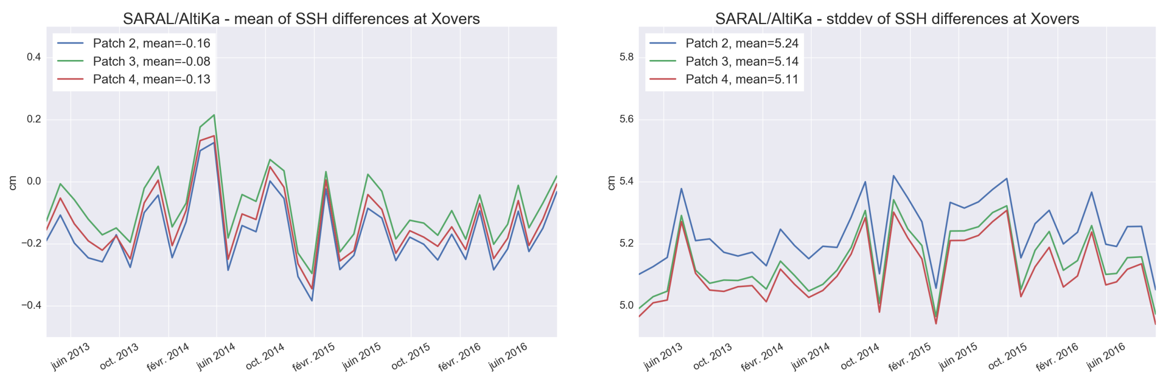

Figure 76: *[left] mean and [right] standard deviation of SSH differences at crossovers for SARAL/AltiKa using three different wet tropospheric path delay retrieval algorithms*

When evaluating wet tropospheric corrections, a classical approach is to compare them to the ECMWF model, both for the mean and standard deviation of differences. Figure 78 displays the daily monitoring of global mean radiometer minus model wet tropospheric path delay differences. While P3 effectively reduces the mean and standard deviation of the wet tropospheric correction with respect to the model, P4 reintroduces a bias and increases the RMS of differences. Moreover, there is a period around December 2015 that shows a sudden increase in the RMS of wet tropospheric differences. This likely indicates that some errors remain to be corrected, either in the correction itself, or in the way its performance was evaluated here (for example no extra editing was performed here but a first analysis suggests that the error might come from data points at very high latitudes).

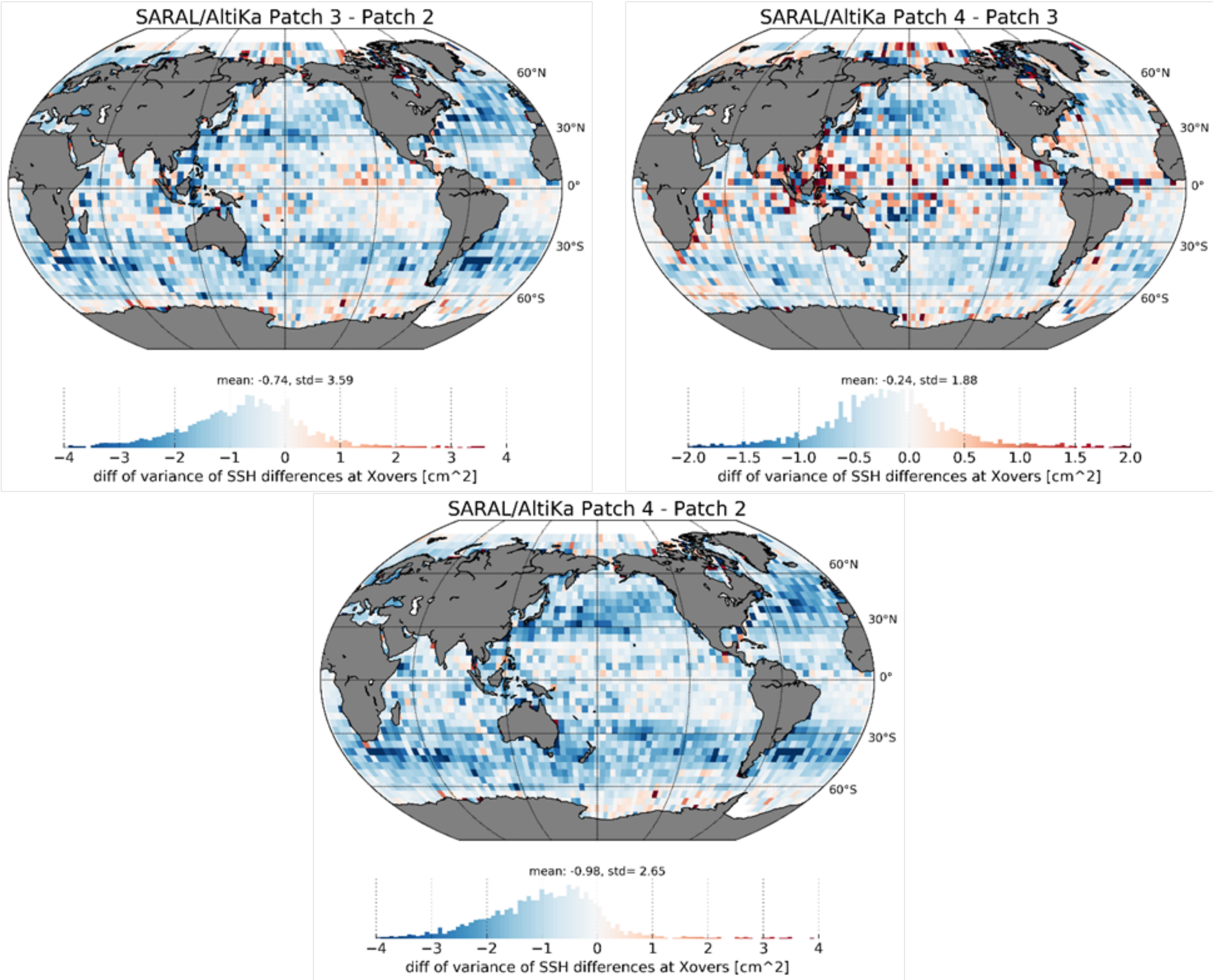

Figure 77: *map of the variance reduction at crossovers from P2 to P3, from P3 to P4 and from P2 to P4*

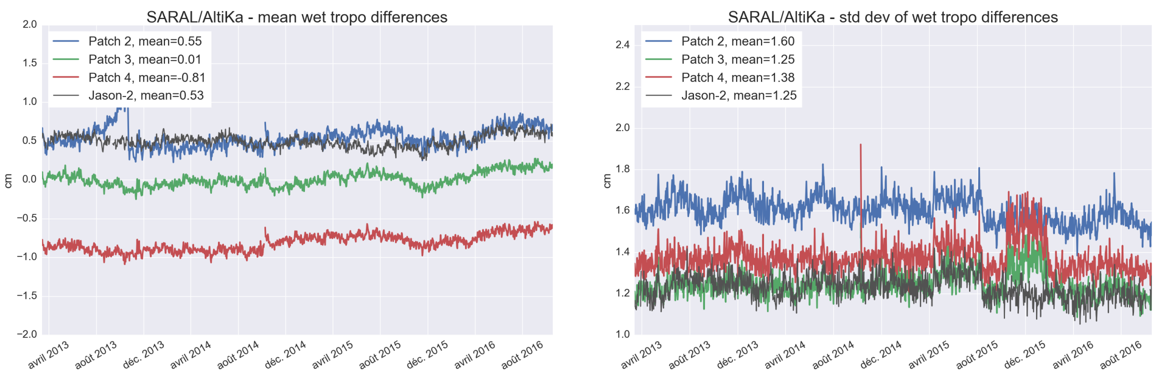

Figure 78: *[left] mean and [right] standard deviation of daily radiometer minus model wet tropospheric differences for SARAL/AltiKa using three different wet tropospheric path delay retrieval algorithms*

7.4. SARAL/AltiKa noise level dependencies to swell and rain

Here we investigate SARAL/AltiKa noise level dependencies to SWH, rain rates and swell characteristics derived from a model. This investigation has been performed on SARAL/AltiKa 1 Hz data for range and backscattering noise levels. Here we consider that noise levels are accurately measured by the standard deviation of high rate elementary measurements (called hereinafter 'range std' and 'sigma0 std' respectively).

To go beyond the relation between range noise level and SWH, we use Wave Watch III model outputs (see Tolman [21, 22]) to investigate the impact of swell height, direction and period on the noise level. Rain rates derived from colocations with meteorological missions are also used to investigate the sensitivity to rain events.

Indeed, results from Sentinel 3A which uses a Synthetic Aperture Radar configuration showed a real impact of the swell direction and period on the range standard deviation. Do similar effects exist on SARAL/AltiKa, which is a conventionnal nadir-looking altimeter, but with a reduced footprint and different frequency with respect to Jason-2?

The results presented here are based on the analysis of two years à SARAL/AltiKa GDR data from cycle 1 to cycle 21 (2013-03-14 to 2015-03-19). Only valid measurements, according to the Cal/Val validity flag are considered. Among the criteria of this flag, at least 20 elementary 40 Hz values of range and backscatter have to be valid, this guarantees that enough values are available to estimate statistically significant standard deviations.

To measure the dependency between the noise level Y and a parameter X, valid measurements are binned depending on X value and a regression is performed to get a model of the dependency $Y = f(X)$. We define the K_{X-Y} coefficient as the percentage of the distribution of Y std that may be explained (and thus possibly corrected) by X using the previously fitted model.

7.4.1. Significant wave height

The significant wave height (SWH hereinafter) is directly extracted from the GDR products. It is derived from the leading edge of the 40 Hz waveforms. All the valid SWH retracked are averaged to produce the 1 Hz SWH.

The strong dependance between range std and the SWH already has been largely studied (see figure 79 left). A simple linear regression is sufficient to fit it with a resulting trend of 1.23 cm/m. The $K_{SWH-range}$ obtained is 37.3 %, making more than a third of the range std distribution explainable by the SWH.

Sigma0 std variations due to the SWH are far more complicated to fit (see figure 79 right). Indeed the specular surface of ocean at small SWH can lead to sigma blooms. An inverse function is necessary to describe correctly the left (specular) part of this curve. Above 2 meters, sigma0 seems quite independant of SWH even if an additional trend of 0.0022 dB/m improves slightly the fit. The resulting $K_{SWH-sigma0}$ is 1.2% signaling a weak dependency between backscattering noise and SWH.

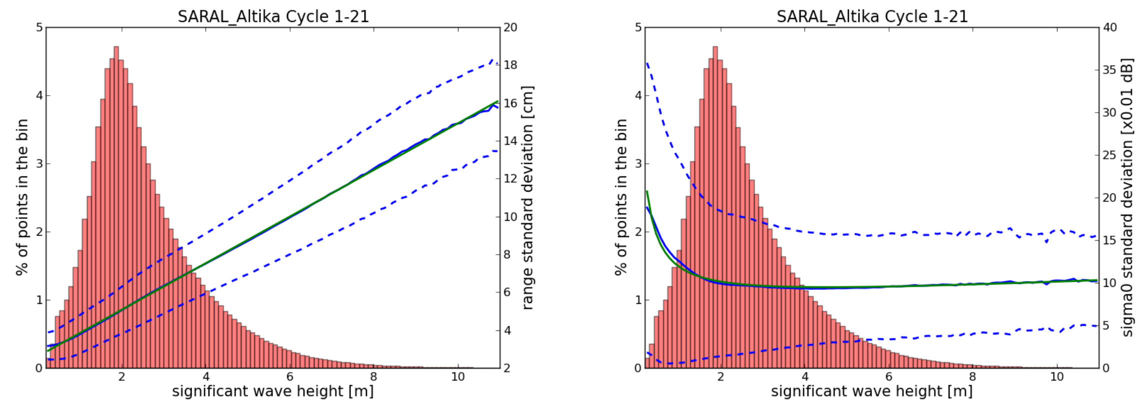

Figure 79: *Variations of range std (left) and sigma0 std (right) against the SWH. The red chart bars set for the fraction of measurement in each bin (number of bins = 100). The blue plain (respectively dotted) line is the mean value (respectively mean value ± standard deviation) of range std in the bin. The green line is the fitting model.*

7.4.2. Rain rate

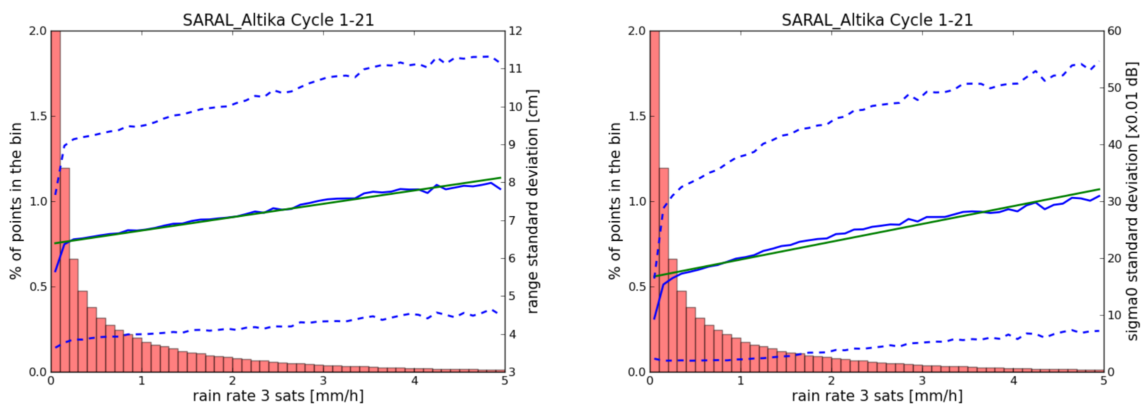

Figure 80: *Variations of range std (left) and sigma0 std (right) against the rain rate. The red chart bars set for the fraction of measurement in each bin (number of bins = 50). Please, note that the first bin correponding to dry measurements is truncated on the plot as it containts more than 70 % of the measurements points. The blue plain (respectively dotted) line is the mean value (respectively mean value ± standard deviation) of range std in the bin. The green line is the fitting model.*

Rain rate values are based on 3 meteorological satellites measurements: SSMIS-F16, SSMIS-F17 and Windsat. As local rain is relatively ephemeral, a maximum time delay of one hour is fixed between the colocated acquisition of SARAL/AltiKa and of the meteorological satelites. Using this time threshold results in actual rain rate colocations for only 70 % of the SARAL/AltiKa 1 Hz measurements.

The dependency of range std on the rain rate is fitted with a 0.35 cm/(mm/h) trend, in figure 80. The coverage on the range std distribution is only 1.715 cm which is far less significant than with the SWH resulting to $K_{rain-range} = 0.8\%$. Nevertheless, $K_{rain-sigma0} = 3.7\%$ showing a significant influence of the rain rate on the backscatter coefficient noise.

For both cases, although a linear regression is used, one may note a clear non linearity for the first bin (containing ≈ 70 % of measurements), where the linear regression used does not perform well. A better model for these dry points may increase significantly the percentage of the noise exmplained by rain rate (K_{rain-Y}).

7.4.3. Swell components

The swell components used here are taken from the Wave Watch III model version 5.16, see [21, 22]. The Ifremer FTP server distributes monthly grids of swell height, direction and period. These grids are based on a Mercator projection with a 0.5^o x 0.5^o resolution. For each measurement point, the Wave Watch III model parameter is lineary interpolated in space and time from the grid. Concerning direction, the grid contains the angle between swell direction and North which is converted to relative angle to the local ground track direction.

As the swell height is very close to the significant wave height, it reveals the same behavior with a correlation of 0.97 between the two parameters. We do not develop these results further.

No evident dependency of sigma0 std with respect to swell direction is observed (see fig. 81). Concerning the range std variations, $K_{swellD-range} = 0.7$ % would be explainable by the direction. The maximum of the model is around 102^o which is statistically more represented in the bins. Therefore, it suggests that both, the range std and the sigma0 may be totally independant to the swell direction as it is expected for conventionnal altimetry where the scene has a cyclindrical symmetry.

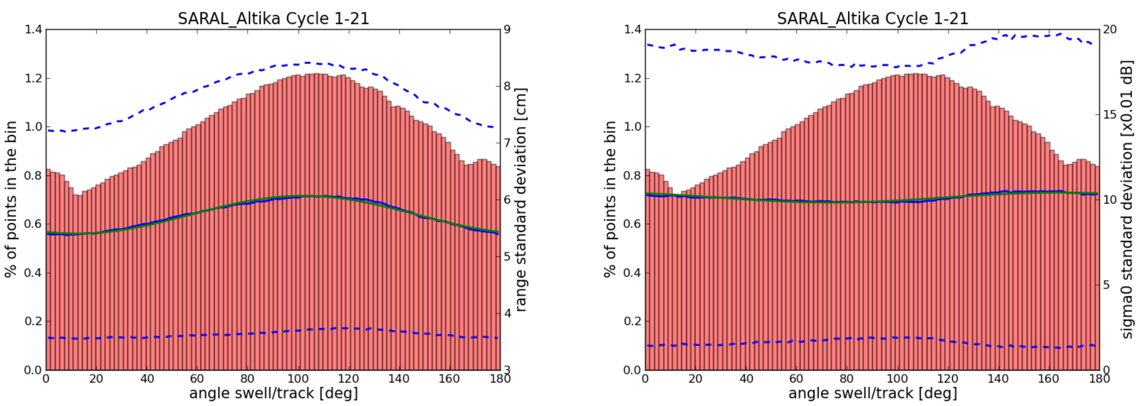

Figure 81: *Variations of range std (left) and sigma0 std (right) against the swell direction. The red chart bars set for the fraction of measurement in each bin (number of bins = 100). The blue plain (respectively dotted) line is the mean value (respectively mean value ± standard deviation) of range std in the bin. The green line is the fitting model.*

At last, figure 82 shows that a 2^{nd} degree polynomial is needed to fit correctly the dependance of range std and sigma0 std on swell period. Despite allowing for this complexity, the extreme bins of the period range which contains statistically few measurements points remain quite far from the model. For the range std, $K_{swellP-range} = 16.9$ % is obtained, about half of $K_{SWH-range}$. The dependance of sigma0 std on swell period results in a fit which has the minimum value at the median swell period, 6.5 s. But this would not be able to explain more than $K_{swellP-sigma0} = 0.5$ %.

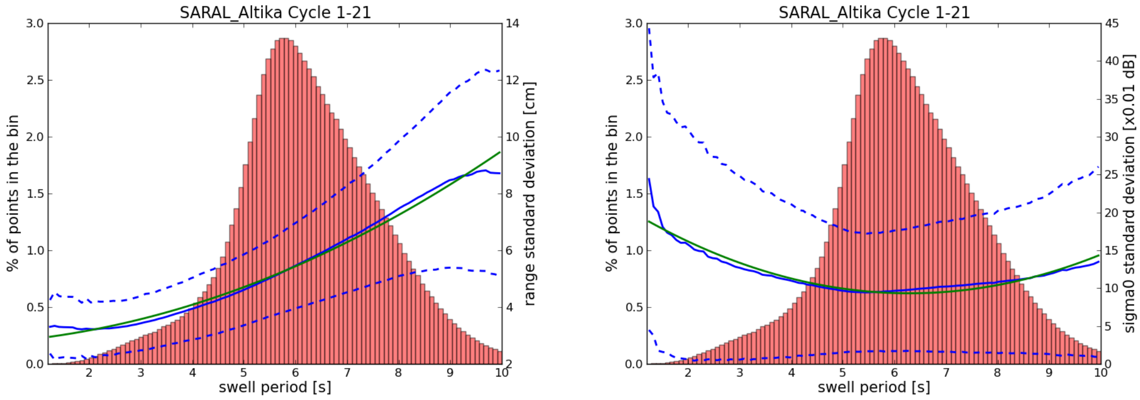

Figure 82: *Variations of range std (left) and sigma0 std (right) against the swell period. The red chart bars set for the fraction of measurement in each bin (number of bins = 100). The blue plain (respectively dotted) line is the mean value (respectively mean value ± standard deviation) of range std in the bin. The green line is the fitting model.*

7.4.4. Interdependance between parameters

The parameters are not independant, thus the description of range std variations with several parameters is not the linear combination of the models of the different single parameters. Table 8 sums up the correlations between the range std modeled with the different parameters.

range std	SWH	rain	SH	SD	SP
SWH	1.0	0.04	0.97	0.16	0.63
rain		1.0	0.03	0.01	-0.02
SH			1.0	0.18	0.63
SD				1.0	0.05
SP					1.0

Table 8: *Average of the correlations between the range std modeled values obtained from the different parameters, for cycles 1 to 21. SWH, rain, SH, SD and SP respectively set for significant wave height, rain rate, swell height, swell direction and swell period.*

The strong correlation between the significant wave height and the Wave watch 3 swell height was expected. This table also shows a quite strong correlation between the swell period and the significant wave height. On the other hand, the rain rate seems not to be correlated with any other parameter. The swell direction would have a slight correlation with the SWH, but this may be due to a statistical bias.

As SWH is the parameter that explains the larger part of the noise variance, it is fitted in association with the others parameters one by one. The results obtained are summarized in table 9. Note that the individual K_{SWH} and K_{param} are determined using the model of the single parameter but only on the measurements which are valid for both SWH and the parameter. It explains why the K value may be slightly different with respect to previous sections.

Parameter	K_{SWH}	K_{param}	K_{tot}
Rain rate	37.37 %	0.59 %	37.79 %
Swell height	40.16 %	36.18 %	39.77 %
Swell direction	40.65 %	0.76 %	40.68 %
			.../...

Parameter	K_{SWH}	K_{param}	K_{tot}
Swell period	40.16 %	22.77 %	40.20 %

Table 9: *modeling the range std with significant wave height and another parameter. K_{SWH},K_{param},K_{tot} are respectively the fraction of range std dispersion explained by SWH, the parameter and the combination.*

At first, one can observe that the combined Swell height and SWH have a lower K than SWH alone. It clearly shows the numerical limit of the optimization algorithm (Levenberg-Marquardt) which cannot converge properly on such dependant parameters. For swell direction and swell period, the K_{tot} does not have a significant increase with respect to K_{SWH}. Concerning swell period which has a single $K_{swellP} = 22.7$ % for a correlation of 0.63, it demonstrates that the dependance of range std on swell period is only due to the covariance with SWH.

At last, adding the rain rate to the range std modeling with SWH results in a very small increase of the K from 37.37 % to 37.79 % ($\Delta K = 0.42$ %) but quite significant with respect to the $K_{rain-range}$ = 0.59 %. According to the correlation between SWH and the rain rate (C = 0.04), one can expect to have a ΔK closer to 0.59 %. In further investigations, this might be improved by providing a better model for the shift on the dry point 80.

7.4.5. Seasonal variations

The variations cycle by cycle of the $K_{X-range}$ values are displayed by figure 83. It clearly shows a seasonal cycle of these values. For SWH, it varies from 35 % in winter to 40 % in summer. The swell period model has an even larger amplitude oscillating beteween 14 % in winter and 23 % in summer. It is correlated with the annual variations of the range std. Nevertheless, the trend resulting from the SWH linear regression is likely constant in time as shown on figure 84).

Figure 85 shows the equivalent variations but for the sigma0 std dependency. Globally, a very similar annual cycle is retrieved even if the parameters amplitudes may differ. For instance, the seasonnal variations of $K_{SWH-sigma0}$ is very weak but still visible. On the other hand, the dependency on the swell period is negatively correlated with its maximum in winter-spring at $K_{swellP-sigma0}$ = 1 % and minimum in summer at $K_{swellP-sigma0} = 0.3$ %. This is actually consistent with the curved shape on the right panel of figure 82.

7.4.6. Summary of the noise level results

We performed an analysis of the noise level dependency of range and backscatter on swell and rain. The main results of this analysis are:

- The significant wave height is the main driver of the range std dispersion. A linear regression leads to a model which can explain 37 % of range std variations in average. The SWH

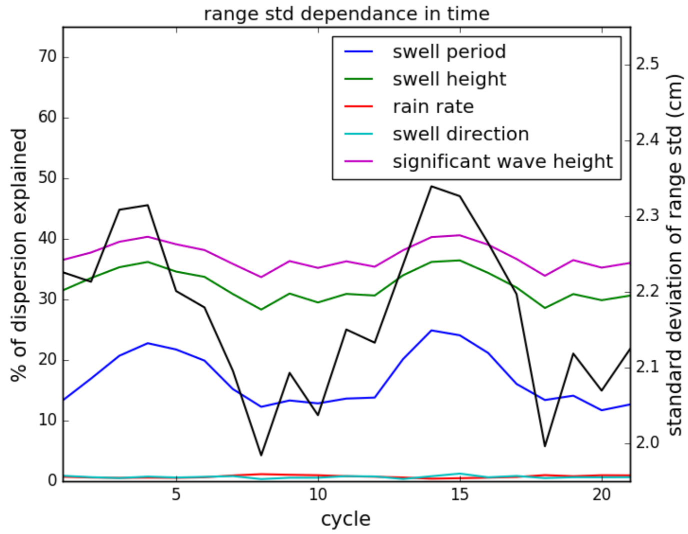

Figure 83: *The colored lines set for the dependance of range std on the different parameters along the cycles (1 to 21) of SARAL/AltiKa. It is the part (in %) of the range std that can be modeled with every single parameter refering to the left Y axis.The black line is the standard deviation of range std along cycles and refers to right Y axis.*

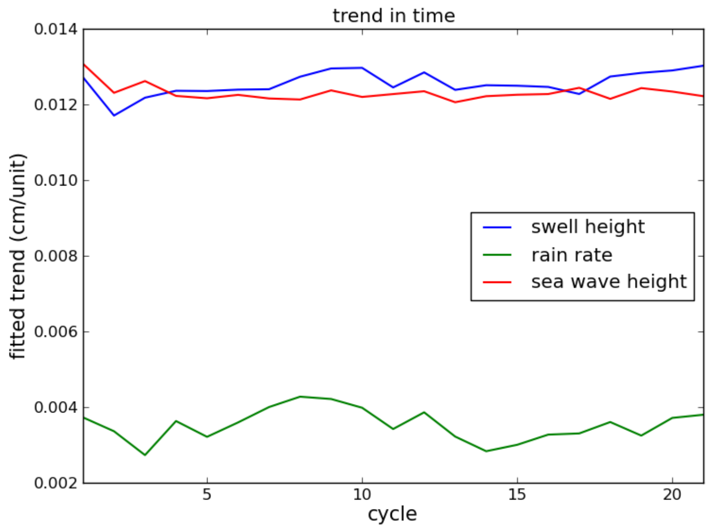

Figure 84: *Variation along cycles of the trends resulting from the linear regressions on the range std value.*

polynomial that fit the best range std is invariant in time but the part of range std explained varies seasonly from 35 % to 40 %.

- The modeled swell height gives results very close to the SWH with a 0.97 correlation. The swell period explains 17 % of the range std but this would be only due to the covariance with SWH. The swell direction does not explain range std nor sigma0 std as the $K_{swellD-Y}$ obtained is very small and probably due to the statistical distribution of this parameter.

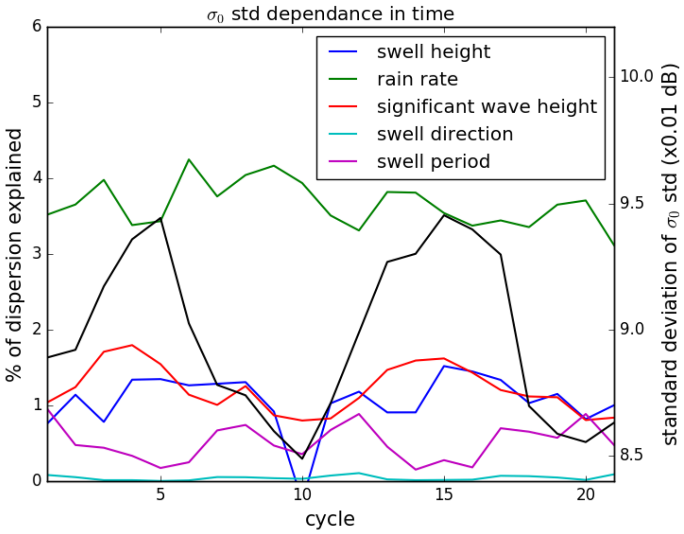

Figure 85: *The colored lines set for the dependance of sigma0 std on the different parameters along the cycles (1 to 21) of SARAL/AltiKa. It is the part (in %) of the sigma0 std that can be modeled with every single parameter refering to the left Y axis. The black line is the standard deviation of sigma0 std along cycles and refers to right Y axis.*

- The rain rate would explain less than 1 % of range std but is independant of SWH. Thus a model combining SWH and the rain rate gives better results than SWH alone. The rain rate is also the only parameter able to explain sigma0 std variations significantly. These investigations also showed a clear gap between the behavior of "dry" measurements and rainy case. Further investigations taking into account this effect would probably have far better results in terms of noise level comprehension.

7.5. Altimetry errors for submesoscale

7.5.1. Error Description

The sea level content provided by most of the conventional altimeters in low resolution mode (LRM) does not allowed the observation of ocean scales smaller than 80-100 km (Dibarboure et al.,2014 [27]). This limitation is mainly due to surface heterogeneities in the altimeter footprint (e.g. rain, sigma blooms) and the white noise level due to the instrumental noise and the measurement estimation. Hereinafter, a quantification of these errors is presented.

A usual way to represent the error budget of altimeter missions at these small scales is to perform spectral analyses of sea-level anomalies. Such spectra based on Fourrier's transform are plotted in figure 86 for Jason-2, Jason-3 and SARAL/AltiKa at global scale and from high rate measurements. The noise level of each altimeter is easily derived from the high frequency plateau of both missions. The white noise level is respectively estimated to 7.3 cm for Jason-2/Jason-3 and 5.4 cm for AltiKa, for significant wave height close to 2.7 m on average. This difference between both missions is mainly explained by the higher frequency rate of AltiKa (40 Hz) with respect to Jason-2/Jason-3 (20 Hz). The noise level do not permit the observation of oceanic structures with a scale smaller than 50 km for SARAL/AltiKa and 60 km for Jason-2/Jason-3. This distance is defined by the ratio between the oceanic signal slope and high frequency plateau equal to 1. This corresponds in figure 86 to the X-axis of the intersection between the high frequency plateau and the oceanic slope (Dufaut et al., 2016 [28]).

Furthermore, a large energy bump for wavelengths higher than few kilometers and lower than 100 km is observed for both Jason-2/Jason-3 and SARAL/AltiKa (figure 86). Dibarboure et al., 2014 [27] described in details this signal and its origin. Basically, it is due to surface heterogeneities in the LRM footprint impacting altimetry measurements as for instance in areas impacted by rain cells or sigma bloom. The comparison of the observed SLA spectrum with the expected spectrum derived from the oceanic slope and the noise level (green, red and blue dash spectra in figure 86) allows the quantification of this error. At 80 km, about 50% of additional energy is measured. Therefore, the addition of this error to the white noise prevents the observation of small oceanic scales lower than 80-100 km (on average) for all the LRM missions.

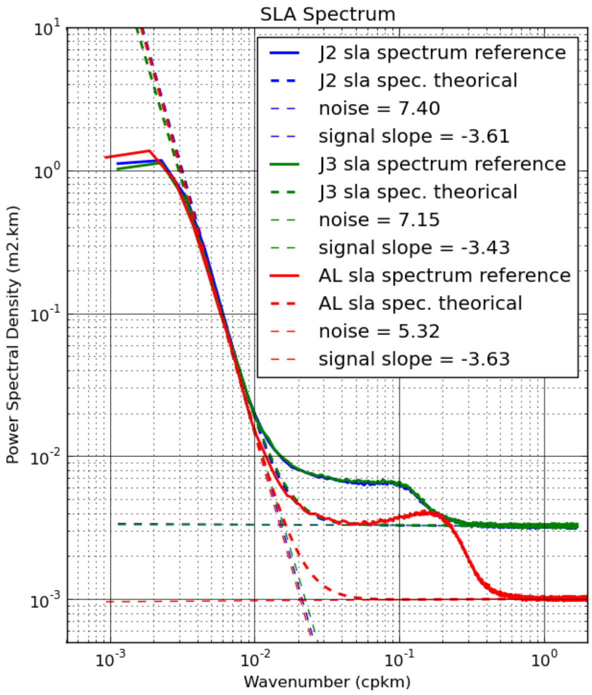

Figure 86: SLA spectra for Jason-2/Jason-3 and SARAL AltiKa from respectively 20 Hz and 40 Hz measurements

7.5.2. Expected Improvements

The altimeter processing may have a strong impact on sea level performances at these small scales, as for instance the choice of retracking algorithms, empirical methods to reduce the altimeter noise or to remove spurious sea-level measurements. Furthermore, the improvements and benefits brought by Delay Doppler altimetry (or SARM) in terms of noise reduction and better across-track resolution allows to avoid this kind of artifact. In this way, the global SAR-mode coverage ensured by the recent Sentinel-3a mission (launched in February 2016), should significantly improve the observation and the understanding of small ocean scales. Hereinafter, two methods have been further investigated to improve LRM measurements at small oceanic scales:

1. The development of a better editing procedure adapted to the high rate measurements (20 hz or 40 hz). The schema below (87) gives the main workflow of the method.
2. The application of the empirical noise reduction method developed by Zaron et al [29], based on the correlation between the altimeter range and significant wave height noise. The computation of the ΔSLA correction is based on the difference ΔSWH between the SWH measurement and the local SWH average: :
   $\frac{\Delta SLA}{\Delta SWH} = \alpha + \beta SWH$.

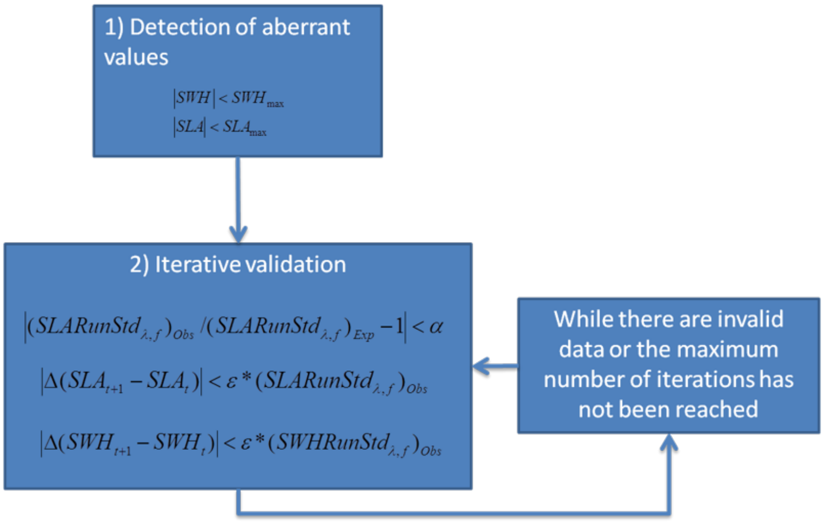

Figure 87: Editing procedure adapted to high rate measurements for Jason-2/Jason-3 and SARAL/AltiKa missions

The impact of both the new editing algorithm and Zaron's method (noted V1 hereinafter) has been compared to Jason-2 data processed with a basic editing procedure (based on duplication of 1-Hz editing flag) and without any reduction flag (noted V0 hereinafter).

Firstly, maps of variance reduction of SLA have been calculated by filtering out along-track signal frequencies lower than 200 km (figure 88). Significant SLA variance reduction is observed especially in areas where waveforms are disturbed by rain cells and sigma bloom events. On average, at global scale, the variance is reduced by about 2 cm^2. This statistic can reach 4-5 cm^2 in rain areas. The improvement in rain cells is mainly due to the new editing algorithm allowing a better detection of bad measurements. It is worth noting that about 8% of additional measurement have been removed (mainly in rain areas) compared to a classical 1-hz editing procedure.

Secondly, SLA spectra have been calculated for each V0 and V1 datasets (figure 89). A significant white noise reduction is observed by about 40% thanks to the Zaron's method. This allows the reduction of the Signal Noise Ratio (SNR) distance from about 45 to 35 km. A reduction of the spectral "bump" - characterizing the LRM errors at small oceanic scales - is also observed for distances lower than 30 km (figure 89 on right panel). However the spectral bump is just slightly modified for distances between 10 and 80 km. Unfortunately, these distances are of main interest for submesoscale studies. This means that the improvements described here do not really improved the observations of mesoscale structures on average at global scale. However, in specific areas with small altimeter range noise (i.e. small SWH), observations of smaller oceanic structures is likely possible. It is also worth noting that SLA spectrum analyses with classical Fourrier's transfom only reflect the altimer sea-level performances in areas with segment long enough (1000 km). In other words, this also means that SLA spectrum analyses are not adapted to measure the improvement in rain areas where segment are too short.

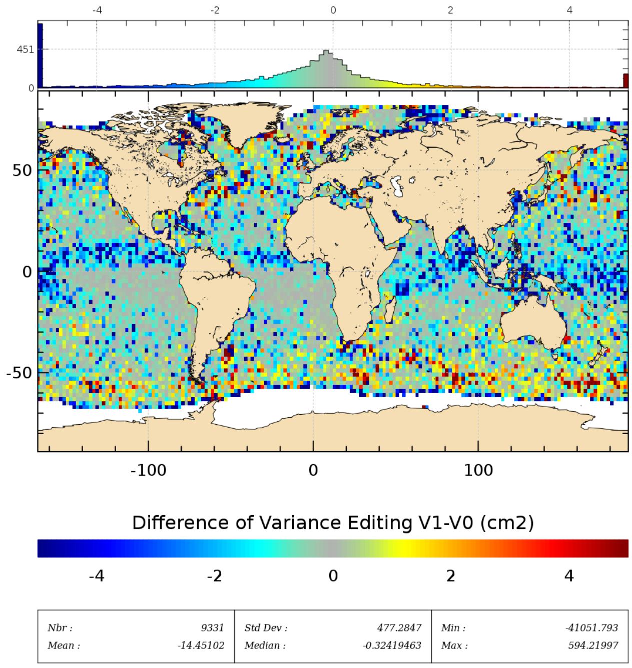

Figure 88: Map of SLA variance reduction applying new editing and Zaron's method (V1) compared to data processed with classical 1-Hz editing procedure (V0), after filtering out along-track data lower than 200 km.

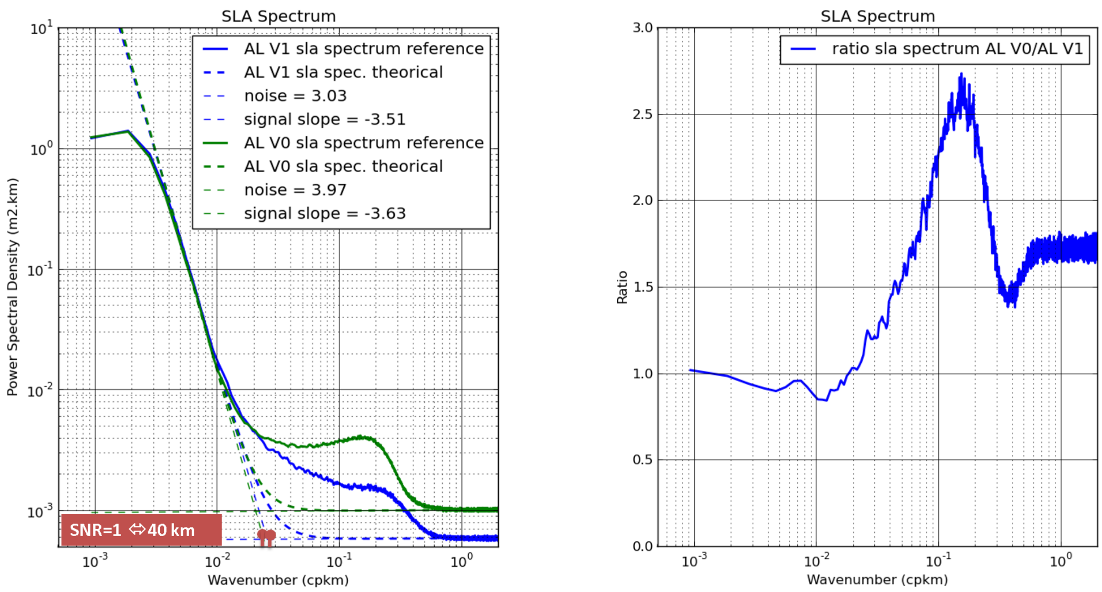

Figure 89: *SLA spectra applying new editing and Zaron's method (V1) compared to data processed with classical 1-Hz editing procedure (V0): classical power spectral density spectra with theoretical spectra superimposed (dashed lines) on left and spectra differences between classical and theoretical spectra on right. Theoretical spectrum is defined from the oceanic slope (as observed by model) and the white noise level (plateau).*

8. Conclusion

SARAL/AltiKa was launched on February, 25th 2013 and has been providing high quality sea surface height measurements for more than three years.

This report summarizes a variety of results, including comparisons with Jason-2 to demonstrate the excellent quality of SARAL/AltiKa data. The main points of this performance assessment are summarized below:

- SARAL/AltiKa provides an excellent coverage of the ocean, with more than 99% of measurements available over ocean,
- data quality is excellent, with only 2.4% of edited measurements, a value lower than for Jason-2,
- SLA statistics show no long term drift with respect Jason-2, SARAL/AltiKa and Jason-2 observe very similar SLA features, both considering the temporal evolution of global averages and geographical patterns,
- standard deviation of daily SLA averages differences between SARAL/AltiKa and Jason-2 is below 5 *mm*,
- at crossovers SARAL/AltiKa shows a performance similar to Jason-2 with a standard deviation of 5.3 *cm*.

The year 2016 is marked by a milestone for SARAL/AltiKa: the end of the repeat cycle phase and start of the drifting phase on July, 4th. As shown throughout the report, this orbit change does not have any measureable impacts on the instrument performance. However, the mean sea surface model is less accurate under the non-repetitive ground track, which has a small impact on the high frequencies of ocean sea level anomalies. SARAL/AltiKa data quality remains excellent.

Mispointing events are still affecting the platform, resulting from random anomalies in reaction wheel friction. However there is no noticeable change in the occurence of these events, which are easily edited and do not affect the data quality.

9. References

References

[1] Dibarboure, G. and A. Lamye, 2017, The drifting phase of SARAL/AltiKa: securing a stable mesoscale sampling with an unmaintained decaying altitude, submitted to *Remote Sensing*

[2] Prandi, P., S. Philipps, V. Pignot and N. Picot, 2015, SARAL/AltiKa Global Statistical Assessment and Cross-Calibration with Jason-2 *Marine Geodesy*, 38, DOI: 10.1080/01490419.2014.995840

[3] Ollivier, A. 2016, Assessment of Orbit Quality through the Sea Surface Height calculation - Yearly report 2016 - SALP activities, SALP-RP-MA-EA-23080-CLS

[4] Prandi, P., V. Pignot, 2015, Saral/ Altika validation and cross calibration activities (Annual report 2015) SALP-RP-MA-EA-22957-CLS available from http://www.aviso.altimetry.fr/fileadmin/documents/calval/annual_report_al_2015_01.pdf

[5] Philipps, S., P. Prandi and V. Pignot, 2013, Saral/ Altika validation and cross calibration activities (Annual report 2013) SALP-RP-MA-EA-22271-CLS available from http://www.aviso.altimetry.fr/fileadmin/documents/calval/annual_report_Altika_2013.pdf

[6] Frery, M.-L. *et al.*, 2014, Correction du canal 37GHz du radiomètre AltiKa, CLS/DOS/NT-14-115

[7] Aouf, L. and J.-M. Lefèvre, 2013, The impact of Saral/Altika wave data on the wave forecasting system of Météo-France : update, Oral presentation at SARAL/AltiKa 1st Verification Workshop, Toulouse, France, available at http://www.aviso.oceanobs.com/fileadmin/documents/ScienceTeams/Saral2013/24_wave_lotfi.pdf

[8] Brown, G.S., 1977, The average impulse response of a rough surface and its application", *IEEE Transactions on Antenna and Propagation*, Vol. AP 25, N1, pp. 67-74

[9] SARAL/AltiKa Products handbook, 2013, *SALP-MU-M-OP-15984-CN* edition 2.3, available at: http://www.aviso.oceanobs.com/fileadmin/documents/data/tools/SARAL_Altika_products_handbook.pdf

[10] Boy, F. and J.-D. Desjonqueres, 2010, Note technique datation de l'instant de reflexion des échos altimètres pour POSEIDON2 et POSEIDON3, *TP3-JPOS3-NT-1616-CNES*

[11] Desjonquères, J. D. , G. Carayon , N. Steunou and J. Lambin, 2010, Poseidon-3 Radar Altimeter: New Modes and In-Flight Performances, *Marine Geodesy*, 33:1, 53–79, available at http://pdfserve.informaworld.com/542982__925503482.pdf

[12] Faugere, Y., A. Delepoulle, F.Briol, I. Pujol, N. Picot, E. Bronner; 2013, Altika in DUACS: Status after 2 months (and perspectives), oral presentation at SARAL/AltiKa 1st Verification Workshop, Toulouse, France, available at http://www.aviso.oceanobs.com/fileadmin/documents/ScienceTeams/Saral2013/34_Altika_in_Duacs_Faugere.pdf

[13] Griffin, D. and M. Cahill, 2013, Use of AltiKa NRT sea level anomaly in the Australian multi-mission analysis, Oral presentation at SARAL/AltiKa 1st Verification Workshop,

Toulouse, France, available at http://www.aviso.oceanobs.com/fileadmin/documents/ScienceTeams/Saral2013/33_multi_mission_gridding_GRIFFIN.pdf

[14] Lillibridge, J., R. Scharroo, S. Abdalla, and D. Vandemark, 2013, One-and Two-Dimensional Wind Speed Models for Ka-band Altimetry, *Journal of Atmospheric and Oceanic Technology*, doi: http://dx.doi.org/10.1175/JTECH-D-13-00167.1

[15] Picot, N., A. Guillot, P. Sengenès, J. Noubel, N. Steunou, S. Philipps, P. Prandi, G. Valladeau, M. Ablain, S. Desai, B. Haines and S. Fleury, 2013, Data Quality Assessment Of The SARAL/AltiKa Ka-band Mission, Oral presentation at OSTST, Boulder, USA, available at http://www.aviso.oceanobs.com/fileadmin/documents/OSTST/2013/oral/Picot_SARAL_Data_Quality_Assessment.pdf

[16] Philipps, S. and V. Pignot, 2014, Saral/AltiKa reprocessing GDR-T Patch2, SALP-RP-MA-EA-22345-CLS/CLS.DOS/NT/14-031

[17] Scharroo, R., and J. L. Lillibridge, 2005, Non-parametric sea-state bias models and their relevance to sea level change studies, in *Proceedings of the 2004 Envisat & ERS Symposium*, Eur. Space Agency Spec. Publ., ESA SP-572, edited by H. Lacoste and L. Ouwehand

[18] Stenou, N., P. Sengenes, J. Noubel, N. Picot, J.D. Desjonquères, J.C. Poisson, P. Thibaut, F. Robert and N. Tavenea, 2013, AltiKa Instrument : In-Flight Stability And Performances, Oral presentation at OSTST, Boulder, USA, available at http://www.aviso.oceanobs.com/fileadmin/documents/OSTST/2013/oral/Steunou_OSTST2013_AltiKa_Instrument.pdf

[19] SARAL System Requirements, *SRL-SYS-SP-010-CNES*

[20] Thibaut, P., O.Z. Zanifé, J.P. Dumont, J. Dorandeu, N. Picot, and P. Vincent, 2002, Data editing: The MQE criterion, *Paper presented at the Jason-1 and TOPEX/Poseidon Science Working Team Meeting, New-Orleans (USA), 21-23 October*

[21] Tolman, H. L., 2014, User manual and system documentation of WAVEWATCH III version 4.18. *NOAA / NWS / NCEP / MMAB Technical Note 316, 194 pp.* available at http://polar.ncep.noaa.gov/waves/wavewatch/manual.v4.18.pdf

[22] The WAVEWATCH III Development Group., 2016, User manual and system documentation of WAVEWATCH III version 5.16. *NOAA / NWS / NCEP / MMAB Technical Note 329, 326 pp.* available at http://polar.ncep.noaa.gov/waves/wavewatch/manual.v5.16.pdf

[23] Prandi, P., V. Pignot and S. Philipps, 2015, Saral/ Altika validation and cross calibration activities (Annual report 2014), SALP-RP-MA-EA-22418-CLS

[24] Roinard, H., S. Philipps and O. Lauret, 2016, Jason-2 validation and cross calibration activities (Annual report 2015), SALP-RP-MA-EA-XXXXX-CLS available at http://www.aviso.altimetry.fr/en/data/calval.html

[25] Roinard, H., P. Matton and S. Philipps, 2015, Jason-2 validation and cross calibration activities (Annual report 2014), SALP-RP-MA-EA-22409-CLS available at http://www.aviso.altimetry.fr/en/data/calval.html

[26] Pujol, M.-I., Y. Faugere, G. Dibarboure, P. Schaeffer, A. Guillot and N. Picot, 2015, The recent drift of SARAL: an unexpected MSS experiment, oral presentation at the 2015 OSTST, Reston, VA

[27] - Dibarboure, G., F. Boy, J. D. Desjonqueres, S. Labroue, Y. Lasne, N. Picot, J. C. Poisson, and P. Thibaut, 2014: Investigating short-wavelength correlated errors on low-resolution mode altimetry. *J. Atmos. Oceanic Technol.*, **31**, 1337–1362, doi:10.1175/JTECH-D-13-00081.1

[28] - Dufau, C., M. Orsztynowicz,G. Dibarboure, R. Morrow, and P.-Y. Le Traon (2016), Mesoscale resolution capability of altimetry:Present and future, *J. Geophys. Res.Oceans*, **121**, doi:10.1002/2015JC010904.

[29] Edward D. Zaron , Robert deCarvalho, 2016. Identification and Reduction of Retracker-Related Noise in Altimeter-Derived Sea Surface Height Measurements. *Journal of Atmospheric and Oceanic Technology*, p201-210, doi:10.1175/JTECH-D-15-0164.1

10. Annex

10.1. Content of Patch 1

Hereafter the content of Patch 1 is recalled. All GDR data up to cycle 7 included were initially produced with this patch. It was used to produce IGDR data from cycle 4 pass 395 to cycle 10 pass 565.

Altimeter calibration file : The altimeter calibration stability has been analysed. Based on the actual data, we have implemented an averaging of the calibrations over a 7 days window for the low pass filter (identical to Jason-2) and 3 days for the internal path delay and total power (not used on Jason-2). This will slightly reduce the daily noise observed in the altimeter calibration data.

Altimeter characterization file : We have updated the altimeter characterization file using the flight calibration of the gain values (4 calibrations performed). The impact is very small (of the order of 0.01 dB).

Retracking look-up tables : We have updated the ocean retracking look-up tables using the flight calibration data (PTR). The impact is very small on the range and sigma0 values but of the order of 15 cms on SWH for low sea states.

MQE : We have analyzed the altimeter flight data and based on the observed MQE values over ocean a threshold of 2.3E-3 (Jason-2 value is 8E-3) is used for the 1Hz data computation.

Neural network : A first linear relation has been computed between the measured BT and the simulated one. This linear relation is applied on the 23.8 GHz only – the same analysis will be conducted on the 37 GHz and sigma0. This generates a bias on the radiometer wet tropospheric correction which is now much more consistent with the model one.

Atmospheric attenuation : The value outputted by the neural algorithm is now recorded in the level2 products (it was set to 0 at the beginning of the mission). Rad_water_vapor and rad_liquid_water: The values have been corrected to comply with the actual unit in the level2 products (kg/m^2). But the rad_liquid_water remains not reliable as an anomaly has been noticed in the neural network.

SSHA : The radiometer wet tropospheric correction is now used to compute this value (the model value was used at the beginning of the mission).

Controls parameters : The threshold values have been updated with in-flight data. This is a first tuning – additional work is necessary.

10.2. Content of Patch 2

Hereafter the content of Patch 2 is recalled. GDR data were produced using Patch 2 from cycle 8 onwards. Cycles 1 to 7 were reprocessed with the Patch 2 to provide a consistent dataset

Wind look-up table : The table provided by NOAA is used. This table is only based on the measured sigma0, taking into account the atmospheric attenuation (sigma0 at the surface). (Reference: Lillibridge et al. [14])

SSB look-up table : The table provided by R. Scharroo is used (same method as in [17]). We use only the significant wave height to compute the SSB.

Radiometer neural algorithm : Taking into account several months of AltiKa measurements, the neural network coefficients have been updated. Note that this modifies the radiometer related parameters (radiometer wet troposphere correction, atmospheric attenuation, radiometer liquid water content and radiometer water vapor content).

Ice-2 retracking algorithm : The algorithm has been updated taking into account the AltiKa Ka band specificities (ice2 algorithm was based on ENVISAT Ku band experience).

FES2012 tide model : This new tide model is included, improving the SSH accuracy in coastal zones. (Reference : http://www.aviso.oceanobs.com/en/data/products/auxiliary-products/global-tidefes2004-fes99/description-fes2012.html)

Matching pursuit algorithm : The algorithm based on J. Tournadre proposal has been tuned to comply to AltiKa Ka band specificities.

MQE parameter scale factor : The scale factor of the MQE has been modified.

Update of the altimeter characterization file : The altimeter characterization file has been modified in order to account for 63 values of altimeter gain control loop (AGC). This has impacts over sea ice and land hydrology, in some cases the AGC was set to default value in current P1 products.

Doris on ground processing (Triode) : The Doris navigator ground processing has been upgraded to reduce the periodic signal observed on the altitude differences with MOE/POE.